Goal-Oriented Angular Adaptive Neutron Transport using a Spherical Discontinuous Galerkin Method

Dion Koeze

December 2011

Supervisor :
dr.ir. Danny Lathouwers

Section Physics of Nuclear Reactors
Department of Radiation Radionuclides Reactors
Faculty of Applied Sciences
Delft University of Technology

Abstract

In neutron transport problems one is often interested in acquiring an accurate detector response, which does not necessarily requires an accurate solution in the whole domain of the problem. In this work the possibilities of a goal-oriented adaptive algorithm for the one speed, steady state, isotropic scatter neutron transport equation are investigated. This method can be expanded to incorporate energy dependency, time dependency and anisotropic scatter.

Three methods are examined on their ability to handle adaptivity and their feasibility of implementation. The discrete ordinates method is included, as this is a widely used method to solve the transport equation. This method allows for quick convergence with source iteration and a sweep algorithm, however it does not allow for adaptivity well. The second method consists of using wavelets as basis functions with the discontinuous Galerkin discretization method. Adaptivity is easily achieved, as wavelets are naturally hierarchical. However, this comes at a price, as the matrix equations that need to be solved are large and not sparse. Also the sweep algorithm cannot be applied to the discrete system of equations obtained with this method. The third and last method is using polynomials as basis functions for the discontinuous Galerkin discretization method. Adaptivity is possible as angular elements (patches) can be refined without altering neighbour patches. The source iteration and sweep algorithm can be applied, which means this method yields discrete equations that are cheap to solve.

A comparison is made between the discrete ordinates method with the Gauss Legendre quadrature and the polynomial discontinuous Galerkin method with linear spatial elements and constant angular elements for one-dimensional problems. For thin scattering materials the discontinuous Galerkin method provides a larger error reduction than discrete ordinates, while for other materials discrete ordinates outperforms discontinuous Galerkin.

Using the adjoint equation we can derive an error estimator for the detector response that is a sum of contributions to the error of each patch. The patches with the largest contribution are refined in an adaptive algorithm. This estimator can be computed with a local or a global approximation of the adjoint solution. This criterion is tested against a traditional refinement criterion that bases its decision on the change in the solution of the angular flux when a patch is refined. The goal-oriented adaptive methods provide a better detector response, while the traditional method provides a more accurate global solution. The estimator that uses the global adjoint approximation is generally a good indicator of the error, while the estimator using the local adjoint approximation is not. They do, however, refine the same patches, so they can both be used as refinement criterion.

The convergence of the uniform and goal-oriented adaptive methods is second order for all test cases in this work. This leads us to expect forth order convergence when linear basis functions are used on the patches.

Contents

List of Figures

List of Symbols

γ	Spatial basis function	
η	Contribution to the error estimator of a patch	$cm^{-3}s^{-1}$
$\mathbf{\Theta}$	Vector of spatial basis functions	
λ	Mean free path of a neutron	cm
μ	Cosine of the polar angle	
μ'	Average polar angle cosine of a patch	
σ_D	Macroscopic detector cross section	cm^{-1}
σ_s	Macroscopic scattering cross section	cm^{-1}
σ_t	Macroscopic total cross section	cm^{-1}
Φ	Scalar neutron flux	$cm^{-2}s^{-1}$
ϕ	Angular neutron flux	$cm^{-2}s^{-1}$
ϕ^*	Exact adjoint solution	
Ψ	Mother wavelet	
Ω	Direction	
$\hat{\mathbf{\Omega}}$	Unit vector of direction of motion	
$\hat{\mathbf{\Omega}}'$	Average direction of a patch	
ω	Azimuthal angle	
$\boldsymbol{A}$	Matrix that holds products of wavelets in streaming term	
$B(u,v)$	Bilinear form in weak formulation of transport equation	
c	Scatter ratio, total over scatter cross section	
E	Energy of a neutron	eV
E_{det}	Error in the detector response	$cm^{-2}s^{-1}$
E_{rms}	Node wise root mean square error of scalar flux	$cm^{-3}s^{-1}$
G	Basis function of a patch	
$\boldsymbol{H}$	Matrix that holds products of wavelets in removal and scatter term	
J	Detector response	s^{-1}
$\boldsymbol{K}$	Matrix with products of spatial basis functiosn in streaming term	

L	Transport operator	
$l(v)$	Linear form in weak formulation of transport equation	
L^*	Adjoint transport operator	
$\boldsymbol{M}$	Matrix with products of spatial basis functions	
$\hat{\boldsymbol{n}}$	Normal vector	
q	Partial scatter source	$cm^{-3}s^{-1}$
$\boldsymbol{r}$	Position vector	cm
R	Volumetric residual	$cm^{-3}s^{-1}$
r	Boundary residual	$cm^{-3}s^{-1}$
S	External source in operator expression	$cm^{-3}s^{-1}$
s	External source in the transport equation	$cm^{-3}s^{-1}$
t	Time	s
$\boldsymbol{U}$	Matrix with products of spatial basis functions on a boundary	
V	Space in which weak solution of transport equation lies	
v	Element of function space used for Galerkin method	
$v(E)$	Speed of a neutron with energy E	cms^{-1}
V_h	Subspace of functions in which the Galerkin discretised solution lies	
W	Weights in quadrature sum obtained from wavelets	
w	Weights in quadrature sum	
$aprx$	Approximate subscript	
Δ	Size of interval or surface area of element	
δ	Boundary of a set or space	
e	Element index subscript	
h	Discrete subscript	
int, ext	Superscript indicating internal and external with respect to an element	
l	l times scattered superscript	
n	Direction subscript	
p	Patch index subscript	
U, D, R	Upwind, Dirichlet, Reflective boundary subscript	
x, y, z	Spatial component subscript	

1 Introduction

In the area of nuclear physics many kind of reactions between atoms and other particles are investigated. One of these reactions is the collapse of an unstable atom, which usually results in smaller atoms and various kinds of radiation. Such a collapse can be induced when a neutron is captured by an atom, it is then called a fission reaction. In the collapse of certain atoms free neutrons are produced, which can induce new fission reactions. Under the right circumstances this can lead to a fission chain reaction.

The first self sustaining nuclear chain reaction produced by man was on December 2 1942 in Chicago. Enrico Fermi and his colleagues built this first reactor from blocks of graphite and three inch wide cylinders of uranium oxide. Shortly after these experiments the United States would invest in research on using atoms for the production of electricity, for medical treatment, as a tool for scientific research and for the production of nuclear weapons. Investments in research in other countries followed shortly after this. In all applications it is important to understand the movement of neutrons, as neutrons induce the reactions with which the energy and radiation is released.

Electricity is often produced by a steam powered generator. Different kind of heat sources can be used to boil the water needed to make steam. A number of sources are used today, including fossil fuels, solar radiation and nuclear fission reactions. The fission reactions take place in a nuclear reactor.

Present day nuclear reactors are designed very different from the early day experiments. Instead of graphite, water is commonly used as moderator. This water can also function as the coolant of the reactor core. The uranium fuel is stored in pellets, which are stacked to form cylinders. One would like to accurately compute the neutron density in such a geometry to be able to predict heat production and fuel burn-up rates.

Another application of nuclear technology is in medical treatments. Radioactive isotopes that are produced in a nuclear reactor can be used as tracers that are injected in a human body. The particles will travel through the veins with the blood, allowing a radiation detector around the patient to see the blood flow. These radioactive isotopes should be short living, as the patient should receive only a minimal dosis. In this and other medical imaging techniques the neutral particles that stream through the patient are used to construct an image of the patient.

Besides using imaging techniques in medical treatments, they can also be used for research on material properties. The structure of material on the smallest scale can be visualized using neutral or charged particles. By irradiating materials with high neutron fluxes we can investigate other properties, like the rate of corrosion of materials in nuclear reactors.

In the examples above the movement, or streaming, and reactions of neutrons are very important. An equation that describes this behaviour was found by adapting the Boltzmann equation, which was used in the nineteenth century to study the kinetic theory of gases. It is called the neutron transport equation and can only be solved analytically for specific geometries. This equation has become an area of active research in the twentieth century, as the research on nuclear applications has become increasingly important since then.

Two different methods of solving the transport equation can be discerned. Monte Carlo methods use random sampling to solve the equation. This can, for example, be accomplished by following single neutrons along their path in the geometry. By sampling many of these neutron histories one can derive properties of the solution of the transport equation. However, different and more sophisticated ways of using random sampling exist.

The other class of methods are the deterministic methods and are the focus of this report. Here the solution to the equation is found by solving the equation with numerical methods. To this end a discretization method must be chosen. Many discretization methods are available and each has its own advantages and disadvantages.

In deterministic numerical methods a mesh is usually defined on the phase space of the equation that is to be solved. The phase space of the transport equation in this report consists of a spatial coordinate and an

angular coordinate. In order to obtain an accurate solution the mesh must be fine, however a very fine mesh will introduce large numerical costs. Numerical cost can be limited in computational aspect or in memory aspect.

A way to minimize the cost for an algorithm is to make it adaptive. Adaptivity means that during the computation some parts of the mesh are refined. This refinement should take place in the regions of phase space where the error contribution is largest. In other words, when using an adaptive method one needs a criterion for determining what parts of the solution introduce the largest error.

Traditionally this criterion is based on a change in the solution upon refinement. This means a local refinement is made and the effect on the total solution is evaluated. This procedure is repeated for all elements. A pre set number of percentage of patches will be refined, these will be the patches that caused the most change in the solution with the local refinement.

Such a refinement criterion does not always work well when the goal is not an accurate global solution, but for example an accurate detector response. The refinement criterion should incorporate that the goal of the refinement is to obtain a detector response. Recently such criteria have been formulated and were tested for different equations . The focus of this work is an algorithm that is adaptive in the angular component of the neutron transport equation.

The amount of neutrons that are travelling in a certain direction can vary a lot with that direction. An example of such a situation is a pencil beam, where neutrons are focussed in a small beam. An accurate representation of the flux can only be found when the resolution of the mesh around the beam is large. However, it is not necessary to use a high resolution mesh in other directions, which will save us on computational cost. An adaptive algorithm should be able to efficiently compute the solution of these situations.

In pencil beam problems where the direction and location of the beam are known, it is not necessary to use an adaptive algorithm to produce a mesh with the right resolution. However, when we cannot predict direction and location of such a beam, an adaptive method is needed. In any problem an efficient adaptive method will ensure that the resolution of the mesh is adequate to obtain an accurate solution.

Besides a criterion for refinement we also need a way of discretizing the transport equation into a set of equations that can be solved numerically. A widely used method for angular discretization is the discrete ordinates method, where one demands the transport equation to hold for a finite set of directions. This method has very low computational costs, although the total costs depend also on the discretization that is used for the spatial part of the problem. A quadrature approximation is used to evaluate integrals for the scatter description, which is the reason why adaptive algorithms are difficult to implement in this method. Most quadratures require that when a direction is added, all other directions will have to be changed. This means all directions will have to be solved again, making it impractical.

Another common approach for discretizing equations is using a finite element or Galerkin approach. In this method basis functions are used to approximate the solution, where the associated coefficients will have to be computed numerically. The basis functions can be chosen to allow for refinement of the mesh that makes only local changes. Two types of basis functions that meet this requirement are investigated in this report, wavelets and polynomial basis functions, for their feasibility of implementation in numerical methods.

Before we explain the structure of this report some words will be spent on the discretization method that is used, the discontinuous Galerkin method. Galerkin methods have been around for almost a century, which are based on the idea that a differential equation which is formulated in the weak sense can be solved on a restricted space, of which we have a finite basis. It is important that the basis is finite, if it were an infinite basis we could not easily use numerical methods to solve the differential equation, as a procedure that needs to be done for each basis vector will never be completed.

Until recently the basis that spans the restricted space consisted of (piece wise) continuous functions. The idea behind this is that discontinuities are not nice, both physically and mathematically. However, allowing for

discontinuities in the basis leads to decoupled equations and can give a more accurate solution. In this report the method is only briefly discussed, for a more detailed explanation we would like to refer to other work.

The body of this report consists of several sections, starting with the mathematical investigation of three possible discretization methods. Three methods are described and investigated as to whether an adaptive algorithm can be formulated based on those methods. First we investigate the discrete ordinates method, which is widely used in deterministic methods. The second method is the discontinuous Galerkin discretization method with polynomial basis functions. The final method we considered is a Galerkin discretization with wavelets as basis functions.

It turns out the discontinuous Galerkin method with polynomial basis functions seems to be the most promising method. Therefore the next section is the formulation of a one dimensional test problem, using constant basis functions as polynomials. This section also presents an overview of the non-adaptive algorithm and the data structure that is used in the code.

Several test cases are used to test the performance of the discontinuous Galerkin method, relative to the discrete ordinates method. These are presented in the section that follows the one-dimensional problem formulation.

After these results, the next section starts by explaining the criteria that are used for determining which patches need to be refined in the adaptive algorithm. A traditional method, which bases its decision on the change in solution when refinement takes place, and two goal-oriented methods, where the goal is to get an accurate detector response, are used. The goal-oriented methods used the adjoint problem, which is explained in this section. Finally in this section an overview of the adaptive algorithm is presented.

The final section of the main body, is the section where all adaptive results are presented. The test consists of comparing error reduction of all methods. The quality of the error estimators is also tested. As a last test we varied the number of patches that is refined in each refinement iteration, to see the effect of this parameter.

After a section with the main conclusions and possible future work, four appendices can be found. The first is a list of all the test problems that are used in this report, together with all geometry and material properties of the problems. The next appendix contains a more detailed derivation of the error estimator and goal-oriented adaptive refinement criterion. Then an appendix with a more detailed, but still brief, derivation of the discretized wavelet equations can be found. The fourth and last appendix is the derivation of the adjoint transport operator and an explanation of the physical interpretation of this operator.

This report is the product of a master thesis research at the Faculty of Applied Sciences of the Delft University of Technology. It was conducted in the group Physics of Nuclear Reactors at the Reactor Institute Delft. It will be the starting point of another master thesis research in the Numerical Analysis group at the Mathematics Department of the same university.

2 The Neutron Transport Equation

In nuclear reactor physics neutrons are very important, since neutrons are necessary for the chain reaction of fission to continue. In fact, since neutrons can travel through the reactor core and fuel is fixed, neutrons are the main subject in reactor physics. The neutron transport equation is the governing equation of free neutrons in the reactor core, or, for that matter, in any geometry or substance. In certain geometries the transport equation can be solved analytically, however for many real world problems numerical solutions are needed. In the process of designing nuclear reactors or other nuclear facilities accurate approximation of the neutron density or neutron flux are needed to predict for example heat production in the core. New numerical techniques are still developed, which will result in more accurate reactor designs. This section contains some basic remarks on the neutron transport equation, which are necessary for this report. A detailed description of the properties and derivation of the transport equation can be found in many nuclear engineering hand books.

2.1 General transport equation

Free neutrons are the neutrons that are important to reactor physics. These neutrons can freely move through the material and take part in reactions with the surrounding material. Common reactions are collisions (scatter) and absorption. Neutrons that are captured in the nucleus of an atom are not important to reactor physics, as these neutrons will not take part in any important reactions. The neutron transport equation therefore considers the free neutrons and desribes the rate of reaction as well as the movement (streaming) of the neutrons. A full derivation of the transport equation, as well as many applications, can be found in [6]. The most general form of the transport equation is

$$\begin{aligned}&\frac{1}{v(E)}\frac{\partial\phi(\boldsymbol{r},E,\hat{\boldsymbol{\Omega}},t)}{\partial t}+\hat{\boldsymbol{\Omega}}\cdot\nabla\phi(\boldsymbol{r},E,\hat{\boldsymbol{\Omega}},t)+\sigma_t(\boldsymbol{r},E,t)\phi(\boldsymbol{r},E,\hat{\boldsymbol{\Omega}},t)=\\&\int_{4\pi}d\Omega'\int_0^\infty dE'\sigma_s(\boldsymbol{r},E'\to E,\hat{\boldsymbol{\Omega}}'\to\hat{\boldsymbol{\Omega}},t)\phi(\boldsymbol{r},E',\hat{\boldsymbol{\Omega}}',t)+s(\boldsymbol{r},E,\hat{\boldsymbol{\Omega}},t)\end{aligned}\tag{2.1}$$

Some of the symbols in this equation are introduced here shortly, a nomenclature can be found in the front of the report. The angular flux ϕ is the quantity of interest, it can be interpreted as the density of the number of neutrons that is at $\boldsymbol{r}$, has an energy E and travels in direction $\hat{\boldsymbol{\Omega}}$ at time t. The total cross section σ_t and the scattering cross section σ_s tell us with what rate the reactions occur.

We will now shortly discuss the physical meaning of each of the terms. The first term on the left hand side is the change in neutron density over time. The next term is the streaming term of the equation, it follows from applying Gauss' theorem on the expression describing the neutrons travelling into a control volume. Finally on the left hand side we have the total removal of neutrons, proportional to the total removal cross section σ_t. The right hand side contains two terms, the second term is an external source, which can be arbitrarily specified. Scattering is described by the first term of the right hand side. This can be considered a source as neutrons with other energies and travelling in other directions can be scattered into the part of phase space considered. Therefore the term contains an integral both over all directions and all energies. Please note that this general form of the transport equation does not describe fission reactions. Fission reactions result in an extra source term that has the same form as the scatter term.

2.2 Common approximations of the transport equation

To test the performance of numerical techniques it is not always necessary to consider the general transport equation. Some approximations or simplifications can be made without altering the behaviour or the complexity of the equation. A number of these adjustments is used in this report, which are discussed in this section.

The time dependence is eliminated in most proofs of principle. When solving a time dependent problem one usually approximates a certain state of the problem at time t as a steady-state problem. To solve a time dependent problem a number of steady-state problems is solved sequentially. Therefore we can equate the first term of the general transport equation to zero: $\frac{1}{v(E)}\frac{\partial\phi(\boldsymbol{r},E,\hat{\boldsymbol{\Omega}},t)}{\partial t} = 0$.

Another common discretization in most solvers is that the energy dependence is discretized into groups. All neutrons are put into energy 'bins' and cross sections are used to determine the number of neutrons that switch bins or stay in the same bin. The driving force of switching bins is scatter, since in scatter reactions neutrons may lose or gain energy. The simplest case is to consider just one bin, this effectively eliminates energy dependence from the problem. This report uses this one group approach.

The scatter source term is further simplified by considering isotropic scatter only. This means the angular dependency of the scatter cross section σ_s is neglected. To account for anisotropic scatter multiple techniques exist, the most common being the expansion of the scatter cross section in spherical harmonics or Legendre polynomials. In this report there is no background information on this.

When applying all these simplifications the transport equation becomes:

$$\hat{\boldsymbol{\Omega}} \cdot \nabla\phi(\boldsymbol{r},\hat{\boldsymbol{\Omega}}) + \sigma_t(\boldsymbol{r})\phi(\boldsymbol{r},\hat{\boldsymbol{\Omega}}) = \frac{\sigma_s}{4\pi}\Phi(\boldsymbol{r}) + s(\boldsymbol{r},\hat{\boldsymbol{\Omega}}) \tag{2.2}$$

where the scalar flux Φ is defined as $\Phi(\boldsymbol{r}) = \int_{4\pi}\phi(\boldsymbol{r},\hat{\boldsymbol{\Omega}})d\hat{\boldsymbol{\Omega}}$.

Some properties of the equation are noteworthy, as they play a role in the performance of numeric solvers. First there is the difference between an optically thick and thin medium. A thick medium means the mean free path λ of neutrons is small. The mean free path compared to the size of the domain determines the probability of neutrons to leak out of the problem. When the domain is much larger than the mean free path the problem is optically thick. The mean free path is determined by the inverse of the total cross section,

$$\lambda = \frac{1}{\sigma_t} \tag{2.3}$$

A thick medium in a small domain can however result in an optically thin problem. Conversely a thin medium, with a large mean free path λ may result in optically thin and optically thick medium. However the size of the domain will be much larger for a thin medium to make a thick problem.

Besides the thickness of the material, one can also vary the ratio with which the two most important reactions, absorption and scatter, occur. This ratio is called the scatter ratio c, and is

$$c = \frac{\sigma_s}{\sigma_t} \tag{2.4}$$

The larger c the more diffusive the material will be. In diffusive materials the transport equation can be approximated by the diffusion equation. In the results it will show that the scatter ratio c of the material influences the performance of numerical methods.

3 Discretization of the Neutron Transport Equation

Discretizing the neutron transport equation is usually done in two steps, an angular and a spatial discretization. The focus of this report is the angular discretization, however we cannot test the angular discretization in practice without a spatial discretization. Therefore later on some words will be spent on spatial discretization. Angular discretization is the focus because we are interested in constructing an angular adaptive method for the transport equation. This means we want a discretization that can handle on the fly refinements of the numerical solutions. This section describes three methods for angular discretization which were investigated to find the method that is best suitable for this goal. The three different methods of angular discretization are the discrete ordinates method, wavelets as basis functions for a discontinuous Galerkin method and polynomials as basis functions for a discontinuous Galerkin method. The discrete ordinates method is the oldest of the three methods, it has its origin in the nineteen fifties and is widely used in numerical codes ever since. Both remaining methods use the discontinuous Galerkin discretization method. This method can be used with different basis functions, for example wavelets. Wavelets are a special class of functions with a hierarchical structure, which could be useful in refinement. The other discontinuous Galerkin method in this report uses polynomials as basis functions. Polynomials have been used in many discretization methods, however to use them on the sphere with the discontinuous Galerkin method has not been done before.

At the end of this section a comparison will be made between these three methods before choosing which method is best suitable for an adaptive algorithm. As it turns out discontinuous Galerkin with polynomial basis functions is chosen. The remaining report will be on the performance of this method.

3.1 Discrete ordinates method

3.1.1 Discrete ordinates description

The discrete ordinates method, simply put, consists of requiring that the transport equation (equation 2.2) holds for a finite size set of directions. Let $\hat{\mathbf{\Omega}}_n$ denote such a direction, where $n = 1, 2, \ldots, N$. The discrete ordinates equation is then

$$\hat{\mathbf{\Omega}}_n \cdot \nabla\phi(\boldsymbol{r}, \hat{\mathbf{\Omega}}_n) + \sigma_t(\boldsymbol{r})\phi(\boldsymbol{r}, \hat{\mathbf{\Omega}}_n) = \frac{\sigma_s}{4\pi}\Phi(\boldsymbol{r}) + s(\boldsymbol{r}, \hat{\mathbf{\Omega}}_n) \tag{3.1}$$

The scalar flux Φ can then be computed using a quadrature in the following manner

$$\int_{4\pi} \phi(\boldsymbol{r}, \hat{\mathbf{\Omega}}) d\hat{\mathbf{\Omega}} = \sum_{n}^{N} w_n(\boldsymbol{r})\phi(\boldsymbol{r}, \hat{\mathbf{\Omega}}_n) \tag{3.2}$$

In this equation the weights should add up to 4π as this is the surface of the sphere. To illustrate this, consider the angular flux ϕ to be unity, the the integral equals 4π. The directions $\hat{\mathbf{\Omega}}_n$ and the distribution of the weights w_n are not specified by the discretization. For an accurate description of the scatter source term the choice of quadrature set needs to meet a number of conditions.

For a two dimensional case there are physical symmetries in the problem, the quadrature set must preserve these. In a two dimensional problem we can save a lot of computational resources by preserving the symmetry in the plane of the problem. Every direction has a mirrored direction which physical meaning is the same. When the plane is in the xy directions, the directions $\hat{\mathbf{\Omega}}_1 = (\Omega_x, \Omega_y, \Omega_z)$ and $\hat{\mathbf{\Omega}}_1 = (\Omega_x, \Omega_y, -\Omega_z)$ have the same influence on the problem. This means we can simplify the scalar flux to an integral over the half sphere

$$\frac{\sigma_s}{4\pi}\Phi(\boldsymbol{r}) = \frac{\sigma_s}{2\pi}\int_{2\pi} \phi(\boldsymbol{r}, \hat{\mathbf{\Omega}}) d\hat{\mathbf{\Omega}} = \frac{\sigma_s}{2\pi}\sum_{n}^{N} w_n(\boldsymbol{r})\phi(\boldsymbol{r}, \hat{\mathbf{\Omega}}_n) \tag{3.3}$$

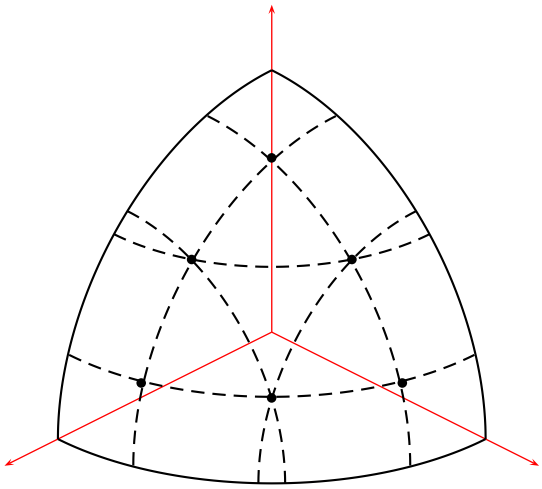

Figure 1: *Set of directions of the level symmetric quadrature for* S_6.

where the weights w_n add up to 4π.

The quadrature should approximate the flux moments well, the scalar flux being the simplest moment, in order to have an accurate scatter source representation. This comes down to being able to approximate polynomials of increasing order on the sphere, the larger the order one can approximate the more accurate the source term.

Also in the diffusion limit of the transport equation the quadrature approximation should work. The diffusion limit is the case where the scatter ratio c goes to unity, in other words neutrons are only scattered, not absorbed. When assuming the angular flux is linear in μ, some requirements must be met to be consistent with the neutron current.

The final property of a discrete ordinate set is that all points should have a positive weight associated with them. This is to prevent the scalar flux from becoming negative, which is not physical. A few basic and new quadrature sets are discussed in Section 3.1.2.

3.1.2 Choice of ordinate sets

For three dimensional problems the most common quadrature is the level symmetric set, which is illustrated in Figure 1. This set has only one degree of freedom, all directions and weights are determined by choosing the first direction.

The most common choice for the ordinate set in the one dimensional case is a Gauss-Legendre quadrature. This quadrature integrates polynomials of order $2N-1$ exactly, where N is the number of quadrature points and weights. These points are the first N zero's of the Nth order Legendre polynomial. However, this quadrature

set does not work with points with a 'compact support', that is, each quadrature point represents functions that live on the whole sphere. Therefore it will not handle discontinuities in the angular flux well. This is best illustrated using an example.

In a one dimensional problem with vacuum boundary conditions, there is a discontinuity in the angular flux. Since there are no neutrons entering the problem, but neutrons leaking out of the problem, there is a discontinuity at $\mu = 0$. The ordinary Gauss-Legendre quadrature set does not handle this well. A solution to this is to use what is called a double Gauss-Legendre quadrature. Where the interval $[-1, 0]$ is approximated separately from the interval $[0, 1]$, i.e. two separate Gauss-Legendre quadratures are used. However, it is not a solution to introduce discontinuities in quadrature sets in three dimensions, since the discontinuities are in general not regular. Other quadrature sets have been proposed to solve this issue. For example quadrature points and weights based on a discontinuous finite element method [7].

The discrete ordinates method is not an adaptive method, one usually chooses a quadrature set for the complete calculation. However, quadrature sets that can be used for adaptive discrete ordinates have been proposed [11]. To construct these sets one has to overcome the problem of adding and removing directions from the quadrature set, which for example cannot be done well in a Gauss-Legendre quadrature.

3.1.3 Spatial solution method and source iteration

The source term of the equation has two contributions, the external source and the scatter source. The left hand side of the dicrete ordinates discretized transport equation (Equation 3.1) is the transport operator. In the first iteration one considers only the external source and solves the transport problem. The obtained flux is the flux of all neutrons that have not scattered. The next iteration uses the scatter source obtained by substituting the not scattered flux in the scatter operator and solving the transport problem with this new source. The flux that is now obtained is the flux of all neutrons that have scattered once or not. This procedure can be formalized as

$$\left[\hat{\boldsymbol{\Omega}}_n \cdot \nabla + \sigma_t\right] \phi^{l+1}(\boldsymbol{r}, \hat{\boldsymbol{\Omega}}_n) = q^l(\boldsymbol{r}, \hat{\boldsymbol{\Omega}}_n) \tag{3.4}$$

where ϕ^{l+1} is the flux of $l+1$ times scattered neutrons and q^l is the source obtained from the l times scattered neutron flux, that is

$$q^l(\boldsymbol{r}, \hat{\boldsymbol{\Omega}}) = \frac{\sigma_s(\boldsymbol{r})}{4\pi} \int_{4\pi} \phi^l(\boldsymbol{r}, \hat{\boldsymbol{\Omega}}') d\hat{\boldsymbol{\Omega}}' + s(\boldsymbol{r}) \tag{3.5}$$

$$= \frac{\sigma_s(\boldsymbol{r})}{4\pi} \sum_{n=1}^{N} w_n \phi^l(\boldsymbol{r}, \hat{\boldsymbol{\Omega}}_n) + s(\boldsymbol{r}) \tag{3.6}$$

This source iteration procedure will converge quickly for absorbing problems, that is, problems where $\sigma_t >> \sigma_s$. For diffusive problems (σ_s is almost equal to σ_t) this will converge very slowly. In these cases it can be sped up by using Diffusion Synthetic Acceleration (DSA), which means another equation is to be solved in each iteration, which approximates the diffusive behavior of the equation.

When using source iteration, solving the transport part of the problem can be done by a 'sweeping' algorithm. Consider neutrons travelling in direction $\hat{\boldsymbol{\Omega}}_n$, they take information through space only in the direction of travel (downwind). Assume that we have discretized the spatial part of the problem by defining a grid, or elements, and solving each element separately from other elements. (This is discussed in the section about Discontinuous Galerkin 3.2.4). Now consider one spatial element, this element has upwind and downwind neighbours, upwind and downwind being defined by $\hat{\boldsymbol{\Omega}}_n$. This element can be solved when all inflowing information is already computed, that is, when the flux in the upwind elements is already computed. An ordering in

the elements (for direction $\hat{\mathbf{\Omega}}_n$) can then be determined. Solving the spatial part of the problem in this ordering ensures that elements are not computed before all upwind fluxes are computed [9]. An illustration of this algorithm can be found in Figure 3.1.3.

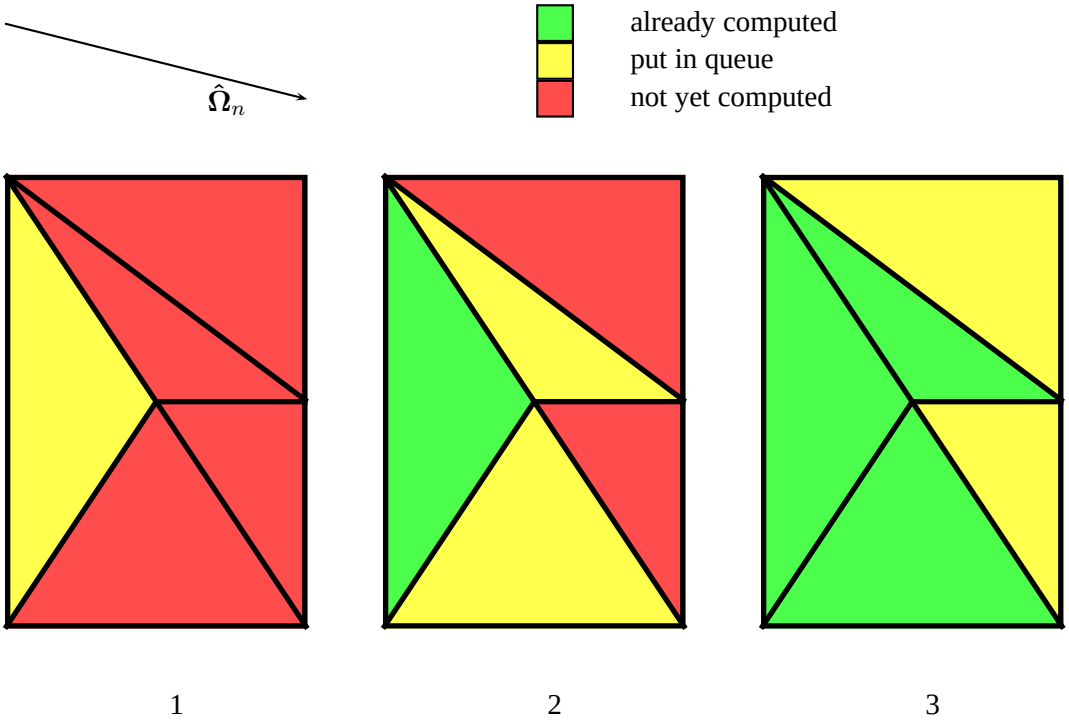

Figure 2: *Illustration of the sweeping algorithm. The rectangular domain is divided into triangular elements. The solution on an element can be computed (the element is 'swept') when all upwind neighbours are already updated. It takes three steps to compute all elements in this example. In each step the elements that can be computed are marked and put in a queue. Upwind neighbours of an element are determined by the direction* $\hat{\mathbf{\Omega}}_n$.

The discrete ordinates method provides an algorithm that can be implemented very cheaply, since only a finite number of directions (usually up to about 100) is considered and spatial discretization cost are not high when using the Discontinuous Galerkin method. The speed of the algorithm lies in the source iteration combined with so called 'sweeps' to solve the transport part of the problem.

3.2 Polynomials with discontinuous Galerkin

The Discontinuous Galerkin method is like a Galerkin method, but with discontinuous basis functions. The theory is almost identical to the regular Galerkin method which originated in the first half of the twentieth century. By using polymials on elements we can give a description of the angular flux on the whole sphere, not just on a discrete set of points like in the discrete ordinates method. The discrete ordinates method does not provide us with a description of the angular flux on the whole sphere, which could result in problems for geometries where specific directions are important. This is overcome by using a finite element method on the sphere.

3.2.1 Galerkin method

The Galerkin method basically requires that the equation is solved in its weak form. This weak form is solved by a function from a constrained space, i.e. the basis functions. Discontinuous Galerkin differs from regular Galerkin method in the choice of basis functions. As the name suggests the composite solution of the basis functions can be discontinuous. It can however only be discontinuous on element boundaries, not inside an element.

The weak formulation of an equation in general is

$$\text{find} \quad u \in V \quad \text{s.t.} \quad \forall v \in V: \quad B(u,v) = l(v) \tag{3.7}$$

where u is the solution to the differential equation. In the context of transport theory u would be the angular flux ϕ. Now we can apply the Galerkin discretization, which consists of putting a constraint on the space V, giving us the space V_h. This constraint could be that we take only polynomials on our chosen elements as functions in V_h. When allowing these functions to be discontinuous between elements we have the Discontinuous Galerkin method. This results in the following formulation

$$\text{find} \quad u_h \in V_h \quad \text{s.t.} \quad \forall v_h \in V_h: \quad B(u_h,v_h) = l(v_h) \tag{3.8}$$

Discretization by the Galerkin method results in an error that lies not in the chosen space V_h, this property is called the Galerkin orthogonality. Suppose we have an exact solution u and a Galerkin solution u_h. Since $V_h \subset V$ we can use v_h as a test function for the space V. Let the error be $\epsilon_h = u - u_h$. It then follows that

$$B(\epsilon_h, v_h) = B(u, v_h) - B(u_h, v_h) = l(v_h) - l(v_h) = 0 \tag{3.9}$$

which means the error lies outside the spaces or in other words the error depends on the choice of spaces.

Discontinuous Galerkin gives a better approximation than a Galerkin method with a continuous solution, even though non-physical discontinuities are introduced. When the grid on which the basis functions live is small enough the discontinuities will almost vanish.

3.2.2 Galerkin methods on the sphere

The Galerkin method uses functions defined on an element (basis function with compact support). In this report the word ‘element’ is used for spatial elements and the word ‘patch’ is used for angular elements. Patches on a sphere can be constructed in many ways, one of the easiest is by a projection from another body. Place such a body in the center of a sphere and let the extremities of the body exactly touch the sphere. Now each point on the sphere can be identified with a point on the body by drawing a line from the point on the sphere to the center of the sphere. The line will intersect the surface of the body, this is the point on the body with which the point on sphere is to be identified. This is illustrated in Figure 3.

The body used for the projection should preferably have some properties that help the adaptivity of the algorithm, in other words it must be possible to cut the patches into smaller patches while still keeping a smooth distribution of patches on the sphere. Examples for the bodies that can be used for this procedure are the octahedron and the hexahedron. Illustrations of the two bodies can be found in Figure 4. In these illustrations it is also shown how the patches can be cut into smaller patches. The mathematical derivation of the Galerkin method on the sphere can be found in Section 3.2.3, it makes use of the patch structure presented here.

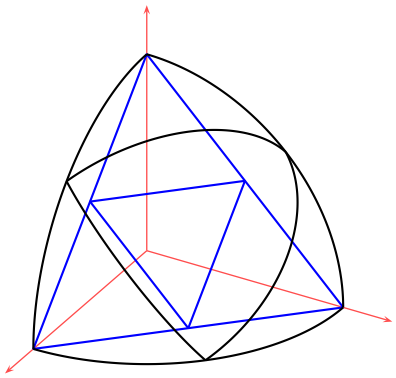

Figure 3: *The blue lines form an octant of the octahedron, which is divided into four smaller triangles, or patches. A projection of the octant to the sphere is made by drawing a line from the origin through the octahedron to the sphere. The points of intersection on the octahedron and sphere are then associated. The projection of the blue lines on the sphere is then the set of black lines, which define a patch structure on the sphere.*

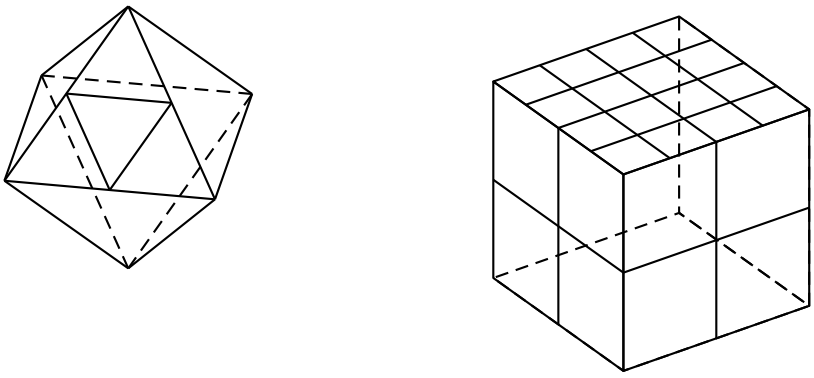

(a) Division of a octahedron (b) Division of a hexahedron

Figure 4: *Divisions of two bodies that can be mapped onto the sphere and have a flexible and hierarchical distribution of patches.*

3.2.3 Angular discretization

The simplified Boltzmann transport equations reads (Equation 2.2)

$$\hat{\mathbf{\Omega}} \cdot \nabla \phi + \sigma_t \phi = s + \frac{\sigma_s}{4\pi} \Phi \tag{3.10}$$

where $\hat{\mathbf{\Omega}}$ is the angular vector, ϕ is the angular flux and Φ is the scalar flux. Now we will apply the Galerkin method to this equation, therefore we first define the space V_h in which the solution will lie. This is done by splitting the angular flux in a spatial and an angular part. The spatial part $\phi_j(\boldsymbol{r})$ will be approximated by first order polynomials in this report, but can in principle be any polynomial. Analogously, the angular part will be approximated by zeroth order polynomials (constant functions) in this report, but can also be other polynomials. This can be formulated as the following sum

$$\phi(\boldsymbol{r}, \hat{\mathbf{\Omega}}) \approx \sum_{j=1}^{M} \phi_j(\boldsymbol{r}) G_j(\hat{\mathbf{\Omega}}) \tag{3.11}$$

where M is the number of patches in a spatial element, or on a spatial location. We can now multiply the equation from the left by an angular test function G_p in our space V_h. Then integrate over the whole angular domain to obtain

$$\int_{4\pi} G_p(\hat{\mathbf{\Omega}}) \left[(\hat{\mathbf{\Omega}} \cdot \nabla + \sigma_t) \sum_{j=1}^{M} \phi_j G_j - s - \frac{\sigma_s}{4\pi} \Phi \right] d\hat{\mathbf{\Omega}} = 0 \tag{3.12}$$

For the scalar flux Φ in this equation we can obtain the following expression, since the patch function G_j is unity on the patch and zero elsewhere.

$$\begin{aligned}
\Phi &= \int_{4\pi} \phi d\hat{\mathbf{\Omega}} && (3.13)\\
&= \int_{4\pi} \sum_{j=1}^{M} \phi_j G_j d\hat{\mathbf{\Omega}} && (3.14)\\
&= \sum_{j=1}^{M} \phi_j \int_{4\pi} G_j d\hat{\mathbf{\Omega}} && (3.15)\\
&= \sum_{j=1}^{M} \phi_j Area(G_j) && (3.16)
\end{aligned}$$

Let from now on ΔG_j denote the area of patch G_j. Please note that G_j is just an indicator of that patch, G_j is unity on the patch and zero outside the patch. The value of the flux on that patch is in the parameter ϕ_j.

Let us now work out the integral of Equation 3.12. Plug in the expression of the scalar flux to obtain

$$\int_{4\pi} G_p(\hat{\mathbf{\Omega}}) \left[\hat{\mathbf{\Omega}} \cdot \nabla \sum_{j=1}^{M} \phi_j G_j + \sigma_t \sum_{j=1}^{M} \phi_j G_j - s - \frac{\sigma_s}{4\pi} \sum_{j=1}^{M} \phi_j \Delta G_j \right] d\hat{\mathbf{\Omega}} = 0 \tag{3.17}$$

Now we can simplify the streaming term and distributing the integral over the terms, including over all the terms in the sums

$$\sum_{j=1}^{M} \int_{4\pi} G_p G_j \hat{\mathbf{\Omega}} \cdot \nabla \phi_j d\hat{\mathbf{\Omega}} + \sigma_t \sum_{j=1}^{M} \int_{4\pi} \phi_j G_p G_j d\hat{\mathbf{\Omega}} - \frac{\sigma_s}{4\pi} \int_{4\pi} G_p d\hat{\mathbf{\Omega}} \sum_{j=1}^{M} \phi_j \Delta G_j - \int_{4\pi} G_p s d\hat{\mathbf{\Omega}} = 0 \quad (3.18)$$

Since the patches all have compact support we know that

$$\sum_{j=1}^{M} \phi_j \int_{4\pi} G_p G_j d\hat{\mathbf{\Omega}} = \phi_p \Delta G_p \quad (3.19)$$

Using this we get the following expression

$$\int_{\Delta G_p} \hat{\mathbf{\Omega}} \cdot \nabla \phi_p d\hat{\mathbf{\Omega}} + \sigma_t \phi_p \Delta G_p - \frac{\sigma_s}{4\pi} \Delta G_p \sum_{j=1}^{M} \Delta G_j \phi_j - \int_{4\pi} G_p s d\hat{\mathbf{\Omega}} = 0 \quad (3.20)$$

This equation can be written more compactly as follows

$$\hat{\mathbf{\Omega}}_p' \cdot \nabla \phi_p + \sigma_t \phi_p = \frac{\sigma_s}{4\pi} \Phi + s_p \quad (3.21)$$

In this equation we have:

$$\hat{\mathbf{\Omega}}_p' = \frac{1}{\Delta G_p} \int_{\Delta G_p} \hat{\mathbf{\Omega}} d\hat{\mathbf{\Omega}} \quad (3.22)$$

$$\Phi = \sum_{j=1}^{M} \Delta G_j \phi_j \quad (3.23)$$

$$= \sum_{j=1}^{M} w_j \phi_j \quad (3.24)$$

$$s_p = \frac{1}{\Delta G_p} \int_{4\pi} G_p s d\hat{\mathbf{\Omega}} \quad (3.25)$$

Note that this equation looks very similar to the Discrete Ordinates discretized equation. There are two differences with the Discrete Ordinates description, firstly the directions $\hat{\mathbf{\Omega}}_p'$ are defined differently. They follow from the patch structure, which also means the length of $\hat{\mathbf{\Omega}}_p'$ is not necessarily equal to unity. The other difference is that there is no freedom in chosing the quadrature, the sum describing the scalar flux follows naturally from the discretization procedure.

3.2.4 Spatial discretization

Several researches have been done on the spatial discretization with Discontinuous Galerkin in the field of neutron transport. This report does not focus on the behavior of the spatial part of the transport equation, but on the angular part. For more on the spatial properties of Discontinuous Galerkin see [13] [14].

We start with the equation we obtained in the previous section:

$$\hat{\mathbf{\Omega}}_p' \cdot \nabla \phi_p + \sigma_t \phi_p = \frac{\sigma_s}{4\pi} \Phi + s_p \quad (3.26)$$

In the spatial part of the problem we use linear basis functions. The spatial domain is cut up into elements and each element has basis functions linear in the Cartesian coordinates. From these basis functions we can define the total solution as a sum of the basis functions. The sums can be written as

$$\phi_p(\boldsymbol{r}) \approx \boldsymbol{\Theta}^T(\boldsymbol{r})\boldsymbol{\phi}_p \tag{3.27}$$

$$\Phi(\boldsymbol{r}) \approx \boldsymbol{\Theta}^T(\boldsymbol{r})\boldsymbol{\Phi} \tag{3.28}$$

where the vector $\boldsymbol{\phi}$ holds the angular flux values associated with the basis functions, in the same way $\boldsymbol{\Phi}$ holds the scalar flux values. $\boldsymbol{\Theta}$ holds the basis functions, that is, each γ_n is a linear function on the spatial element. Suppose we have K spatial elements, then depending on the dimension of the problem (1, 2 or 3) P_K basis functions are needed to span our space.

$$\boldsymbol{\Theta} = [\gamma_1(\boldsymbol{r}), ..., \gamma_{P_K}(\boldsymbol{r})]^T \tag{3.29}$$

$$\boldsymbol{\phi}_p = [\phi_{1,j}, ..., \phi_{P_K,p}]^T \tag{3.30}$$

$$\boldsymbol{\Phi} = [\Phi_1, ..., \Phi_{P_K}]^T \tag{3.31}$$

We can now apply the Galerkin discretization by multiplying with a test function $\boldsymbol{\Theta}$ and integrating over the spatial domain. Using the divergence theorem to rewrite the streaming term we obtain

$$\int_{\delta V_e} \hat{\boldsymbol{\Omega}}_p' \cdot \hat{\boldsymbol{n}} \Theta_e \sum_{k=1}^{P_K} \phi_{k,p}^b(\boldsymbol{r}) d\delta V - \int_{V_e} (\hat{\boldsymbol{\Omega}}_p' \nabla \cdot \sum_{k=1}^{P_K} \Theta_k) \Theta_e \phi_{k,p} dV + \int_{V_e} \Theta_e \sum_{k=1}^{P_K} \left[\sigma_t \Theta_k \phi_{k,p} - \frac{\sigma_s}{4\pi} \Theta_k \phi_{k,p} - s_p(\boldsymbol{r}) \right] dV = 0 \tag{3.32}$$

In this equation $\phi_{e,j}^b$ is the angular flux at the boundary of a cell. Now we will assign to each element face its angular flux, e is the element index, f is the element face index. To do this we need to compose the total element boundary out of the individual element faces. Each of those individual faces is a plane or line, in order to be able to define an outward normal vector. This gives us the following expression

$$\delta V_e = \sum_{l=1}^{N_{faces}} \delta V_{e,l} \tag{3.33}$$

The flux on this boundary is chosen to be the upwind flux. This means we have to make a distinction between directions as

$$\phi_{e,p,l}^b = \begin{cases} \phi_{e,p} & \text{if} \quad \hat{\boldsymbol{\Omega}}_p' \cdot \hat{\boldsymbol{n}}_l > 0 \\ \phi_{e,p}^{\text{upwind in } l} & \text{if} \quad \hat{\boldsymbol{\Omega}}_p' \cdot \hat{\boldsymbol{n}}_l < 0 \end{cases} \tag{3.34}$$

Plugging this into the equation we arrive at a matrix equation that has the final discretized form. The matrices are square and have the size of the number of basis functions that are in one spatial element. The matrix equation that is to be solved for each patch on each element is then

$$\sum_{l=1}^{N_{faces}} \Omega_p' \boldsymbol{U}_{e,p,l} \boldsymbol{\phi}_{e,p,l}^b + (-\Omega_p' \boldsymbol{K}_e + \sigma_t \boldsymbol{M}_e) \boldsymbol{\phi}_{e,p} = \frac{\sigma_s}{4\pi} \boldsymbol{M}_e \boldsymbol{\Phi}_e + \boldsymbol{s}_{e,p} \tag{3.35}$$

where

$$\boldsymbol{U}_{e,p,l} = \int_{\delta V_{e,l}} n_l \boldsymbol{\Theta}_e \boldsymbol{\Theta}_e^T d\delta V \tag{3.36}$$

$$\boldsymbol{K}_e = \int_{V_e} (\nabla \boldsymbol{\Theta}_e) \boldsymbol{\Theta}_e^T dV \tag{3.37}$$

$$\boldsymbol{M}_e = \int_{V_e} \boldsymbol{\Theta}_e \boldsymbol{\Theta}_e^T dV \tag{3.38}$$

$$\boldsymbol{s}_{e,p} = \int_{V_e} \boldsymbol{\Theta}_e s_p(\boldsymbol{r}) dV \tag{3.39}$$

$$= \int_{V_e} \int_{4\pi} \boldsymbol{\Theta}_e G_p s(\boldsymbol{r}, \hat{\boldsymbol{\Omega}}) d\hat{\boldsymbol{\Omega}} dV \tag{3.40}$$

3.2.5 Continuity relations between spatial elements

Two neighbouring elements do not necessarily have the same angular distribution of patches. There are two cases that can be discerned, (a) neutrons flowing from a coarse to a fine element and (b) from a fine to a coarse element. In general neutron conservation for neutrons crossing a plane can be formulated as

$$\int_{\hat{\boldsymbol{\Omega}} \cdot \hat{\boldsymbol{n}}^{\text{upwind}} < 0} \hat{\boldsymbol{\Omega}} \cdot \hat{\boldsymbol{n}}^{\text{upwind}} \phi^{\text{upwind}}(\hat{\boldsymbol{\Omega}}) d\hat{\boldsymbol{\Omega}} = \int_{\hat{\boldsymbol{\Omega}} \cdot \hat{\boldsymbol{n}}^{\text{downwind}} > 0} \hat{\boldsymbol{\Omega}} \cdot \hat{\boldsymbol{n}}^{\text{downwind}} \phi^{\text{downwind}}(\hat{\boldsymbol{\Omega}}) d\hat{\boldsymbol{\Omega}} \tag{3.41}$$

[12]. In this equation ϕ^{upwind} is the flux in the upwind element and ϕ^{downwind} is the flux in the downwind element. Similar notation is used for the outward normal vectors $\hat{\boldsymbol{n}}$.This condition should be met in all points $\boldsymbol{r}$ along the boundary of the two elements, as this insures continuity of the neutron current. When the patches on the sphere are constant this will result in some simple continuity relations, they are derived here.

(a) Streaming from coarse to fine element

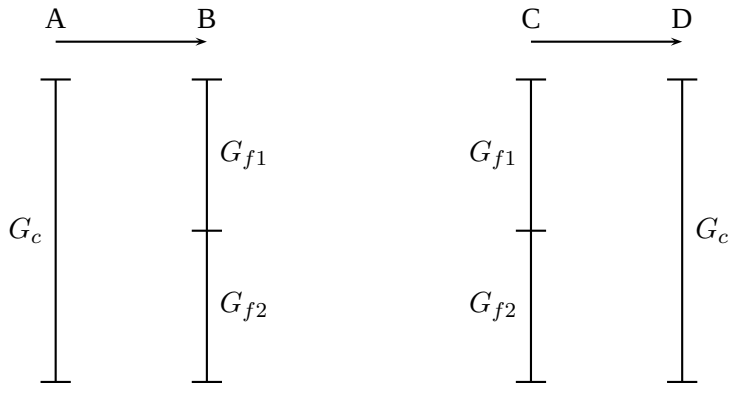

(a) Coarse to fine (b) Fine to coarse

Figure 5: *Two cases of different angular distribution of patches in neighbouring elements. To ensure neutron conservation relations between the discrete patches need to be derived.*

Take two elements A and B and consider the angles such that neutrons flow from A to B. Suppose element A has one patch G_c and element B has two patches G_{f1} and G_{f1}, this is illustrated in Figure 5(a). The continuity relation in Equation 3.41 can be expressed as follows

$$\int_{\Delta G_c} \hat{\boldsymbol{n}} \cdot \hat{\boldsymbol{\Omega}} \phi(\hat{\boldsymbol{\Omega}}) d\hat{\boldsymbol{\Omega}} = \int_{\Delta G_{f1}} \hat{\boldsymbol{n}} \cdot \hat{\boldsymbol{\Omega}} \phi(\hat{\boldsymbol{\Omega}}) d\hat{\boldsymbol{\Omega}} + \int_{\Delta G_{f2}} \hat{\boldsymbol{n}} \cdot \hat{\boldsymbol{\Omega}} \phi(\hat{\boldsymbol{\Omega}}) d\hat{\boldsymbol{\Omega}} \tag{3.42}$$

$$\int_{\Delta G_c} \hat{\boldsymbol{n}} \cdot \hat{\boldsymbol{\Omega}} \phi_c G_c d\hat{\boldsymbol{\Omega}} = \int_{\Delta G_{f1}} \hat{\boldsymbol{n}} \cdot \hat{\boldsymbol{\Omega}} \phi_{f1} G_{f1} d\hat{\boldsymbol{\Omega}} + \int_{\Delta G_{f2}} \hat{\boldsymbol{n}} \cdot \hat{\boldsymbol{\Omega}} \phi_{f2} G_{f2} d\hat{\boldsymbol{\Omega}} \tag{3.43}$$

$$\phi_c \int_{\Delta G_c} \hat{\boldsymbol{n}} \cdot \hat{\boldsymbol{\Omega}} d\hat{\boldsymbol{\Omega}} = \phi_{f1} \int_{\Delta G_{f1}} \hat{\boldsymbol{n}} \cdot \hat{\boldsymbol{\Omega}} d\hat{\boldsymbol{\Omega}} + \phi_{f2} \int_{\Delta G_{f2}} \hat{\boldsymbol{n}} \cdot \hat{\boldsymbol{\Omega}} d\hat{\boldsymbol{\Omega}} \tag{3.44}$$

Since the union of the support of patches G_f1 and G_f2 is equal to the support of G_c ($G_f1 \bigcup G_f2 = G_c$) we can simplify this to

$$\phi_c \int_{\Delta G_c} \hat{\boldsymbol{n}} \cdot \hat{\boldsymbol{\Omega}} d\hat{\boldsymbol{\Omega}} = \phi_{f1} \left[\int_{\Delta G_{f1}} \hat{\boldsymbol{n}} \cdot \hat{\boldsymbol{\Omega}} d\hat{\boldsymbol{\Omega}} + \int_{\Delta G_{f2}} \hat{\boldsymbol{n}} \cdot \hat{\boldsymbol{\Omega}} d\hat{\boldsymbol{\Omega}} \right] \tag{3.45}$$

$$\phi_c \int_{\Delta G_c} \hat{\boldsymbol{n}} \cdot \hat{\boldsymbol{\Omega}} d\hat{\boldsymbol{\Omega}} = \phi_{f1} \int_{\Delta G_{f1} \bigcup \Delta G_{f2}} \hat{\boldsymbol{n}} \cdot \hat{\boldsymbol{\Omega}} d\hat{\boldsymbol{\Omega}} \tag{3.46}$$

$$\phi_c = \phi_{f1} \tag{3.47}$$

by assuming that $\phi_{f1} = \phi_{f2}$. It is natural to assume this, as the two patches G_{f1} and G_{f2} are equally as important. This result is also what one intuitively would expect. Even though the downwind element B can handle a more accurate solution of the flux, that information is not available. So the two patches G_{f1} and G_{f2} will represent the exact same angular flux as in the upwind element.

(b) Streaming from fine to coarse element

Now suppose we have refined element C and a coarser element D. On C we have two patches, G_{f1} and G_{f2}, and on element D there is only one patch G_c. This is illustrated in Figure 5(b). We will use the same continuity condition as for the former case, which can be found in Equation 3.41. Applying this condition yields

$$\int_{\Delta G_c} \hat{\boldsymbol{n}} \cdot \hat{\boldsymbol{\Omega}} \phi_c d\hat{\boldsymbol{\Omega}} = \int_{\Delta G_{f1}} \hat{\boldsymbol{n}} \cdot \hat{\boldsymbol{\Omega}} \phi_{f1} d\hat{\boldsymbol{\Omega}} + \int_{\Delta G_{f2}} \hat{\boldsymbol{n}} \cdot \hat{\boldsymbol{\Omega}} \phi_{f2} d\hat{\boldsymbol{\Omega}} \tag{3.48}$$

$$\phi_c \int_{\Delta G_c} \hat{\boldsymbol{n}} \cdot \hat{\boldsymbol{\Omega}} d\hat{\boldsymbol{\Omega}} = \phi_{f1} \int_{\Delta G_{f1}} \hat{\boldsymbol{n}} \cdot \hat{\boldsymbol{\Omega}} d\hat{\boldsymbol{\Omega}} + \phi_{f2} \int_{\Delta G_{f2}} \hat{\boldsymbol{n}} \cdot \hat{\boldsymbol{\Omega}} d\hat{\boldsymbol{\Omega}} \tag{3.49}$$

Note that since ϕ is constant on a patch we can pull out this variable. Rewriting this equation brings us to the final expression

$$\phi_c = \frac{\phi_{f1} \int_{\Delta G_{f1}} \hat{\boldsymbol{n}} \cdot \hat{\boldsymbol{\Omega}} d\hat{\boldsymbol{\Omega}} + \phi_{f2} \int_{\Delta G_{f2}} \hat{\boldsymbol{n}} \cdot \hat{\boldsymbol{\Omega}} d\hat{\boldsymbol{\Omega}}}{\int_{\Delta G_c} \hat{\boldsymbol{n}} \cdot \hat{\boldsymbol{\Omega}} d\hat{\boldsymbol{\Omega}}} \tag{3.50}$$

This result can be interpreted as a weighted sum of the current through the two refined patches G_{f1} and G_{f2}, which will be clear after rewriting the equation as follows

$$\phi_c = \frac{\phi_{f1}\hat{\boldsymbol{n}} \cdot \int_{\Delta G_{f1}} \hat{\boldsymbol{\Omega}} d\hat{\boldsymbol{\Omega}} + \phi_{f2}\hat{\boldsymbol{n}} \cdot \int_{\Delta G_{f2}} \hat{\boldsymbol{\Omega}} d\hat{\boldsymbol{\Omega}}}{\hat{\boldsymbol{n}} \cdot \int_{\Delta G_c} \hat{\boldsymbol{\Omega}} d\hat{\boldsymbol{\Omega}}} \tag{3.51}$$

$$= \frac{\phi_{f1}\Delta G_{f1}\hat{\boldsymbol{n}} \cdot \hat{\boldsymbol{\Omega}}'_d + \phi_{f2}\Delta G_{f2}\hat{\boldsymbol{n}} \cdot \hat{\boldsymbol{\Omega}}'_e}{\Delta G_c \hat{\boldsymbol{n}} \cdot \hat{\boldsymbol{\Omega}}'_f} \tag{3.52}$$

The sum of the fluxes ϕ_{f1} and ϕ_{f2} is weighted by the patch size and component of the average direction in the outward normal of the element. Please note that by Equation 3.22 we have $\Delta G_c \hat{\boldsymbol{\Omega}}'_f = \Delta G_{f1}\hat{\boldsymbol{\Omega}}'_d + \Delta G_{f2}\hat{\boldsymbol{\Omega}}'_e$.

3.2.6 Spatial solution methods in discontinuous Galerkin

The source iteration of the equation, which is described for Discrete Ordinates in Section 3.1.3, can still be applied when the angular part of the equation is discretized using Discontinuous Galerkin. The transport part of the equation (left hand side) and the source and scatter part of the equation (right hand side) can be computed sequentially in each iteration, with the newest available information.

In Section 3.1.3 the sweeping algorithm is also described. This is an algorithm used for solving the transport part of the problem. The idea of the algorithm is that all upwind neighbours of an element must have been updated before the element itself can be updated. There are two ways of applying this in the Discontinuous Galerkin method.

First is the easily implemented, but less accurate method. At the start of the algorithm there is a certain distribution of patches on the sphere. These patches have their average direction, which can be used to determine an ordering in the elements for neutrons travelling in the direction of that patch. This ordering is determined only at the beginning and is then used throughout the algorithm. When refinement would take place there is no update to the ordering. Using this method it could happen that not all upwind patches are updated before the fluxes are used for the downwind element update.

The other method consists of counting all upwind dependencies of all patches, in other words counting the patches that stream in to a patch. When a patch is updated the dependency to the patch it streams in to can be removed. One can then use the criterion that when no more upwind dependencies are left the patch is ready to be updated. It is not yet clear whether this algorithm can get stuck, by a ring of dependencies (or how to prevent this).

3.3 Wavelets

The first theories on specific wavelets date from the early twentieth century by Alfréd Haar, although the concept of a general wavelet was developed much later. In the nineteen seventies and eighties much progress has been made in constructing more families of wavelets. Since then wavelets have been used in a number of fields of research. Its main application is in storing and processing image and sound data.

3.3.1 Mathematics of wavelets

A family of wavelets (in multiresolution analysis) consists of a mother wavelet, which is a function with some special properties, and all its descendants. In this section we will illustrate everything in the one dimensional

case. The mother wavelet Ψ has to fulfil the following requirements:

$$\int_{-\infty}^{+\infty} \Psi(t)dt = 0 \tag{3.53}$$

$$\int_{-\infty}^{+\infty} |\Psi(t)|^2 dt = 1 \tag{3.54}$$

furthermore it is a function in $L^2(\mathbb{R})$.

All translations by integer increments of this mother wavelet form the set V_0. In the same way dilatation of the mother wavelet with 2^j and taking all translations form the set V_j. These sets V_j, with $j = ..., -1, 0, 1, ...$, are ordered by inclusion and the closure of the infinite inclusion spans up the whole space $L^2(\mathbb{R})$.

$$... \subset V_2 \subset V_1 \subset V_0 \subset V_{-1} \subset V_{-2} \subset ... \subset L^2(\mathbb{R}) \tag{3.55}$$

Also the infinite intersection is the zero function. These properties are needed to use these functions as a one-to-one representation of a function $f \in L^2(\mathbb{R})$. In other words we can represent f by a set of coefficients c_{jk}, which belong to the wavelet $\Psi_{jk}(t) = 2^{-j/2}\Psi(\frac{t}{2^j} - k)$. Various algorithms that use these properties to efficiently store and process image and sound data are in use. Similarly, this can be used to give a description of the angular flux ϕ in the transport equation. More information on wavelets and multiresolution analysis can be found in [2] [5] [10].

3.3.2 Wavelets in neutron transport

There are two ways to implement wavelets in neutron transport theory. The first is by defining spherical wavelets and applying the multiresolution analysis as described above. This is more involved than a multiresolution analysis in carthesian coordinates. This report will not explain such a multiresolution analysis in depth, as it is not practical to implement in a production code. A lot of computational power is spent on determining the coefficients of wavelets that are not needed to get an accurate solution. The full multiresolution analysis is not needed to obtain an accurate solution.

The other method uses patches on the sphere, in the same way as the discontinuous Galerkin method uses patches, see Section 3.2. Defining a tesselation of the sphere into patches one can define wavelets on the patches. Each vertex of the tesselation is the center point of a wavelet, which is identical (neglecting rotation) in each patch. An illustration of such a wavelet can be found in Figure 6.

The wavelets are the basis functions with which the transport equation is solved, by cutting the patches into smaller patches the solution will become more accurate. However all wavelets remain necessary to describe the angular flux, once a patch is refined it does not mean the associated wavelet can be neglected [3]. Other wavelets can also be used to discretize the angular component of the transport equation, for example Daubechies' wavelets [4].

In the end, the algorithm one obtains is a Finite Element method that uses wavelets as basis functions. This means the angular flux ϕ can be written as

$$\phi(\boldsymbol{r}, \hat{\boldsymbol{\Omega}}) = \sum_{n=1}^{N} W_n \Psi_n(\boldsymbol{r}, \hat{\boldsymbol{\Omega}}_n) \tag{3.56}$$

where the Ψ_n is a certain wavelet on the sphere. Plugging this expression in the transport equation and following the Galerkin discretization procedure yields the wavelet discretized transport equation. This is just an angular discretization, the wavelet method still needs to be combined with a spatial discretization. The discontinuous Galerkin method could also be used for the spatial discretization.

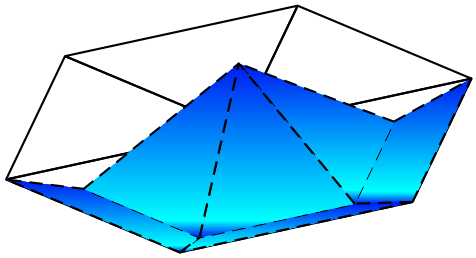

Figure 6: *Spherical wavelet defined on patches, each vertex is the center of such a wavelet. The patches show on the far side.*

3.3.3 Cost of wavelet algorithm

Since wavelets are not independent of each other the matrices in the discretized transport equation become rather large. In fact, say the number of wavelets is N and the number of spatial basis functions in an element is M, then the matrices will be $NM \times NM$.

To illustrate the sparseness of the matrices we will show the most sparse matrices that are used in the wavelets method [3]. These matrices consist of the entries (Ω_i is a component of $\hat{\mathbf{\Omega}}$, with $i = x, y, z$)

$$a_{ij} = \int_{4\pi} \Omega_i G_i(\hat{\mathbf{\Omega}}) G_j(\hat{\mathbf{\Omega}}) d\hat{\mathbf{\Omega}} \tag{3.57}$$

For this example the octahedron is used as body to determine the patch distribution. In this example it is assumed the octants are independent of each other, so in the fully dependent case the matrices would be less sparse. A schematic overview of the refinement used can be found in Figure 7. There are three large wavelets, on the red nodes. There are also three first order wavelets, the green nodes represent those wavelets. Furthermore there are nine second order wavelets and seven third order wavelets, respectively the blue and the yellow nodes. The fill of the matrix with the entries in Equation 3.57 is showed in Figure 8. The matrix is not at all sparse, therefore solving and storing it will not be very efficient and practical.

Besides the problems with large matrices the sweeping algorithm is difficult to implement in the wavelet method (see Section 3.1.3 for the sweeping and source iteration algorithm). The interdepency of the wavelets also troubles application of the sweep method. All wavelets in an element must be solved at the same time, because of the interdependency. This means an ordering for a specific direction cannot be made, i.e. elements of which the upwind flux are not yet determined must sometimes be computed. This means a lot more computational power will go into solving the transport part of the problem. However, the source iteration algorithm can in principle be applied.

3.4 Comparison of three discretization methods

The remainder of this research focusses on one of the three methods described above. The goal is to make an angular adaptive algorithm. Of the three methods, the most suitable for this end is the Discontinuous Galerkin

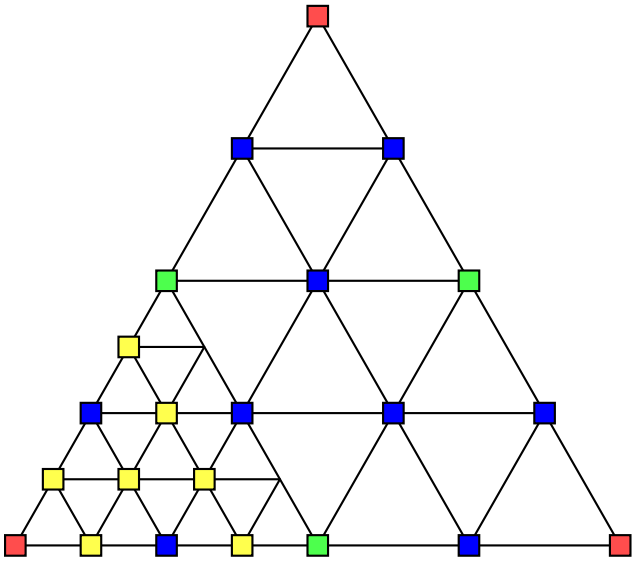

Figure 7: *Wavelets used in the example of the sparseness of the matrices in the wavelets method. Every coloured square is the location of the peak of a wavelet, so every square can be associated with the coefficient the needs to be computed.*

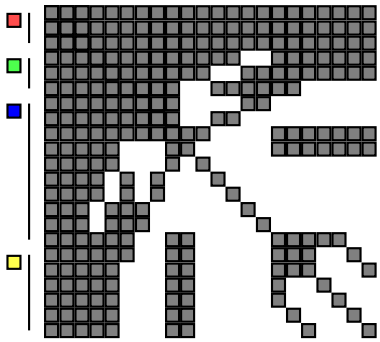

Figure 8: *The matrix with only angular variables that needs to be solved when using the wavelet method. Gray squares indicate a non-zero entry.*

method. Table 1 shows in short the advantages and disadvantages of the methods. A more detailed discussion can be found below.

Discrete Ordinates Discrete Ordinates has been widely used because it is a very cheap algorithm. Only a relatively small number of angular variables is used and the source iteration combined with sweeping algorithms make it very fast. The lack of difficult integrals that need to be computed also contribute to the speed of the algorithm.

There still is a choice of the quadrature set that is used to approximate the scalar flux. In terms of speed it does not matter much which quadrature is used, as this is determined by the number of directions.The accuracy, however, can be greatly improved by using an appropriate quadrature. Active research is still being done in

	S_N	DG	Wavelet
Hierarchical	-	+	+
Flexible basis functions	+	+	0
Storage	+	0	-
Computational cost	+	0	-
Easy to refine	-	+	0
1D cost	+	+	+
3D cost	+	0	-
Pencil beams	-	+	+
Overall	0	+	-

Table 1: *Short overview of the advantages and disadvantages of the three methods.*

this area. However there are not many quadrature sets that allow local refinement. When one wants to refine a certain direction in most sets all directions and weights will be changed. So this method is quick for one calculation, but does not allow for local refinement well.

Another problem, related to the difficulty of refining, are the so called ray effects. When the directions are not chosen properly rays may occur in the solution that are not physical. This is due to an insufficient angular resolution in absorption dominated problems.

Discontinuous Galerkin The Discontinuous Galerkin method is a relatively cheap method, albeit a little more expensive than the Discrete Ordinates method. It is, actually, as cheap as S_N when using constant basis functions on the patches. For higher order basis functions an extra matrix equation needs to be solved.

Local angular refinement is very easy to perform and has little consequences on the cost, in comparison with the Wavelets method. The sweeping algorithm will still work, which makes this method not much more expensive than Discrete Ordinates.

The scalar flux in this method is also approximated with some kind of quadrature. However, it cannot be arbitrarily specified. This quadrature follows naturally from the discretization procedure. It depends on the order of the basis functions that are used on the patches.

Spatial adaptivity can be easily combined with this method, as both the spatial and angular parts of the problem are discretized using the same procedure. One could say that the whole ‘phase space’ of the spatial and angular parts combined is discretized by that procedure.

Wavelets Wavelets naturally have a hierarchical structure, that is the way they are constructed. This can be easily used for refinement, however it also introduces equations with large matrices that are not sparse. Therefore the wavelets method is expensive both in computational power and storage.

The method does provide accurate results, in the same way as Discontinuous Galerkin does. In quality of the solution wavelets are to be preferred over Discrete Ordinate.

Another problem is the sweeping algorithm, since wavelets have overlapping support. This means all angular variables must be computed at the same time, by solving an equation with large matrices. Therefore one cannot make an ordering of the spatial elements such that elements are only updated when all upwind elements are already updated.

3.4.1 Similarity of the three methods

In certain conditions the three methods have a striking similarity, in fact they are almost the same. When using constant basis functions on patches in Discontinuous Galerkin and Haar wavelets in the wavelets method, all three methods have constant basis functions in the angular part of the problem.

Discontinuous Galerkin with constant patches can have patches with an average direction which length is not equal to unity, while the Discrete Ordinates method always has unit length directions. However they can point in the same direction, when also the quadrature in Discrete Ordinates is chosen with weights equal to the surface area of the patch, the methods are almost the same.

The wavelets method still has the dependency between wavelets on the sphere. This results in more computational cost in this method. However the space of function in which the solution lives is the same as the space of the constant basis functions in Discontinuous Galerkin, provided the same distribution of patches is used.

Still Discontinuous Galerkin is to be preferred. This method is the most flexible (in choice of basis functions), most accurate (in three dimensions it is likely more accurate than Discrete Ordinates and as accurate as Wavelets) and is the simplest method to implement when compared to the Wavelets method. Therefore the remainder of this report is on the Discontinuous Galerkin method.

4 Formulation of One-Dimensional Problem

The research presented in this report focusses on one-dimensional problems. With only one spatial dimension the transport equation is simplified and the code of the algorithm is less complex. The behaviour of the method, however, does not change.

To get to the one dimensional problem we assume the geometry to be homogeneous in two dimensions, say in x and y. The only variation in material properties are in the z direction. A consequence of this is that the solution of the transport equation is constant in the x and y directions. So we can discard these components of the equation. We can write the three-dimensional transport equation as

$$\Omega_x \frac{\partial \phi}{\partial x} + \Omega_z \frac{\partial \phi}{\partial z} + \Omega_z \frac{\partial \phi}{\partial z} + \sigma_t \phi = \frac{\sigma_s}{4\pi} \Phi + s \tag{4.1}$$

where the streaming term is expanded. The assumption of homogeneity described above can be formulated as setting $\Omega_x \frac{\partial \phi}{\partial x}$ and $\Omega_y \frac{\partial \phi}{\partial y}$ equal to zero. Usually the z direction is taken to be the non homogeneous direction, as this results in the easiest component of the directions vector: $\Omega_z = \mu$. The transport equation then becomes

$$\mu \frac{\partial \phi}{\partial z} + \sigma_t \phi = \frac{\sigma_s}{4\pi} \Phi + s \tag{4.2}$$

The other terms in the equation do not change due to this assumption. They are invariant along the x and y directions.

First the patch distribution for the one dimensional case is discussed, which is different from the general three dimensional case. After that an overview of the non-adaptive algorithm used in this report is presented. This section concludes with the data structure used for storing the patch structure and the solution.

4.1 Patch structure in one dimension

In the one dimensional case we only need to look at the dependence in the polar angle, so we can write the problem in terms of μ. The azimuthal angle ω can be integrated out due to the symmetry in the x and y directions. This is easily done since the value of the angular flux will not change when ω is running. Let μ run from -1 to 1 and ω from 0 to 2π. The scalar flux can be computed by

$$\begin{aligned} \Phi &= \int_{4\pi} \phi d\hat{\mathbf{\Omega}} && (4.3) \\ &= \int_{-1}^{1} \int_{0}^{2\pi} \phi d\omega d\mu && (4.4) \\ &= 2\pi \int_{-1}^{1} \phi d\mu && (4.5) \end{aligned}$$

Another consequence of integrating out the ω dependence is that we can create patches with a ring shape, since the flux only varies along the polar angle μ. This patch structure is illustrated in Figure 4.1. A good choice for the division of μ is to have no patches that are exactly centered around $\mu = 0$, which is then also the average direction. This means the average direction of this patch does not have any component in the z direction, so it has no influence on the one dimensional transport equation.

The coarsest patch distribution used in this report consists of two patches: $\mu \in [-1, 0]$ and $\mu \in [0, 1]$. Every time a patch is refined, μ is divided into two equal parts. This is shown in Figure 4.1.

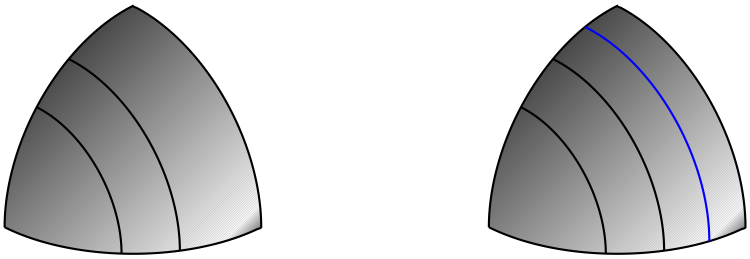

Coarse patches. *Refined patches.*

Figure 9: *Ring shaped patch structure in the one dimensional transport equation. There is always a patch boundary at $\mu = 0$. When a patch is refined the ring is divided into two rings with equal length intervals in μ.*

4.2 Discretization of one-dimensional equation

Each spatial cell is simple, since it is only a line segment. Each cell has two faces, left and right, at which the solution can be discontinuous. The basis functions are first order polynomials, or linear functions. In general in this report the word 'element' is used to denote the spatial cells used with the discontinuous Galerkin method, while the word 'patch' is used for the angular cells. An element has two basis functions and lives between the left most and right most x values of the element:

$$\gamma_1 = \begin{cases} 0 & x < x_{left} \\ \frac{x_{right}-x}{x_{right}-x_{left}} & x_{left} < x < x_{right} \\ 0 & x_{right} < x \end{cases} \tag{4.6}$$

$$\gamma_2 = \begin{cases} 0 & x < x_{left} \\ \frac{x-x_{left}}{x_{right}-x_{left}} & x_{left} < x < x_{right} \\ 0 & x_{right} < x \end{cases} \tag{4.7}$$

This is illustrated in Figure 10.

The transport equation 3.21 becomes:

$$\left[\mu_p' \hat{\boldsymbol{n}}_z \boldsymbol{M} \boldsymbol{\phi}_p\right]_{left} + \left[\mu_p' \hat{\boldsymbol{n}}_z \boldsymbol{M} \boldsymbol{\phi}_p\right]_{right} + (-\mu_p' \boldsymbol{K} + \sigma_t \boldsymbol{M})\boldsymbol{\phi}_p = \frac{\sigma_s}{4\pi} \boldsymbol{M} \boldsymbol{\Phi} + \boldsymbol{S}_p \tag{4.8}$$

where

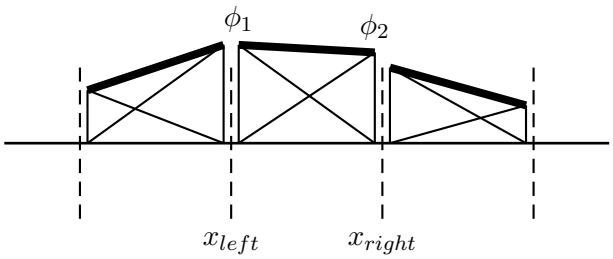

Figure 10: *Illustration of the basis functions used in the one dimensional problem. Cell boundaries are dashed, basis functions multiplied with their coefficient are thin lines and the solution is the thick line.*

$$\mu'_p = 2\pi \int_{\Delta G_p} \frac{\mu \sin(\cos^{-1}(\mu))}{\Delta G_p} d\mu \tag{4.9}$$

$$\boldsymbol{\Phi} = \sum_{j=1}^{M} \Delta G_j \boldsymbol{\phi}_j = \sum_{j=1}^{M} w_j \boldsymbol{\phi}_j \tag{4.10}$$

$$\boldsymbol{K} = \int_{V_e} \frac{\partial \boldsymbol{\Theta}}{\partial z} \boldsymbol{\Theta}^T dV \tag{4.11}$$

$$\boldsymbol{M} = \int_{V_e} \boldsymbol{\Theta}\boldsymbol{\Theta}^T dV \tag{4.12}$$

$$s(z) = 2\pi \int_{-1}^{1} G_p s(z,\mu) \sin(\cos^{-1}(\mu)) d\mu \tag{4.13}$$

$$\boldsymbol{S}_p = \int_{V_m} \boldsymbol{\Theta} s(z) dV \tag{4.14}$$

4.3 Overview of algorithm

A schematic overview of the algorithm is given in Figure 11. Once the algorithm is started we arrive at the initialization of the finite element matrices (Set up FEM). These matrices are defined in equations 4.9 through 4.14. In this stage all necessary arrays for storing material properties and flux values are allocated. In the next section the data structure used for storage of the flux values is described. By allocating these arrays one chooses the patch distribution that will be used throughout the algorithm.

The next stage is updating the source, which, in the first iteration, is only computing the external source. We then perform the first sweep, solving for all angular fluxes throughout the domain. A transport sweep consists two sweeps, one left going and one right going. The order does not matter, as long as Dirichlet boundary conditions are used. In this stage the matrices defined in the set up are used. After the sweep we arrive at 'Update scalar flux', where the scalar flux Φ for each element will be determined. The scalar flux is also linear discontinuous, therefore two scalar flux values per element are computed.

We then arrive at the stage where the source is updated again. Now, however, the latest scalar flux is available so we can add the scatter source. This is the only coupling between directions in the algorithm. The last three steps will be repeated until a preset number of iterations is reached. The total number of iterations is based on a manual convergence test.

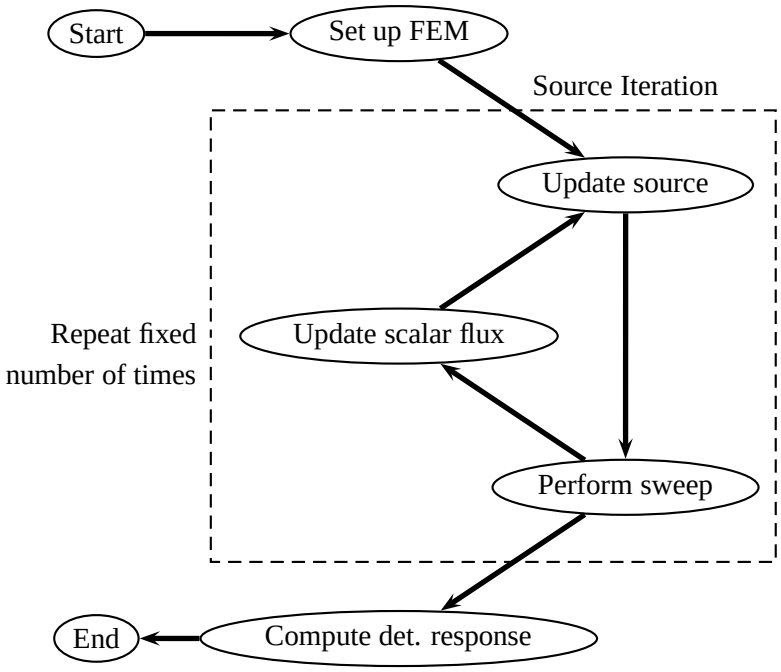

Figure 11: *Schematic overview of the solution methodology used with the discontinuous Galerkin discretization with polynomial basis functions.*

4.4 Data structure

A number of requirements must be met by the data structure that is used in this program. All material properties need to be stored for easy reference. Since the patches are to be refined the data structure must allow for changes in the mesh during computation. A final requirement is the ability to look up neighbouring flux values, that is, flux values of patches in the element next to the current element. This is needed to add the streaming term to the equation.

In the data structure we can take advantage of the hierarchical structure of the patches. The patches in the one dimensional case form a binary tree, in other words each patch has two children and one parent. Figure 12 is an example of a binary tree. In this figure one can also see the ID numbers given to the patches. At the end of the parent ID number a '1' is appended for the left child, analogously at the end of the ID number of the right child a '2' is appended. Not all patches in the tree are used for the calculation of the scalar flux Φ. The patches that are used are called 'active', the others are 'inactive'. When the tree is refined to a deeper level than the two initial patches, the parent patches are not deleted. They can be used to navigate through the tree. Since patches are stored in an array there are two ways to navigate through this tree. First is by parents and children and second by the array structure.

The information that is stored in a tree entry can be found in Figure 13. Every patch has a unique ID number, which is at the same time the route in the tree to that patch. With this ID number similar patches in different spatial elements can be found. Also, the location on the sphere is stored, as an interval of the variable μ, which can be used for quick reference. One can also navigate through the tree by looking up the locations

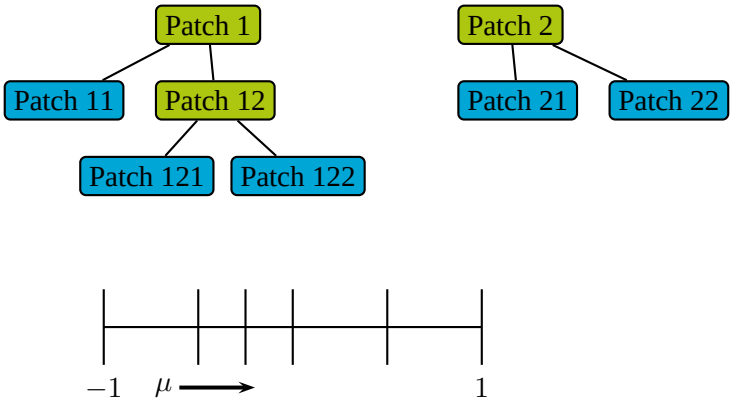

Figure 12: *Binary tree of patches in the one dimensional case. The active patches are blue, the inactive are green. ID numbers of patches are also shown, the ID number of the left child has a '1' appended to the parent ID, while for the right child this is a '2'. Below the patch division of the tree on the line segment is shown.*

of the parent of the current patch, or the locations of the two children of the current patch. The last piece of information that is stored is whether this patch is active, or in other words, whether the patch is used in the solution. In this way the tree structure is maintained, while not all patches are used in the calculations.

Patch ; ID , μ range, μ' , $\int \mu d\mu$, parent , children , active

Figure 13: *For each patch the information in this figure is stored. An array of patches makes a tree, through which one can navigate by parent children relations or by the array structure.*

5 Performance of Angular Discontinuous Galerkin

Some results on the Discontinuous Galerkin Discretization method are presented in this section. The results here are all based on a uniform refinement of all patches. In other words we can compare the DG method to the discrete ordinates method.

The discrete ordinates method and discontinuous Galerkin method will be compared using two error measures. The error is then plotted against the number of unknowns in the discrete problem. For the discrete ordinates method this comes down to twice the number of elements times the number of directions. The number of unknowns for the discontinuous Galerkin method is just twice the total number of patches. In such a plot one can see the efficiency of the method, as the number of unknowns is a crude measure of the computational power that is used in solving the problem. The data points in the results of this section are obtained by running the program with finer initial meshes, no refinement takes place during calculation.

The first error measure is that of the detector response, for which we first have to define the detector response. Many kinds of detector configurations are possible, but only a limited amount is physically relevant. Two detector configurations are used in this report, a volumetric detector and a boundary detector. The volumetric detector response can be formulated as

$$J(\phi) = \int_V \int_{4\pi} \sigma_D \phi(\boldsymbol{r}, \hat{\boldsymbol{\Omega}}) d\hat{\boldsymbol{\Omega}} dV \tag{5.1}$$

In this expression, the cross section σ_D determines the rate at which neutrons are being measured. The dimensions of the detector are contained in this cross section. In regions where the detector is not present we take the cross section to be zero. Since we integrate over the whole detector region without discrimination in angle, neutrons in each direction have the same contribution to the detector.

As the name suggests, the boundary detector measures the number of neutrons that cross a boundary. This detector response can be expressed as

$$J(\phi) = \int_{\delta V} \int_{\hat{\boldsymbol{\Omega}} \cdot \hat{\boldsymbol{n}} > 0} \hat{\boldsymbol{n}} \cdot \hat{\boldsymbol{\Omega}} \phi(\boldsymbol{r}, \hat{\boldsymbol{\Omega}}) d\hat{\boldsymbol{\Omega}} d\delta V \tag{5.2}$$

There is no detector cross section σ_D in this expression, as it simply counts the neutrons that cross a plane. The location of the plane is determined by the set ∂V. The outward normal of the plane is $\hat{\boldsymbol{n}}$. In the expression above only angles that point outward respective to the plane are included in the integral.

With these detector responses we can define an absolute error measure, which is

$$E_{det} = |J_{ref} - J_h| \tag{5.3}$$

where J_{ref} is the 'exact' detector response and J_h is the detector response calculated with the current discrete solution.

The other error measure with which we can compare methods is the root mean square error of the scalar flux Φ. This error is taken node wise, instead of integral wise:

$$E_{rms} = \sqrt{(\boldsymbol{\Phi}_{ref} - \boldsymbol{\Phi}_d) \cdot (\boldsymbol{\Phi}_{ref} - \boldsymbol{\Phi}_d)} \tag{5.4}$$

In this equation $\boldsymbol{\Phi}_h$ is the vector of scalar fluxes on the nodes of the current discrete solution. $\boldsymbol{\Phi}_{ref}$ is again the 'exact' solution, however, it is now a vector quantity.

When there is a comparison to the exact error in this report we do not use the exact error. A reference error is computed using a very fine angular mesh and this is taken to be equal to the exact error. The spatial elements

are small, in the sense that the spatial part of the problem is converged. There will not be any spatial component in the error.

Two sections can be found below, one on the homogeneous slab, the other on separate source detector problems. The test cases in these sections are used to gain some general insight in the Discontinuous Galerkin method in the angular component of the transport equation. An overview of all tests cases, with geometry, material properties and solution, used in this report can be found in Appendix A.

5.1 Homogeneous slab (cases A and B)

Test case A is optically thick and highly scattering, the scatter ratio and total cross section is 0.99. Figure 14 shows a plot of the error decrease of the detector response versus the total number of patches of both DO and DG. Every data point in the plot holds twice as many patches as the previous data point, since each patch is cut into two new patches.

One can observe that both the uniform DG as the DO (Discrete Ordinates) converge second order. In fact, DO outperforms DG in this case, which is due to the scattering medium. DG with constant basis functions on patches has trouble with diffusive materials, more on this in the section with the adaptive results, Section 7. This is in contrast with the optically thin slab (test case B), which is less scattering. A similar plot of the error reduction versus the total number of patches is shown in Figure 17. The rate of convergence is still second order, but DO performs slightly less than DG. DG has an advantage here because the slab is thin, which means the effects of leakage at the edges propagate through the whole domain of the problem. Leakage at the boundaries results in discontinuities in the angular flux ϕ, since there are neutrons leaking out, but no neutrons are entering from the vacuum. DO handles this discontinuity poorly, as the quadrature, the Gauss-Legendre set, handles discontinuities poorly. The quadrature set is designed to integrate spherical harmonics well, which are not discontinuous. DG can handle these discontinuities well, since all patches are discontinuous by definition.

Figures 16 and 17 show the rms error reduction of respectively test case A and B. In these plots the rms error is plotted versus the total number of patches. The same behaviour can be seen in these plots as in the plots of the error in the detector response. This is mainly due to the geometry being homogeneous. In a sense the two error measures are the same when source and detector both span the whole domain of the problem. To illustrate this consider the detector response, which is calculated as an integral over the whole angular domain. The scalar flux is is also an integral over the whole angular domain, the only difference is the detector cross section σ_D. However, the detector response is computed by then taking the integral over the whole spatial domain, while the root mean square error is obtained by taking an inner product of the scalar flux values.

It is remarkable that the convergence is second order for both the detector response error and the root mean square error. When a mix of polynomials with different orders is used one cannot a priori say what the convergence rate will be. However, since constant basis functions are used for the patches, we can expect fourth order convergence with linear patches.

5.2 Source detector (cases C, D, E and F)

Four test cases with a separate source and detector are used in this report. A volumetric source is positioned on the left hand side of the domain, one tenth of the width of the domain. On the opposite side, the right hand side, a volumetric detector can be found, also one tenth of the width of the domain. The cross sections are homogeneous throughout the domain, and different for each test case. C is thick and diffusive, D is thin and scattering, E is somewhat thick and lightly scattering and F is also somewhat thick, but purely absorbing. The complete description of the test cases can be found in Appendix A.

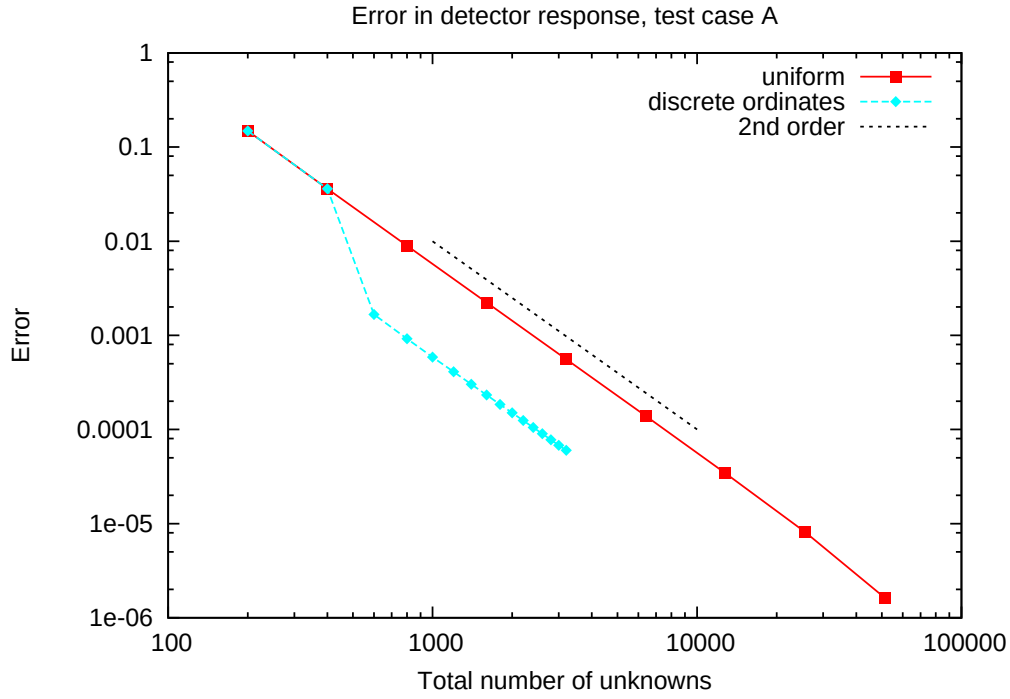

Figure 14: *Error in detector response of test case A, the thick slab. Discrete ordinates outperforms the discontinuous Galerkin method, both converge second order.*

In Figure 18 a plot of the error in the detector response versus the total number of patches of all four separate source detector test cases can be found. Note that the same behaviour as in the homogeneous slab case can be found. In diffusive materials DO outperforms DG, see Figure 18(a), while in optically thin problems DG outperforms DO, see Figure 18(b). In optically thin cases with little scatter, see Figure 18(c) DO outperforms DG by a large amount, which is also the case for the purely absorbing test case shown in Figure 18(d).

In diffusive materials DO outperforms DG, but in thinner less scattering materials DG slightly outperforms DO. However, once the scatter becomes unimportant for the detector response, DO again outperforms DG. In all four cases the rate of convergence is second order. For the same reason as in the homogeneous test cases DO outperforms DG in thick diffusive materials, while DG outperforms DO in thin less scattering materials. When the material is not scattering at all, DO again outperforms DG, which is due to the fact that there is no coupling between directions without scatter. The set of directions obtained from the Gauss Legendre set gives a better approximation than the set of directions obtained from DG. The Gauss Legendre directions are not uniformly distributed, but are more numerous near $\mu = -1$ and near $\mu = 1$. These directions are more important for an accurate detector response than directions near $\mu = 0$. DG provides us with uniformly distributed directions, which will therefore perform worse. In other words, when there are no discontinuities in the angular flux, the set of directions in discrete ordinates performs better.

DG with constant patches (constant basis functions on patches) has trouble representing the linear flux profile in the thick highly scattering medium of test case C (see Figure 18(a)). Many piece wise constant functions are needed to approximate a linear function well. That is why the discrete ordinates method performs much better. However when the material is thin the constant patches are better able to describe the angular flux well, as can be seen in Figure 18(b). The flux profile becomes exponential in the angular variable μ. Constant

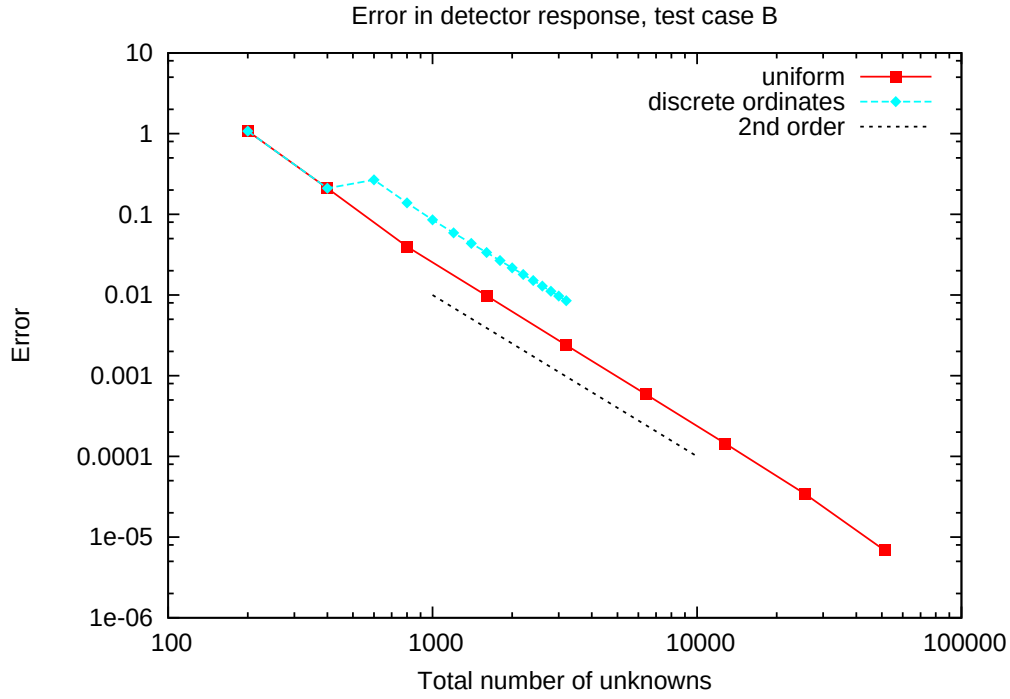

Figure 15: *Error in detector response of test case B, the thin slab. The discontinuous Galerkin method outperforms discrete ordinates, both converge second order.*

patches can describe the tail of the exponent well, which gives a better description than a linear profile.

Another thick case is test case E, Figure 18(c), where discrete ordinates outperforms the discontinuous Galerkin method. This case is mostly absorbing, so the flux profile will be mostly exponential, which should be in the benefit of discontinuous Galerkin. However since this test case is optically thick, DO does not have the disadvantage of leakage effects propagating through the domain, therefore DO still outperforms DG.

A concluding remark about the error in the volumetric detector response is that for a source detector problem the angular flux in the detector region is most important to obtain an accurate detector response. To obtain an accurate angular flux at that end of the domain one needs an accurate representation of the angular flux in the middle of the domain, as the neutrons will have to traverse this part of the domain to get to the detector from the source. The edge effects at the end of the source, for all material properties, are in that respect not very important. It is however important to get an accurate description of the leakage at the detector end, as the leakage will effect the detector response.

The rms error versus the total number of patches of the four source detector test cases is shown in Figure 19. Please note that in the rms error measure DG outperforms DO in all cases except for the diffusive source detector problem. So DG provides a better overall solution than DO does, which is likely due to the discontinuity in the angular flux at the boundaries of the geometry. For all material properties and domain sizes the leakage has effect on the rms error, which is not necessarily the case with a small volumetric detector. The Discrete Ordinates method with a Gauss Legendre quadrature set cannot handle such a discontinuity well, it is however in the nature of DG to handle discontinuities well. Also note that the rate of convergence is still second order. As will become clear later, for each test case the rate of convergence is second order. This is not necessarily what one would expect for constant basis functions.

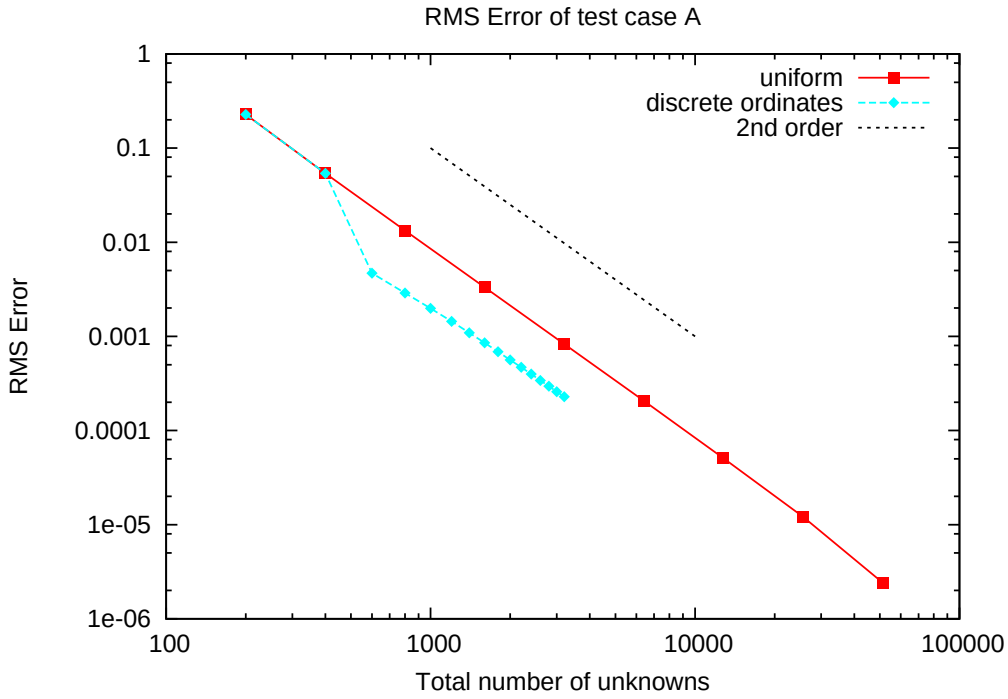

Figure 16: *Node wise root mean square error of scalar flux, test case A. Same behaviour as with the error in the detector response, discrete ordinates outperforms the discontinuous Galerkin method. Remarkably the convergence is still second order.*

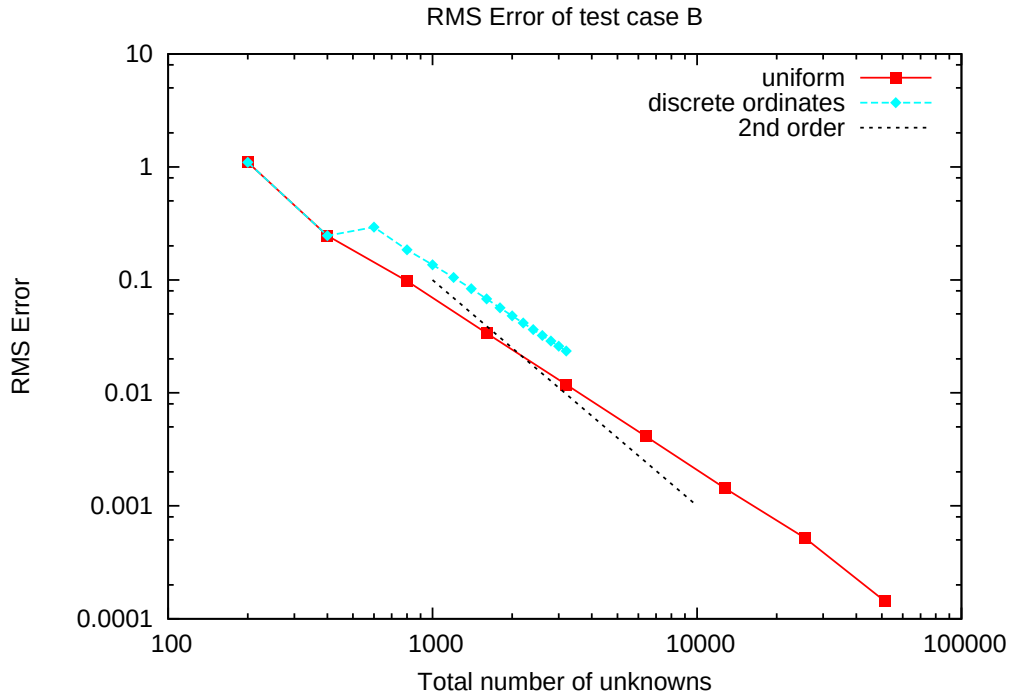

Figure 17: *Node wise root mean square error of scalar flux, test case B. Same behaviour as with the error in the detector response, the discontinuous Galerkin method outperforms discrete ordinates. Remarkably the convergence is still second order.*

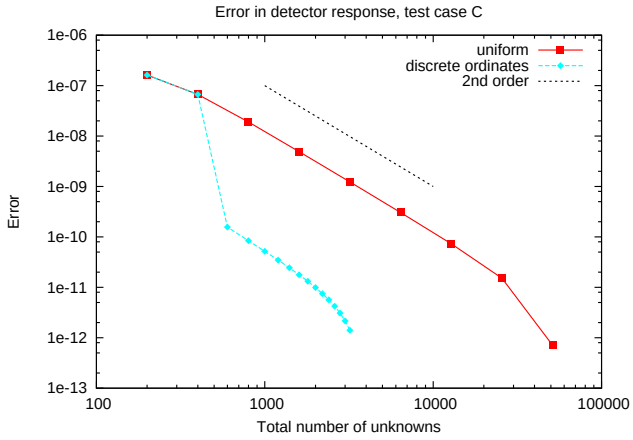

(a) *Test case C, thick highly scattering medium.*

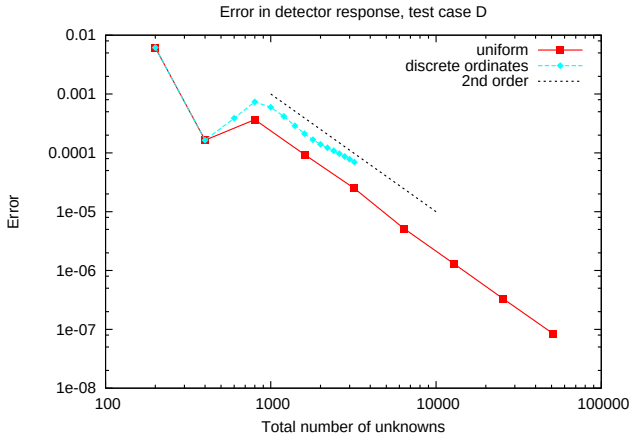

(b) *Test case D, thin scattering medium.*

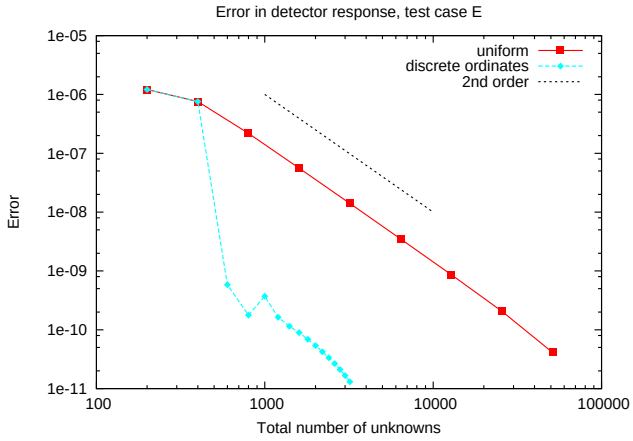

(c) *Test case E, absorbing medium.*

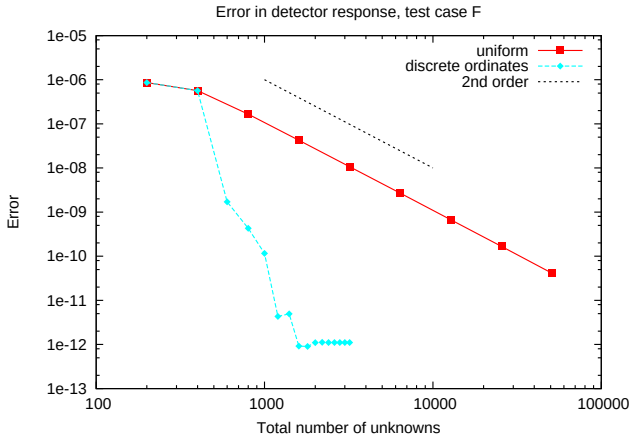

(d) *Test case F, purely absorbing medium.*

Figure 18: *Error of all source detector test cases.*

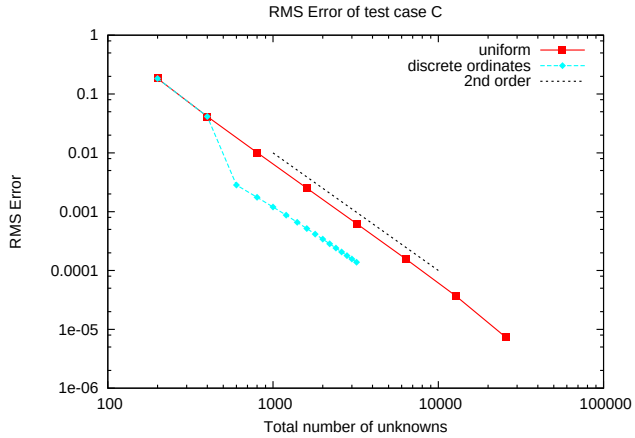

(a) *Test case C, thick highly scattering medium.*

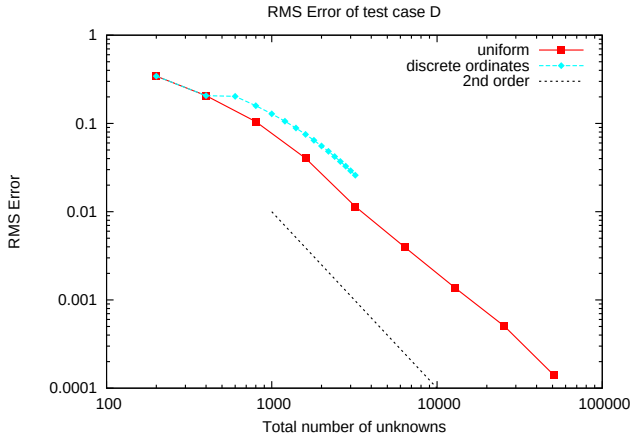

(b) *Test case D, thin scattering medium.*

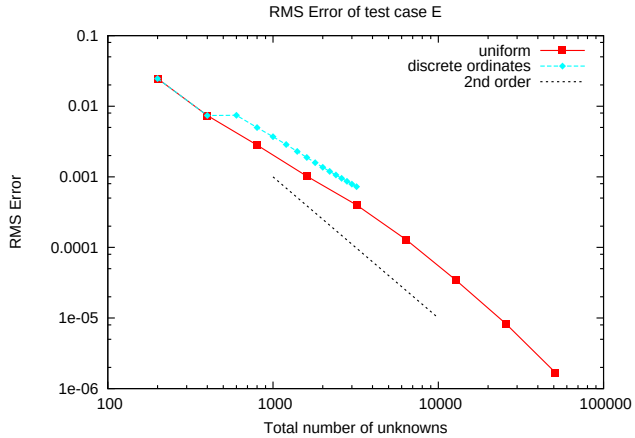

(c) *Test case E, absorbing medium.*

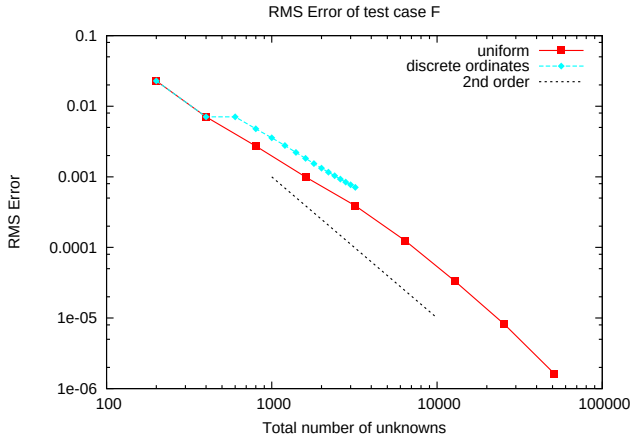

(d) *Test case F, purely absorbing medium.*

Figure 19: *RMS Error of all source detector test cases.*

6 Refinement Strategies

An adaptive method is a method where refinement in the mesh will take place during calculation, that is the mesh is not stationary. The advantage of such a method is that, with a good refinement strategy, the computational power can be used in regions of the domain that contribute most to the error. Which leads to a more efficient method. The efficiency of an adaptive method depends for a large part on the refinement strategy that is used.

A refinement strategy is a method of selecting the locations where refinement will take place. In this case that will be selecting the patches that are cut into two, equally sized, refined patches. Two classes of strategies are tested in this report, traditional and goal-oriented methods. Within the class of the goal-oriented methods two different 'flavours' are tested, using the full adjoint solution and a local adjoint solution. More on the adjoint problem and the goal-oriented refinement strategies can be found in Section 6.2.

Traditional methods are based on the change in solution when a local refinement in the mesh is performed. The local refinements with the largest decrease in error are considered to be useful. The traditional method used in this report can be found in Section 6.1.

In Section 7 the comparison between the different refinement strategies is made. They are also compared to the performance of the discrete ordinates method. These results will also tell us whether this method of discretization combined with a goal-oriented refinement strategy proves to be a useful method.

The final part of this section is an overview of the adaptive algorithm that is used in this report. This is an expansion of the algorithm that can be found in Section 4.3. The algorithm as described in that section is used to calculate the solution after patches are refined.

6.1 Traditional refinement

Traditional refinement methods can be found in many areas of mathematics and physics, however the method described here does not necessarily apply to all these areas. It is however widely used in numerical neutron transport and other fields. All traditional methods are based on the same idea. A local refinement and solution is computed and compared to the original non-refined solution. The elements or patches that have the largest change in solution will keep the refinement, the other elements will go back to their original distribution.

We now need to quantify 'change in the solution'. The solution in this case is the angular flux ϕ and the change will be looked at in phase space. In other words, we will look at the square of the change in the angular flux integrated over phase space of a patch η, which reads

$$\begin{aligned} \eta &= \int_{\Delta x}\int_{G_i}(\phi_{h/2}-\phi_h)^2 d\hat{\mathbf{\Omega}}dx && (6.1)\\ &= \int_{G_i} d\hat{\mathbf{\Omega}}\int_{\Delta x}(\phi_{h/2}-\phi_h)^2 dx && (6.2)\\ &= 2\pi\Delta G_i\int_{\Delta x}(\phi_{h/2}-\phi_h)^2 dx && (6.3)\end{aligned}$$

Since the integrand of the angular integral is a constant function, we can pull it out. That leaves us with the spatial integral, which can be formulated in terms of the matrices in Equation 4.12:

$$\eta = \int_{\Delta x}\int_{G_i}(\phi_{h/2}-\phi_h)^2 d\hat{\mathbf{\Omega}}dx = 2\pi\Delta G_i(\boldsymbol{\phi}_{h/2}-\boldsymbol{\phi}_h)^T\boldsymbol{M}(\boldsymbol{\phi}_{h/2}-\boldsymbol{\phi}_h) \quad (6.4)$$

The change can be determined in different ways, for example refine the whole domain and select the elements where the solution changed most. Or, another example, refine each element locally and determine its solution. The change in solution of this local refinement is then used as criterion.

One specifies a fixed percentage of patches that is to be refined in each iteration. That percentage of patches with the largest change, as in the above definition, will be refined. In this report $\phi_{h/2}$ is determined in the local approximation. A patch is locally refined and the new solution is computed on this patch. This means the upwind flux values that are used in the computation of this patch are of the coarse level and are not updated. Also the scalar flux Φ is not updated before computing the solution on the finer patches. After the change has been computed that patch is coarsened again, before going on to the next patch.

This method clearly tries to get an accurate solution of ϕ on the whole domain, it's goal is to let ϕ vary as little as possible. However, we are interested in an accurate calculation of the detector response. The goal of the traditional refinement strategy does not necessarily result in an accurate detector response. As opposed to traditional methods goal-oriented methods take into account the quantity one wants to accurately determine, in this case the detector response.

6.2 Goal-oriented refinement

The goal in this report is obtaining an accurate detector response, to incorporate this in a method of selecting patches that are to be refined one needs a way of determining the importance of a patch to the detector response. This importance can be obtained by using the adjoint or dual problem [1].

This section starts by deriving the adjoint transport problem and examining its physical interpretation. Using this adjoint problem we can then formulate an error estimator, which is derived in the following section. From this estimator we can also obtain a criterion for selecting patches that will be refined. This criterion will, as opposed to traditional methods, take into account our goal of obtaining an accurate detector response. Finally some words are spent on the approximations of the exact adjoint solution one can use.

6.2.1 Adjoint or dual neutron transport problem

The fields of mathematics and physics do not agree on the name of the expression used for the error estimation in this report. Mathematicians say it is the dual problem, however nuclear physicists call it the adjoint problem. From now on it will be called the adjoint problem.

The simplified neutron transport equation, Equation 2.2, can be written as an operator equation

$$L\phi = S \tag{6.5}$$

In this equation the operator L is the transport operator, which deals with the transport, removal and scatter term of the transport equation. The right hand side S is the external source.

Using the operators we can define the adjoint operator L^* as

$$< \phi^*, L\phi > = < \phi^*, S > \qquad \Longleftrightarrow \qquad < L^*\phi^*, \phi > = < \phi^*, S > \tag{6.6}$$

The binary operator $< \bullet, \bullet >$ denotes an inner product of functions, computed as the integral over phase space of the product of the two functions. We are free to chose the right hand side of the adjoint transport equation, or in other words which equation we solve. A useful choice of the right hand side is

$$L^*\phi^* = \sigma_D \tag{6.7}$$

as this results in a detector response that can be written as

$$J =< \sigma_D, \phi >=< \phi^*, S > \tag{6.8}$$

After a tedious derivation, which is included in Appendix D, it follows that the adjoint transport operator L^* differs only in the streaming term from the transport operator L. This term has changed sign, resulting in the following adjoint transport equation

$$-\hat{\mathbf{\Omega}}_i' \cdot \nabla \phi_i^* + \sigma_t \phi_i^* = \frac{\sigma_s}{4\pi}\Phi^* + \sigma_D \tag{6.9}$$

The difference with the normal transport equation, Equation 3.21, is the sign of the streaming term and a different external source.

Above, the adjoint neutron transport equation was derived on purely mathematical reasoning. This equation does, however, also have a physical interpretation. There are two differences with the normal transport equation, which we will examine.

Instead of the physical source s_i we now have the detector cross section σ_D as the source. Apperently the 'adjoint neutrons' originate from the detector. Keeping that in mined we can also see that a change of sign in the transport equation can be understood as a change in direction. All directions are effectively reversed, meaning the 'adjoint neutrons' stream in the opposite direction of the physical neutrons. Combining these observations we can interprete the 'adjoint neutrons' as the the importance of that location in phase space to the detector. The larger the adjoint angular flux ϕ^* the larger the probability that neutrons in that location in phase space are detected.

Solving the adjoint transport equation is actually solving the importance that is 'flowing' out of the detector into the geometry of the problem. As we will see later in this section, this importance can be used for refining specific directions that contribute a lot to the error in the detector response.

In the complete derivation of the adjoint transport operator one needs to assume boundary conditions for the adjoint problem in order to obtain the formulation above, Equation 6.6. At the boundaries, when using Dirichlet boundary conditions, there is no in flow of neutrons in the normal or forward transport problem. For the boundary terms to cancel out we need to assume that the out flow of importance of neutrons in the adjoint transport problem is zero. A more detailed derivation of the adjoint transport problem and its physical interpretation can be found in Appendix D.

6.2.2 Error estimation

An error estimate can now be formulated, using the forward and adjoint transport equation. The complete derivation of this error estimate can be found in Appendix B, in this section only the important steps and results are presented.

During the discretization of the transport equation using the discontinuous Galerkin method the equation is multiplied by a basis function and integrated over phase space. This can be found in Sections 3.2.3 and 3.2.4. We can write that equation in the following form [8], which is the weak form

$$B(\phi, v) = l(v) \qquad \forall v \in V \tag{6.10}$$

In that equation v is the test function and ϕ is the angular flux that is to be solved. V is the space of all basis functions used in the Discontinuous Galerkin discretization. Please note that the linear form l contains only the source terms, the bilinear from B contains all other terms.

Using the detector response in Equation 5.1 we can define the error in the detector response as

$$\Delta J = J(\phi) - J(\phi_h) \tag{6.11}$$

where ϕ is the exact solution and ϕ_h is the discrete solution. The detector response operator $J(\phi)$ is linear, so we can simplify this to

$$\Delta J = J(\phi - \phi_h) \tag{6.12}$$

We can rewrite this using the adjoint problem

$$\Delta J = B(\phi - \phi_h, \phi^*) \tag{6.13}$$

In Section 3.2 the orthogonality property of the Galerkin method was derived. In short this property states that the error lies outside the space V, which allows us to rewrite the former equation as

$$\Delta J = B(\phi - \phi_h, \phi^* - \phi_h^*) \tag{6.14}$$

Finally we can use Equation 6.10, in other words consistency, to obtain

$$\Delta J = l(\phi^* - \phi_h^*) - B(\phi_h, \phi^* - \phi_h^*) \tag{6.15}$$

When we plug in the expressions for l and B we obtain a sum over all patches, which we can write as

$$\Delta J = \sum_e \sum_p \eta_{e,p} \tag{6.16}$$

The indices e and p are, respectively, the sum over the elements and over the patches. In this sum we see that the quantity η of each patch is weighted by the surface area of that patch. η itself follows from the derivation and can be written as

$$\begin{aligned}
\eta_{e,p} \;=\; & \Delta G_{e,p} \int_e R_h(\phi^* - \phi_h^*) d\boldsymbol{r} + \Delta G_{e,p} \mathbf{1}_{p \in \Omega_U^-} \int_{\partial e^- \setminus \{\partial V_D \cup \partial V_R\}} (\boldsymbol{\Omega'}_{e,p} \cdot \hat{\boldsymbol{n}}) r_{h,U} (\phi^* - \phi_h^*)^{int} d\boldsymbol{r} \\
& + \Delta G_{e,p} \mathbf{1}_{p \in \Omega_D^-} \int_{\partial e^- \cap \partial V_D} (\boldsymbol{\Omega'}_{e,p} \cdot \hat{\boldsymbol{n}}) r_{h,D} (\phi^* - \phi_h^*)^{int} d\boldsymbol{r} \\
& + \Delta G_{e,p} \mathbf{1}_{p \in \Omega_R^-} \int_{\partial e^- \cap \partial V_R} (\boldsymbol{\Omega'}_{e,p} \cdot \hat{\boldsymbol{n}}) r_{h,R} (\phi^* - \phi_h^*)^{int} d\boldsymbol{r}
\end{aligned} \tag{6.17}$$

Please note that the η of a patch is an integral of the residual of a patch, weighed by the importance that one obtains from solving the adjoint equation.

The error is expressed as a sum over the patches, where each patch has a contribution proportional to its size, its residual and the importance of the patch to the detector response. This seems to be a very natural way to express the error in the detector response. Since the patches have individual contributions to the error we can use this to decide which patches to refine. A fixed percentage of patches with the largest contributions will be refined. This is the goal oriented adaptive criterion used in this report. For a detailed derivation of this expression we refer to Appendix B.

6.2.3 Approximation of exact adjoint solution

In the expression for the error estimator we see that we need the exact adjoint solution ϕ^*. As the adjoint problem cannot always be solved analytically, it will be solved in the same discretized way as the forward transport problem. This means the exact adjoint solution ϕ^* is not available and must be obtained or approximated in a different way.

For clarity we will use the symbol ϕ^* for the exact adjoint solution, the symbol ϕ^*_{aprx} for the approximation of the exact adjoint solution and ϕ^*_h as the discrete adjoint solution. We can take ϕ^*_{aprx} then to be the adjoint solution on a finer patch distribution than ϕ^*_h. It would be best to take this on a deep as possible level, however for practical reasons in this report we take ϕ^*_{aprx} to be refined to one level deeper than ϕ^*_h. This means each patch that is part of the solution of ϕ^*_h is refined once to obtain the patch distribution on which ϕ^*_{aprx} is computed.

With this choice of approximating ϕ^* with ϕ^*_{aprx} that lives on a patch distribution one level deeper one is still left with the choice of how to compute ϕ^*_{aprx}. There are two distinct ways of computing this solution, globally or locally. Global means one solves the adjoint problem completely on the finer patch distribution. Locally means one solves the adjoint problem on the same patch distribution as the forward level and refines the adjoint patch locally when the error needs to be computed. After refining and before computing the error one will solve the adjoint flux ϕ^*_h on this patch using the non refined neighbour flux values and non updated adjoint scalar flux Φ^*_h.

With these two methods the same difference between levels of refinement is used, however the cost of the locally computed adjoint solution is much lower than the globally computed adjoint solution. This is due to the fact that in the global computation the adjoint solution will need to be converged on a deeper level, using more unknowns, than when using the local computation. In the results in Section 7 we will examine the effect of both methods.

6.3 Overview of adaptive algorithm

An overview of the fully adaptive algorithm is presented here. This algorithm can be used for both the traditional and goal oriented criteria.

The adaptive algorithm is actually an expansion of the non-adaptive algorithm presented earlier, see Section 4.3. This non-adaptive algorithm is used between refinement iterations to compute the solution. In each refinement iteration the error per patch η for all elements is computed, which are then sorted in descending order. The error can be computed using different methods. The three methods examined in this report are the traditional refinement and two types of goal-oriented refinement, using the globally or locally refined approximation of the exact adjoint solution. A fixed percentage of patches that are on top of the list will then be refined. The effect of different percentages will be examined in Section 7.5.

We will now explain the flow of the algorithm and what needs to be done in each step. The algorithm starts again with setting up the matrices needed for the spatial finite element method, also the arrays that store material properties and patches are allocated. This is the patch distribution that is used at the start of the algorithm and will change during the algorithm.

As in the uniform case the source in first iteration consists of just the external source term. After updating the source term the transport sweep can be performed. The matrices are needed at this stage. With the newly available angular flux we can update the scalar flux. From this stage the algorithm can go to two directions. Until the fixed number of inner iterations is reached the algorithm will continue with updating the source. In this way the transport problem is solved until convergence with the current patch distribution. These steps in the inner iteration are performed for both the adjoint and forward problems.

Once the preset number of inner iterations is reached the algorithm continues by calculating the error for

each patch. To this end the adjoint transport problem has to be solved first. This is done in similar fashion as the inner iteration of the forward problem. However the patch distribution can be different. After calculating the error contribution per patch we can order the patches to find out which have the largest contribution. A fixed percentage of patches is then refined.

After refining the inner iteration will start again, with the new finer patch distribution. The inner iteration will again loop until the preset number of iterations is used. The number of times the outer iteration is repeated is also fixed and preset.

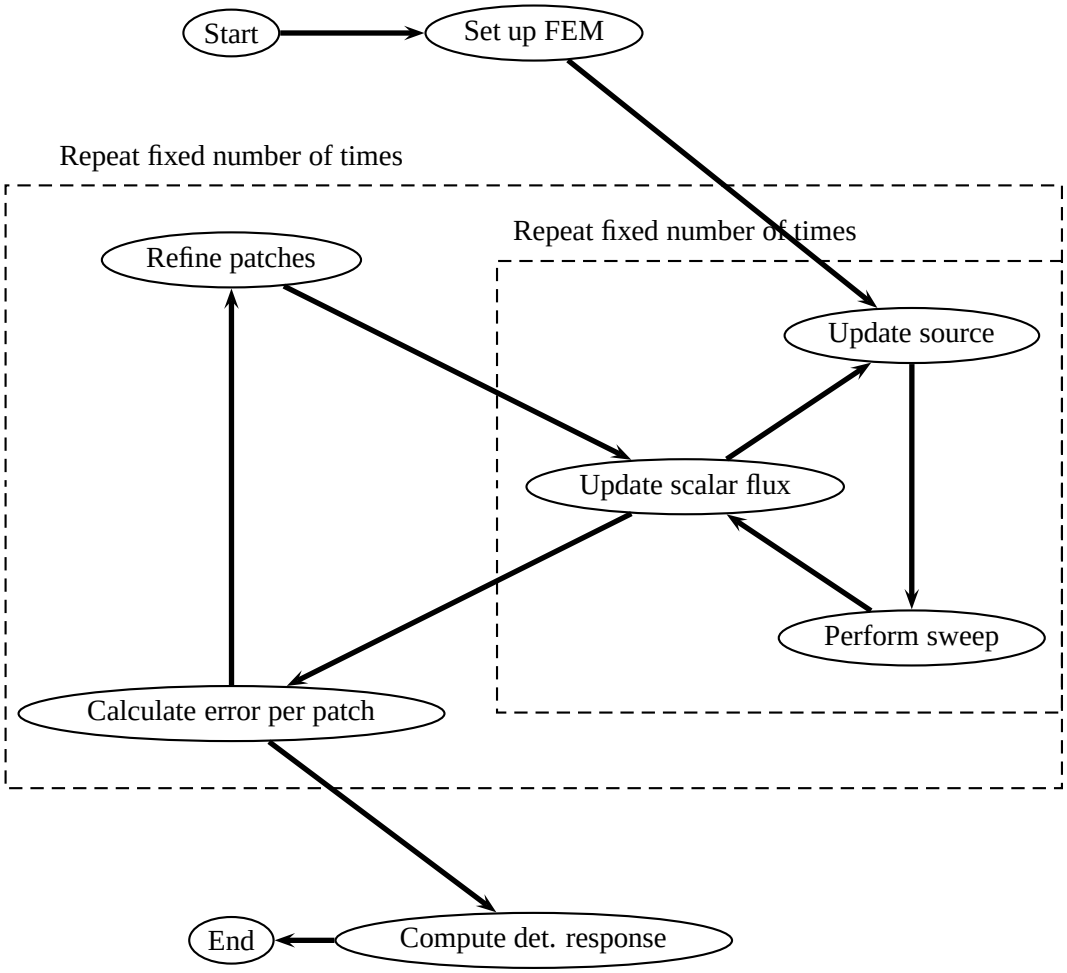

Figure 20: *Schematic overview of the adaptive algorithm.*

7 Results of Adaptive Methods

In this section the results of the various adaptive algorithms are presented. Ten cases are used to illustrate the performance of the algorithm, these test cases can be found in Appendix A. Each of the cases will test different aspects of the adaptive methods. In all test cases the adaptive algorithms refine 30 per cent of the patches in each refinement iteration, unless stated otherwise.

For the tests in this section we will use the same error measures as in Section 5, the error in the detector response E_{det} and the node wise root mean square error of the scalar flux E_{rms}. The errors are again computed using a reference value for the detector response and the scalar flux. This reference value is computed at a much deeper level of refinement.

For all test cases a figure with the error plotted against the total number of patches. This shows how the refinement in each step improves the solution. In this way different adaptive methods can be compared on performance. The discrete ordinates method is also included in these plots, although it is not an adaptive method. However, one can compare the cost in number of unknowns of the discrete ordinates method and the adaptive methods.

The quality of the error estimator for the two goal-oriented methods is also examined. To this end we compare the estimated error with the reference error, which is computed at a much deeper level. We examine the quality to find out whether we can use the error estimator as a trustworthy representation of the error. This would mean that in future work the reference error does not necessarily have to be computed.

A final comparison between the adaptive methods is an investigation into the effect of the refinement ratio, that is the percentage of patches that is refined in each refinement iteration. The adaptive algorithm is run several times with different percentages. The error versus the total number of patches for all methods is then plotted in one figure, which shows the most effective refinement ratio.

The first test cases have a homogeneous slab geometry, with different materials. The next test cases have a separate source and detector in a homogeneous material. A volumetric detector is mostly used, however a boundary source is also investigated. Thereafter the source detector test case is extended by placing a shielding region in the middle of the domain, between the source and detector. The final tests are on the effect of the refinement ratio on the convergence.

A final remark has to be made on all plots that are shown in this section, the legend holds names for the different method that are presented in this work. ‘Uniform’ is the discontinuous Galerkin method with uniform refinement, i.e. in each refinement iteration all patches are refined. ‘Traditional’ refers to the traditional refinement criterion that can be used with the discontinuous Galerkin method. The two goal-oriented adaptive methods are referred to as ‘full adjoint’ and ‘local adjoint’. The full adjoint is the criterion that bases its decision for which patches to refine on the adjoint solution of patches that are one level deeper (they are refined once more) than the patches of the forward solution. The other criterion bases its decision on a local refinement of the adjoint solution and is therefore called local adjoint. We also have the discrete ordinates method which is referred to as ‘discrete ordinates’. Finally a line that represents second order convergence is plotted for convenience, this line is referred to as ‘2nd order’.

7.1 Homogeneous slab (cases A and B)

The first test case is the homogeneous slab, both optically thick and thin. The exact specifications of these test cases are presented in Appendix A. In Figure 21(a) one can find the plot of the detector response error versus the total number of patches of test case A, the thick scattering slab. In this plot we note that convergence is eventually second order for all methods that are presented. The error with uniform refinement of patches decreases constantly, while the error of all other methods decreases faster in the beginning, i.e. with few

patches. Therefore the traditional, full and local adjoint and discrete ordinates methods eventually have an advantage of an estimated factor of two, measured in the number of patches needed to get a certain error. The similarity in error decrease of the different methods is probably due to the homogeneity of the problem.

Turning to the plot of detector response error decrease versus the total number of patches in case B, Figure 21(b), we see that all methods again perform somewhat similar. This time the uniform method (all patches are refined in each refinement iteration) performs slightly better than the other methods. The error decrease for all methods is again about second order.

In both cases the adaptive algorithms perform about the same, also the Discrete Ordinates method performs about the same as the adaptive algorithms. The uniform refinement performs, however, different in case A and B. In case A the adaptive algorithms perform slightly better, while in case B the uniform refinement performs slightly better. An answer to this can be found in the spatial patch distribution, which is shown in Figure 22. In these plots the number of patches in an element is plotted against the x position of that element.

Case B has quite a uniform patch distribution in space. Therefore one would expect the uniform and adaptive methods to work similarly. However in case A the patch distribution is far from uniform, more patches are used near the edge of the domain. Near the edges the angular flux is more difficult to compute, because of the leakage. In the middle of the domain there is little effect of the leakage, because the material is optically thick. Therefore the adaptive algorithms can provide a better solution.

Another remarkable result is the steps in the patch distribution of test case A. These are an artefact of the refinement algorithm, when a smaller fraction of patches is refined these steps disappear and the distribution becomes exponential. The exponential behaviour might be due to the fact that effects of leakage decrease exponentially when propagating through the domain, because a ray of neutrons also decreases exponentially.

The lack of difference between the three adaptive methods can be explained by the homogeneity of the problem. Since the volumetric detector is in the whole domain there is little difference between the traditional and goal oriented criteria. One could say that a refinement that changes the solution of the angular flux ϕ most will probably also result in a better detector response and vice versa. Therefore we will turn to other test cases.

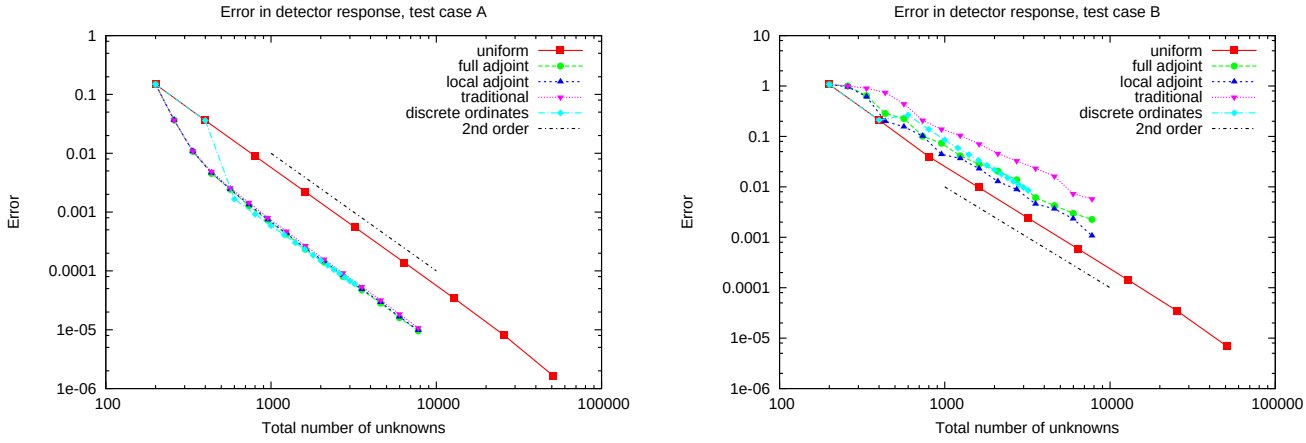

(a) *Test case A, thick highly scattering medium.*

(b) *Test case B, thin scattering medium.*

Figure 21: *Error in the detector response of the two homogeneous slab test cases. In the optically thick case all methods perform better than the uniform method, because the optimal distribution of patches is not flat. However in the optically thin case the optimal distribution is almost flat, therefore the uniform refinement works well.*

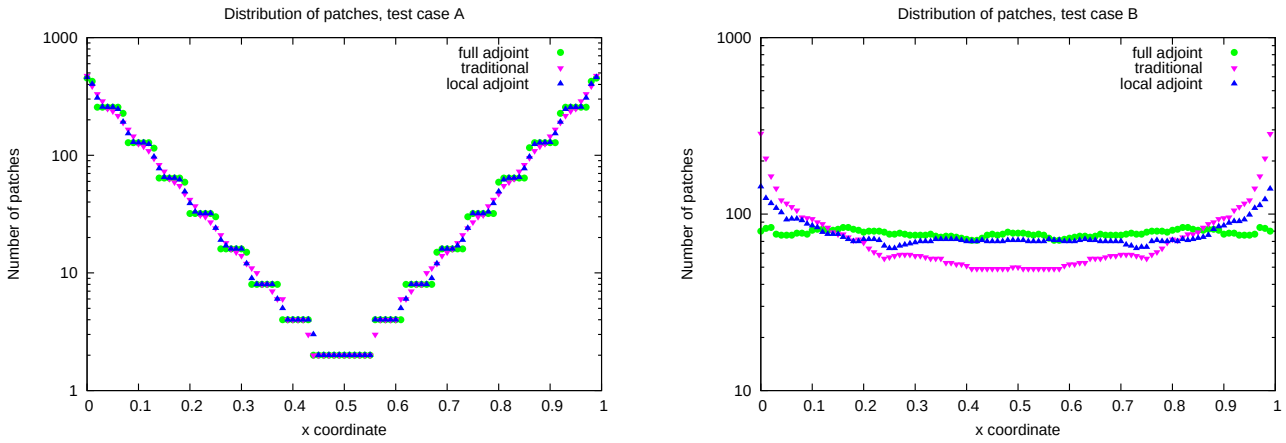

(a) *Test case A, thick highly scattering medium.*

(b) *Test case B, thin scattering medium.*

Figure 22: *Spatial patch distribution, in one spatial element all patches are counted and plotted at its position. The steps in the optically thick case disappear when a smaller refinement ratio is used. The optimal distribution of patches in the optically thin case is almost uniform.*

7.2 Source detector (cases C, D, E and F)

In these test cases a geometry with a separate source and detector for different materials is presented. The four materials are thick scattering, thin scattering, thin absorbing and a material with medium thickness and some scattering. For each of the test cases the material properties are listed in Appendix A.

Figure 23 shows the error in the detector response versus the total number of patches of all source detector test cases. We see for all four test cases the same second order convergence of the uniform method. For test cases C, E and F we see somewhat the same behaviour. The discrete ordinates method outperforms all other methods, while the traditional refinement criterion with discontinuous Galerkin performs the worst of all, since there is almost no error decrease. The two goal-oriented adaptive methods, full and local adjoint, converge second order and perform at least as good as the uniform method. In case D the full adjoint goal-oriented method performs best, while all other methods perform comparably.

An explanation for this behaviour can be found looking at the angular flux profile. In the thick and diffusive cases the flux profile is almost linear while in the absorption case it is exponential. Since we're using constant basic functions (patches) different behaviour can be expected when the solution has a different angular flux profile. A linear function is harder to approximate with constant patches, as it needs a fine representation for all directions. An accurate approximation of exponential functions with constant functions only needs a fine representation where the derivative of the exponential function is largest.

When comparing the uniform and adaptive methods one finds that the goal-oriented adaptive methods are at least as good as the uniform method. The traditional adaptive method does a very poor job. These differences between the methods can be explained by the patch distributions, which are shown in Figure 24. In this figure we will take a closer look at the spatial patch distribution of cases C and E. In case C we saw that the goal-orientated methods have an equal error reduction as the uniform method, which can be explained by the diffusivity of the problem. Constant patches cannot approximate diffusive problems well, because the angular flux profile is linear. Since we need a fine mesh to approximate a linear function by constant basis functions, this means the whole domain of the problem will be refined. Figure 24(a) shows the flat spatial distribution

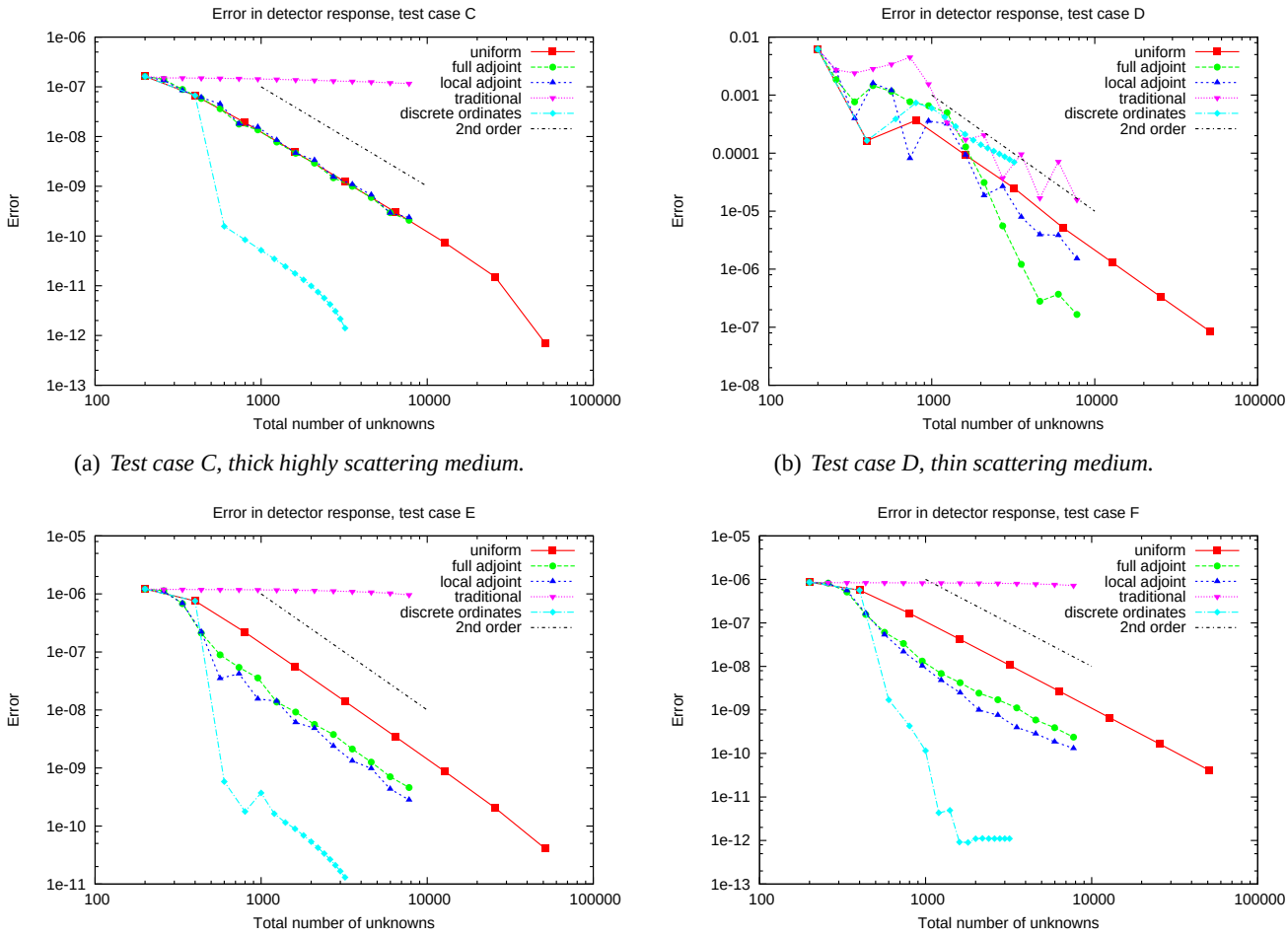

(a) *Test case C, thick highly scattering medium.*

(b) *Test case D, thin scattering medium.*

(c) *Test case E, absorbing medium.*

(d) *Test case F, purely absorbing medium.*

Figure 23: *Error in the detector response of all source detector test cases.*

of the two goal-oriented adaptive methods. This figure also shows why the traditional method performs so poorly. Most refinement is on the left hand side of the problem, while the detector is on the right hand side of the problem, which results in a bad detector response. The traditional criterion refines patches of which the solution changes most when they are refined, which will be around the source region in the domain and not around the detector region, as the solution is much larger in the source region.

The patch distribution of test case E shows why the goal orientated adaptive methods outperform the uniform method. Even though the spatial distribution is still quite flat, more refinement took place on the border of the source region and the detector region. Since this problem is less scattering the patch distribution is less flat. Also in this case the traditional method refines locally around the source and not at all around the detector.

It is also worth looking at the node wise root mean square error (rms error) of the flux. Since this error measure looks at the whole domain of the problem instead of just the detector region. Figure 25 shows a plot with the rms error versus the total number of patches. The traditional adaptive method provides us with the smallest error of all methods and discrete while the goal oriented adaptive methods show almost no decrease in error. This behaviour can be expected since the goal of the goal-oriented methods is to get the detector response

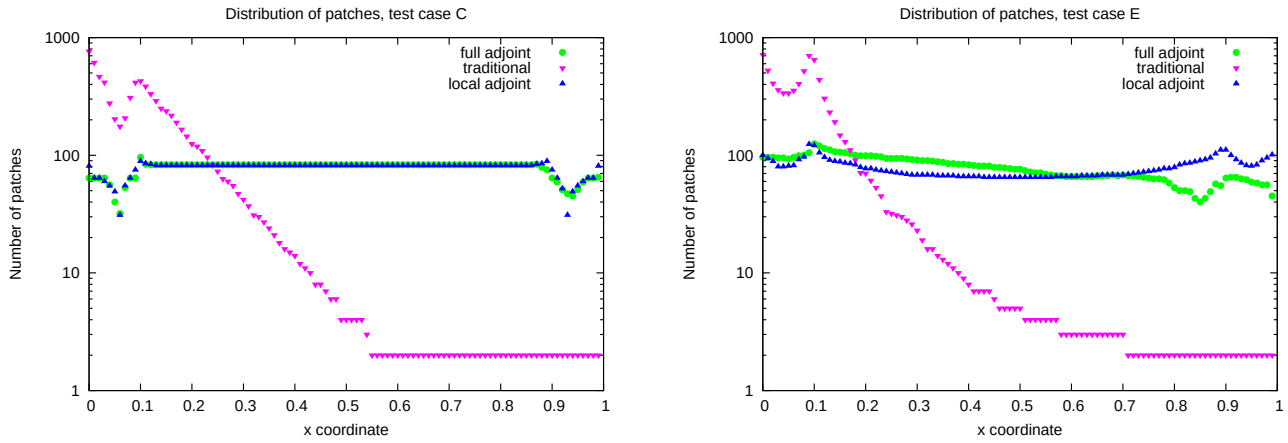

(a) *Test case C, thick highly scattering medium.*

(b) *Test case E, absorbing medium.*

Figure 24: *Spatial patch distribution, in one spatial element all patches are counted and plotted at its position. The traditional adaptive method mostly refines around the source, not around the detector. The absorbing medium has a larger refinement near source and detector for the goal oriented adaptive methods, while the thick case has an almost flat distribution. This is needed for an accurate representation of a diffusive problem.*

as accurate as possible, which not necessarily needs an accurate description of the solution in the whole domain. We furthermore note that the uniform method converges about second order and that the discrete ordinates method performs similar to the uniform method.

We also present a comparison between a source detector problem with a volumetric detector and a boundary detector. The two cases with a boundary detector are G, with a thick scattering medium, and H, with a thin scattering medium. In Appendix A the test cases are described and the material properties are listed. Figure 26 shows the error reduction versus the total number of patches of cases G and H. We see a similarity between cases G and C, and between H and D. To start with G and C, in both cases the discrete ordinates method performs best and the traditional method worst. The uniform method and the two goal-oriented adaptive methods show similar error reduction. In cases H and D we see a uniform method that converges second order and all other methods perform similar, albeit with a spread around the uniform error reduction. This shows that using a boundary detector instead of a volumetric detector does not change much in the behaviour of the methods.

Some differences in behaviour can however be found when examining the spatial patch distribution of the two cases. Figure 27 shows a plot of the number of patches in an element versus the spatial position of that element for both cases. Comparing the plot for case G with that for C we see that between $x = 0.9$ and $x = 1$ the number of patches increases slightly near the boundary of the domain for case G, while in case C we see a dimple in that region. In both cases we see a slight increase in number of patches near the boundary of the detector, that is for case C $x = 0.9$ and for G $x = 1$. This is probably to have an accurate description of the angular flux that enters the detector. The same behaviour can be seen for case H and D, although the full adjoint actually shows a slight decrease in number of patches near the right boundary. In all cases the full and local adjoint differ slightly from each other both in error decrease and in patch distribution, therefore we conclude this is not a fundamental difference between the methods.

The traditional refinement criterion results in a slightly different spatial patch distribution in the cases G and H, as well as in the case C and E. In cases E and H the patch distribution has a relative larger peak around the source region. This can be explained by looking at the solution of the flux, as this also has a larger peak for

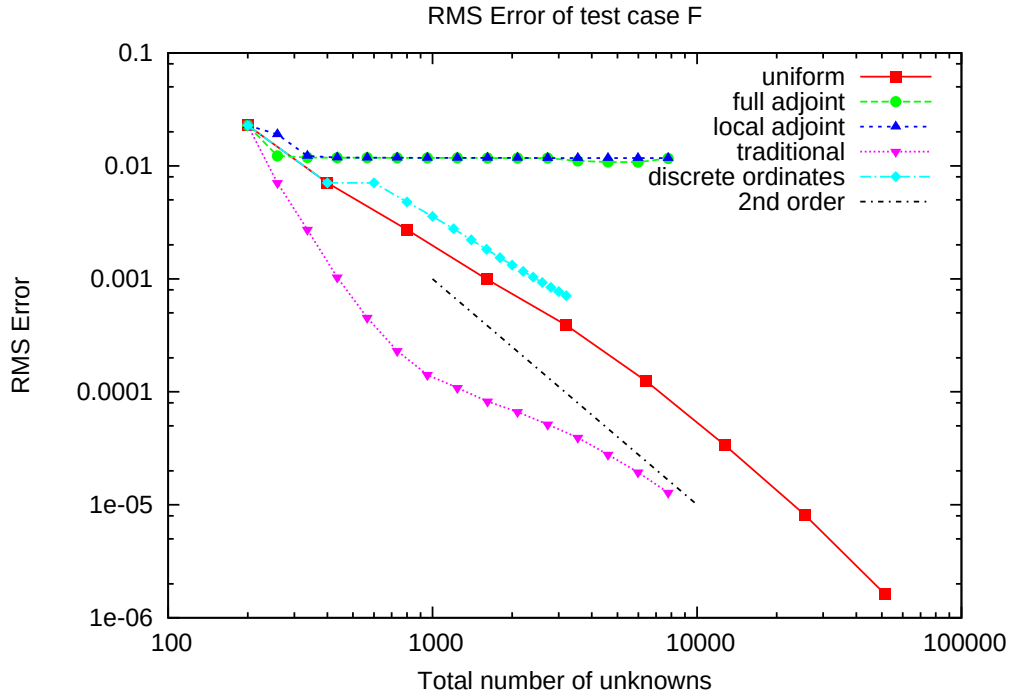

Figure 25: *Node wise root mean square error of scalar flux of test case F. In the root mean square error measure we see the traditional adaptive method being more effective than the goal oriented adaptive methods. The goal of the goal oriented adaptive methods, an accurate detector response, is therefore not the same as an accurate overall solution.*

cases E and H. This shows that the traditional refinement criterion is sensitive to regions where the angular flux is largest.

Finally we remark that the goal oriented adaptive and uniform methods all converge second order in the both error measures, as we would expect from the previous test case. This leads us to believe that using linear basis functions on patches will result in fourth order convergence of these error measures.

7.3 Shielding (cases I and J)

This test case is similar to the previous test case but with an extra shielding region in the middle of the domain. Two types of material are tested which are both optically thick, one is scattering and the other is purely absorbing. So far we have not tested different material properties in one domain, which is done with these tests. The boundaries between the different materials are of interest, as an accurate description of the angular flux is needed at these points for an accurate detector response. For this test case a good performance of the goal oriented adaptive methods was expected. The exact material properties can be found in Appendix A.

Figure 28 holds plots of the detector response error versus the total number of patches. The discrete ordinates method provides us with the largest decrease in error, and again the traditional refinement criterion provides us with the least decrease. The uniform and both goal-oriented methods perform similarly, all resulting in second order convergence. In case J these three methods also result in second order convergence, however the error decrease is slightly larger with the goal-oriented methods. Also in this case the discrete ordinates results in the largest error decrease and the traditional refinement criterion in the least decrease.

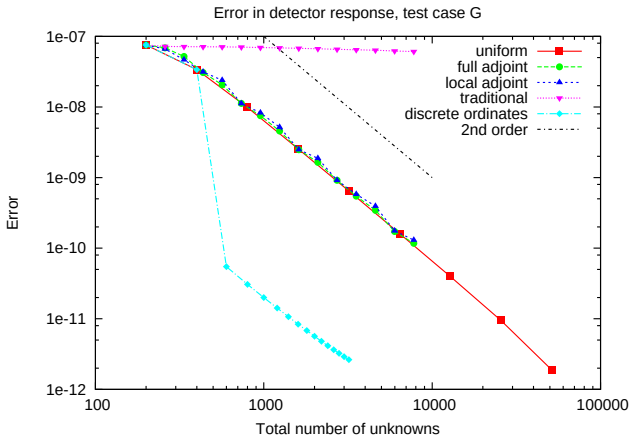

(a) *Thick source boundary detector, test case G.*

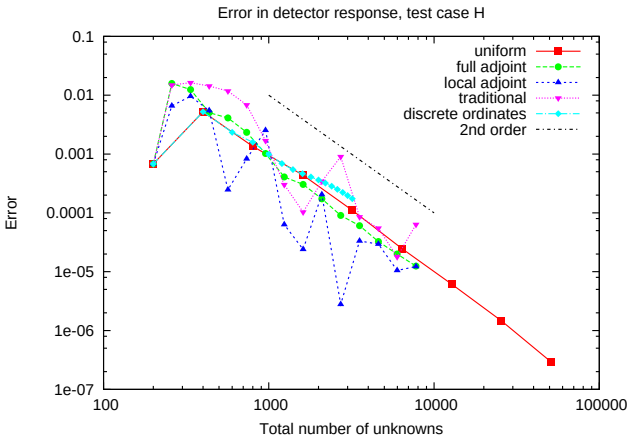

(b) *Thin source boundary detector, test case H.*

Figure 26: *Error in the detector response of the source boundary detector test cases. The behaviour is similar to that of the source volumetric detector test cases.*

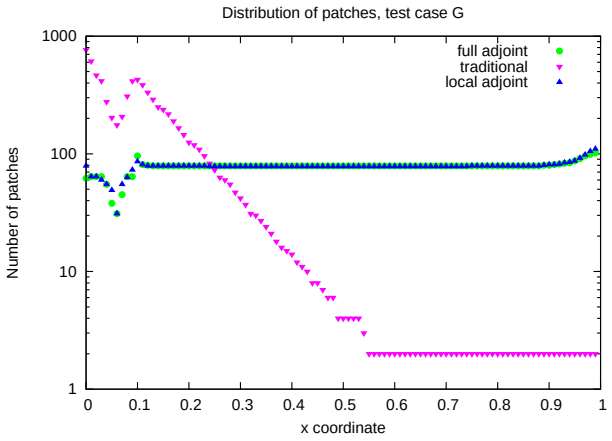

(a) *Thick source boundary detector, test case G.*

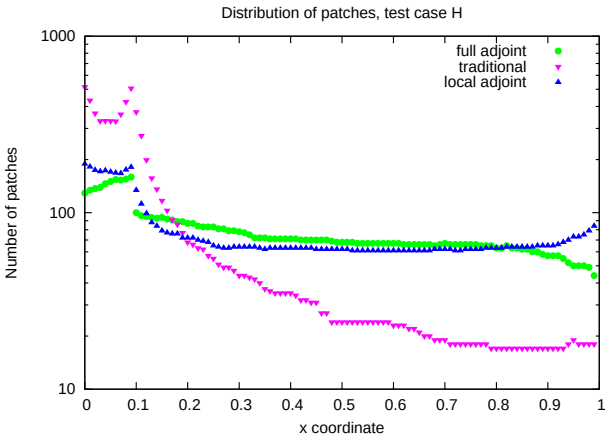

(b) *Thin source boundary detector, test case H.*

Figure 27: *Spatial patch distribution of the source boundary detector test cases. Where in the source volumetric detector test cases the detector is located, no extra refinement takes place in the source boundary detector test cases.*

For the diffusive case I the performance is not as good as expected because the constant patches cannot approximate the linear profile of the angular flux very well. That is, it can approximate it well only by refining many patches. Using linear basis functions on the patches could overcome this, since it will take few basis functions to approximate the linear profile of the angular flux. We have seen this before in other highly scattering cases.

The other case, the fully absorbing shielding test case, has an exponential angular flux profile, which performs better than the scattering case. This is probably due to the fact that constant patches have a problem with the part of the profile with a large derivative. The directions where the angular flux is almost constant do not pose a problem. This is also a recurring observation throughout the test cases.

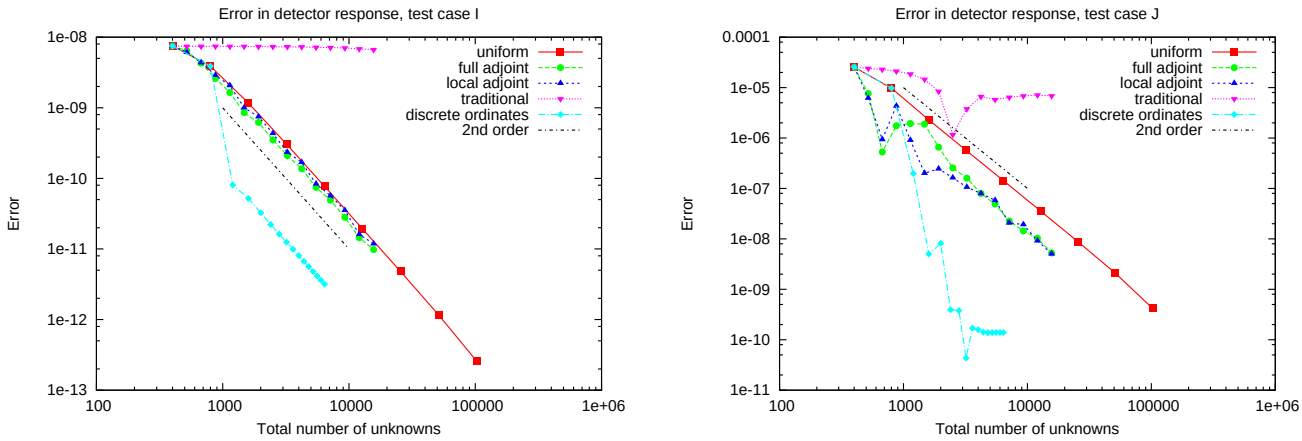

(a) *Test case I, thick highly scattering medium.*

(b) *Test case J, thick absorbing medium.*

Figure 28: *Error in the detector response of the two shielding test cases. Discrete ordinates performs better in diffusive problems, therefore also in this thick scattering case. In the thick absorbing case the set of directions of discrete ordinates give a better approximation of the detector response than that of discontinuous Galerkin.*

It is useful to examine the node wise root mean square error of these test cases. The plots of the decrease of the rms error versus the total number of patches are shown in Figure 29. First of all we see that the uniform refinement strategy converges second order, as is the case in all test cases. We see again that the traditional adaptive method gives a more accurate solution in this error measure, while the goal oriented adaptive methods give a better approximation of the detector response. This fact is also seen in the angular patch distribution, which is shown in Figure 30. This figure shows a plot of the inverse patch size ($1/\Delta\mu$) versus the direction of that patch (μ). Looking at the traditional method we see that directions that are important for getting an accurate scalar flux are refined, which are the directions with positive small μ (there are no negative μ with non zero flux since there is no scatter). The solution of the angular flux improves most when a finer patch structure is used to determine which patches to refine. However, the goal oriented methods mostly refine directions that are important for the detector response, which are directions with a large positive μ are refined, since neutrons travelling in these directions cover the least ground to get to the detector and therefore contribute most to the detector response.

The spatial distribution of patches is shown in Figure 31, where the number of patches in a spatial element is plotted versus the location of that element. In Figure 31(a) one can see that the goal-oriented adaptive methods refine extra near the boundaries of the shielding regions. However, the increase is only small, since many patches are already needed to accurately describe the diffusive behaviour of the medium around the

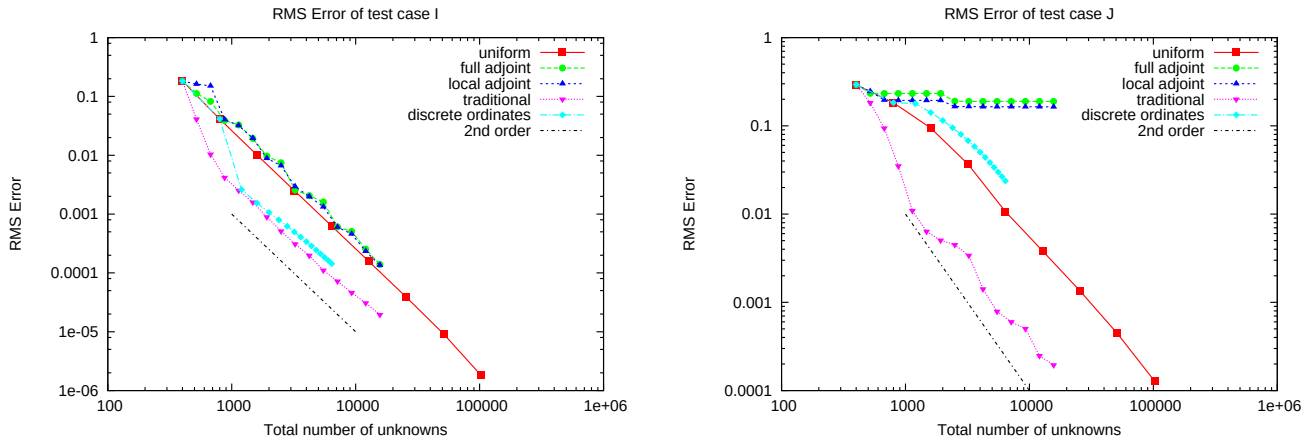

(a) *Test case I, thick highly scattering medium.*

(b) *Test case J, thick absorbing medium.*

Figure 29: *Node wise root mean square error of the scalar flux of the two shielding test cases. The traditional adaptive method provides the most accurate overall solution, in both cases. The goal oriented adaptive methods perform well in the thick scattering case, since all directions are important for an accurate detector response, so the overall solution will be accurate. However in the thick absorbing case only directions toward the detector are important, therefore these methods do not provide an accurate overall solution.*

shielding region. The material of the shielding region can actually be accurately computed with a less fine patch distribution than the medium around it, as this material is mostly absorbing.

Figure 31(b) in contrast has a larger difference between the number patches inside and outside the shielding region. A more coarse patch distribution outside the shielding region suffices to accurately describe the angular flux, however inside the shielding region more patches are needed. An accurate detector response depends on an accurate description of the neutrons that pass through the shielding region, therefore this regions is refined most.

In both shielding test cases we see that the traditional refinement criterion does not help in computing an accurate detector response, as the patches on the right hand side, the detector side of the domain, are not refined at all. The angular flux is very small in this region, which results in only small changes in the angular flux when a patch is refined, as opposed to the left hand side of the domain. Therefore most refinement is around the source region.

7.4 Quality of error estimator

Besides using the error estimate as a criterion for refinement we can also use it as an estimator for the error in the detector response. In many cases the exact error is not available, as we do not have an exact solution to the neutron transport problem. To reliably use the estimator as error indicator we first need to test its performance. This test consists of examining the error ratio, that is the ratio between the estimated and exact error. Since the exact error is not available we will use a reference error, which is computed on a much finer patch distribution. In this section we will look at three test cases (A, E and G) where the estimator behaves differently.

In each of the figures presented here three data sets are plotted, ‘uniform’, ‘full adjoint’ and ‘local adjoint’. We will treat them in reverse order, starting with the local adjoint. The local adjoint criterion consists of the goal-oriented error estimator (see Section 6.2), where the exact adjoint solution is approximated by a local

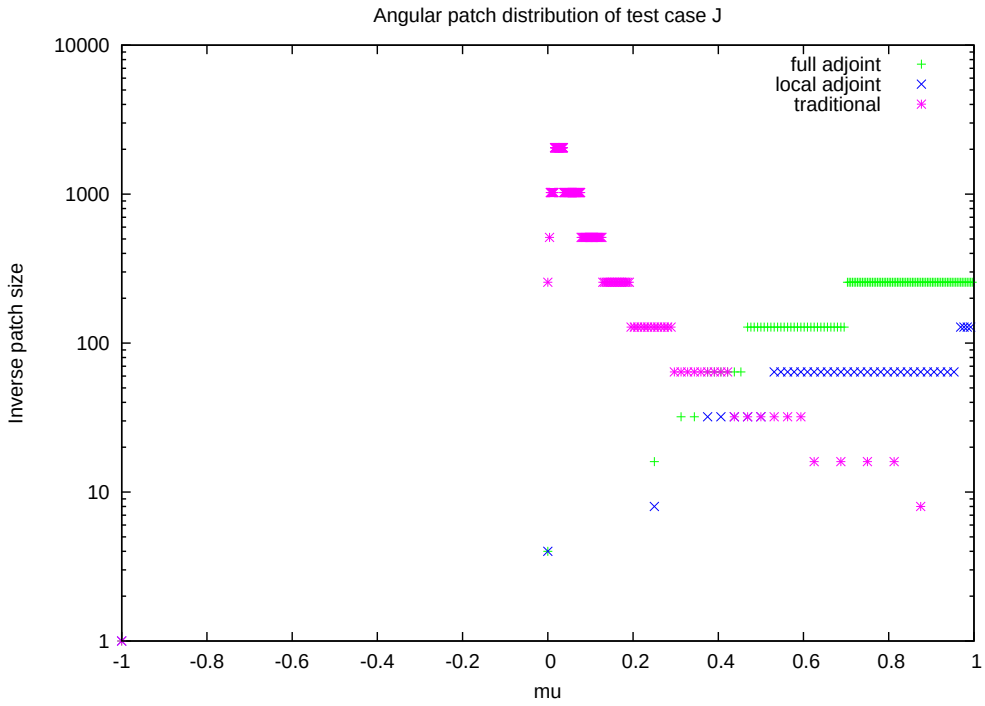

Figure 30: *Angular patch distribution of test case J, thick absorbing shielding problem. This is the distribution at* $x = 0.3$*. Goal oriented methods refine the directoins toward the detector, since those are important for an accurate detector response. The traditional adaptive method refines mostly in other directions, which leads to a more accurate overall soluton. The directions toward the left are not refined since there is no scatter.*

refinement of the associated adjoint patch. That is, to compute the error contribution of a certain patch in the forward patch distribution, we refine the associated adjoint patch once locally, resulting in a representation on one level deeper. Besides using the error estimator the refinement criterion based on the error contribution is also used. Turning to the full adjoint criterion, this method uses the same criterion as the local adjoint, only the exact adjoint solution is now approximated by computing the adjoint solution on a patch distribution that is refined to one level deeper than the forward patch distribution. This results in an adjoint that is computed on a distribution that is globally one level deeper than the forward distribution. The last data set is obtained by using the full adjoint error estimator on a uniform refined patch distribution. This means in each refinement iteration all patches are refined, so the adaptive criterion for refinement is not used. However, we can test the error estimator that is obtained from the adaptive criterion using this patch distribution.

The error ratio's for the thick homogeneous slab, test case A, are shown in Figure 32(a), where the ratio of the error estimator and the reference error is plotted against the total number of patches. We expect the error estimator to asymptotically go to the reference error, this means the ratio should tend to unity. We can see that for case A the ratio tends to unity for the uniform method, however not asymptotically. It is expected that this will happen when linear patches are used, as constant patches cannot approximate linear flux profiles well. The same criterion but with adaptive refinement, the full adjoint case, has somewhat the same behaviour. It has some wiggles, but the trend is the same as the uniform case. In contrast to this, the local adjoint case has a very different behaviour. The ratio lies significantly below the reference error and it even becomes a worse estimator when more patches are used. For this case it cannot be used as an error indicator.

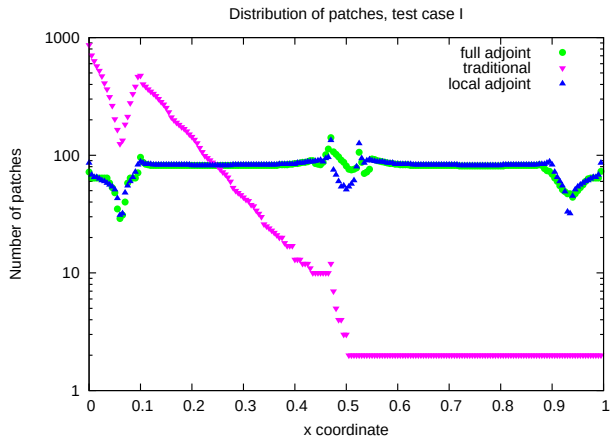

(a) *Spatial patch distribution of test case I, the thick scattering shielding case.*

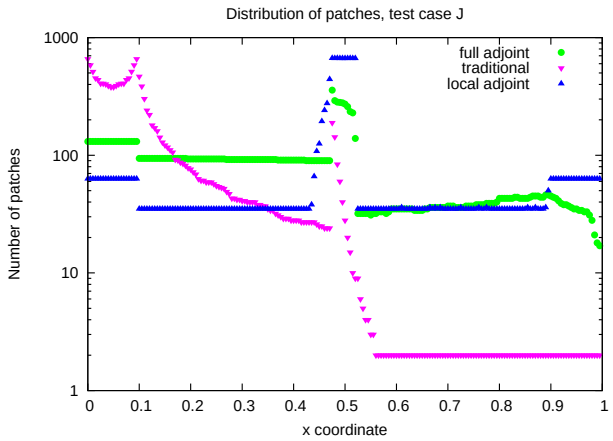

(b) *Spatial patch distribution of test case J, the thick absorbing shielding case.*

Figure 31: *Spatial patch distribution of the shielding test cases. The thick scattering case does not have a large increase in patches in the shielding region, because many patches are already needed to describe the flux in the whole domain, due to the diffusivity. The absorbing case has a large increase in patches, since the shielding region absorbs many more neutrons an accurate solution for the neutrons that travel through is needed to obtain an accurate detector response.*

Turning to test case E, the absorption source detector problem, we see in Figure 32(b) that the full adjoint case does not always provide an accurate error estimator. The error ratio does not tend to unity as patches are refined, which means we cannot use it as a reliable indicator for the error in this case. The uniform refined method still tends to unity, but again not asymptotically. The local adjoint estimator performs even worse in this case, compared to case A. We can certainly not use this as an indicator for the error.

The final case in this section is test case G, the thick boundary detector case. The error ratio's are shown in Figure 32(c). In this case the full adjoint the uniform methods give almost the same error estimator, which tends to unity. However, the local adjoint estimator is still off. In all cases the local adjoint estimator seems to provide us with an underestimate of the error, which cannot be used as an indicator for the error.

An interesting fact is that the local and full adjoint error estimators do not agree on the error estimator, the full adjoint provides us with a reasonably good estimator, while the local adjoint estimator is too much off. The two methods do, however, refine almost the same patches, resulting in similar patch distributions. This can be seen in the patch distribution plots shown earlier. This means that when the error estimator is not important, the local adjoint method, which is cheaper than the full adjoint method, can be used to decide which patches to refine.

7.5 Effects of ratio of refined patches

Usually one takes a ratio of patches to be refined instead of a set number, as the set number gets relatively smaller every refinement iteration. All results in the previous sections were generated with the ratio set to 0.3, in other words 30% of the total number of patches was refined. Every patch that is refined results in two new patches, a net increase of one patch per refined patch. In this section some results on the ratio of patches that is refined in each iteration are presented. This is done for two test cases, the thick homogeneous

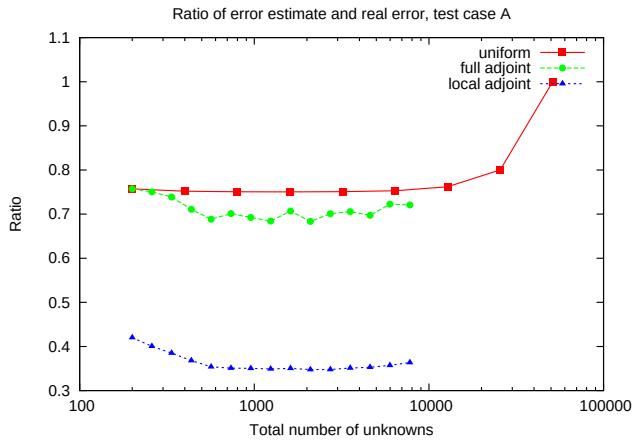

(a) *Ratio of error estimator and reference error of test case A, the thick scattering homogeneous slab problem. The full adjoint gives an accurate error when uniformly refined, the estimator is also quite accurate when refined adaptively. However, the local adjoint estimator gives an inaccurate estimator.*

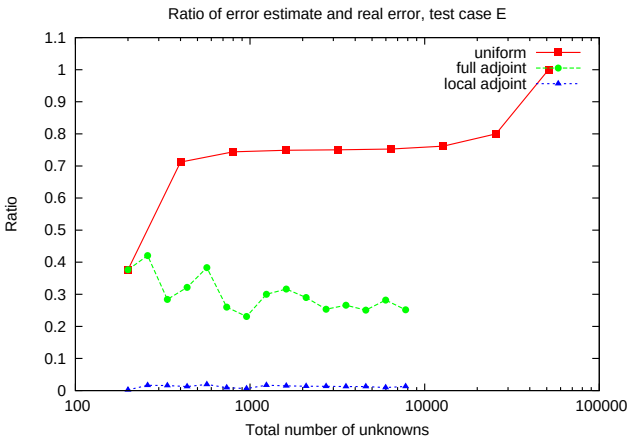

(b) *Ratio of error estimator and reference error of test case E, the absorption source volumetric detector problem. In this case the full adjoint estimator gives an accurate estimator when refinement takes place uniformly, however not when the refinement takes place adaptively. The local adjoint estimator does not provide an accurate estimator.*

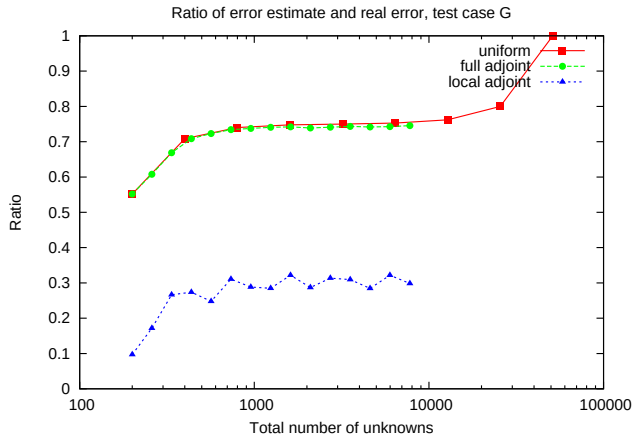

(c) Ratio of error estimator and reference error of test case G, the thick source boundary detector problem. The full adjoint refinement criterion gives us an accurate estimator, in contrast to the local adjoint estimator.

Figure 32: *Ratio's of error estimators and reference error. The reference error is computed using a very deep refinement, much deeper than where the tests took place.*

slab case A (called RA) and the thin source detector case D (called RD). The figures here show plots of the detector response error versus the total number of patches for different methods. The effects of the ratio of refined patches is investigated for the following percentages, 1%, 5%, 10%, 20%, 30% and 40%. For reference purposes we included the data sets of the uniform and discrete ordinates method, as well as a line representing second order convergence.

For the thick scattering homogeneous slab test case (case RA), there is little difference to be seen in Figure 33. The symmetry and homogeneity of the problem are the likely cause of this. This means we can best choose

a large refinement ratio in this case, as this takes least time to be computed. We can, so to speak, get away with a large ratio of patches refined in each iteration. This is due to the fact that we saw that large regions in the domain are refined, it is not very concentrated (see Figure 22(a)).

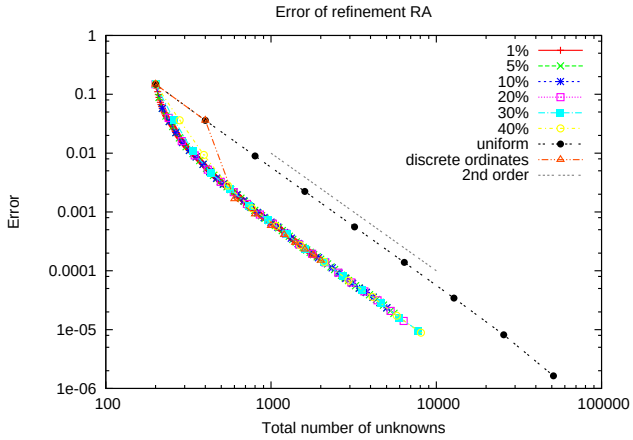

(a) *Full adjoint estimator.*

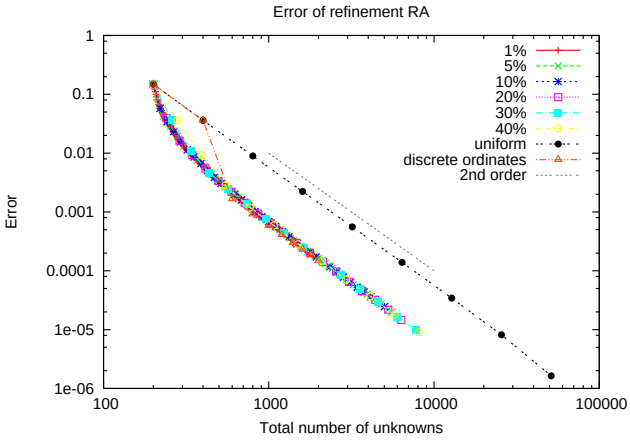

(b) *Local adjoint estimator.*

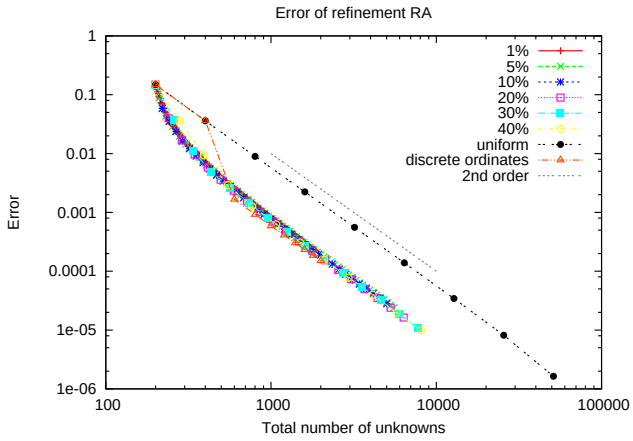

(c) *Traditional estimator.*

Figure 33: *Error of test case A, for different refinement ratio's, per refinement method. All methods perform the same, which is probably due to the uniformity and homogeneity of the problem.*

Turning to test case RD, the source detector with a thin scattering material, we see that the refinement ratio affects the accuracy. There is much variation of the error decrease within each method, however we can see that a ratio of refinement between five and thirty per cent generally seems to result in the largest error decrease for the two goal-oriented adaptive methods. In the traditional method we see that the forty per cent method results in the largest decrease, however the variability of this method is large. In the previous data points it does not perform better than other methods.

Furthermore note the dip in the error around three hundred patches, this is due to a sign change in the difference between the computed and the reference detector response. Since we defined the detector response error measure as the absolute value of that difference, we see it as a dip in the error.

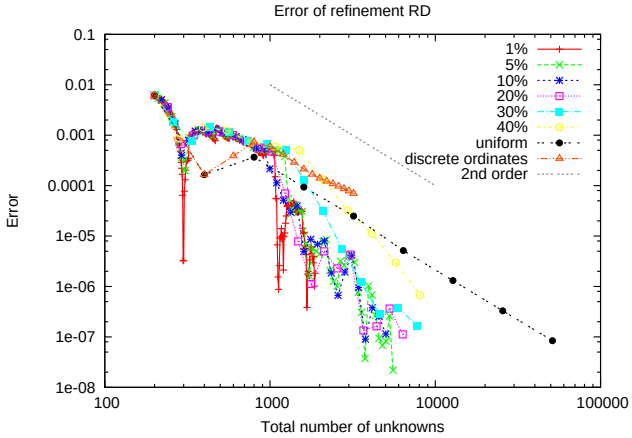

(a) *Full adjoint estimator.*

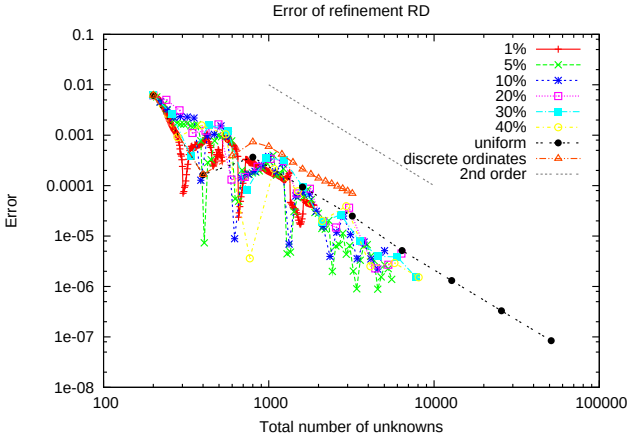

(b) *Local adjoint estimator.*

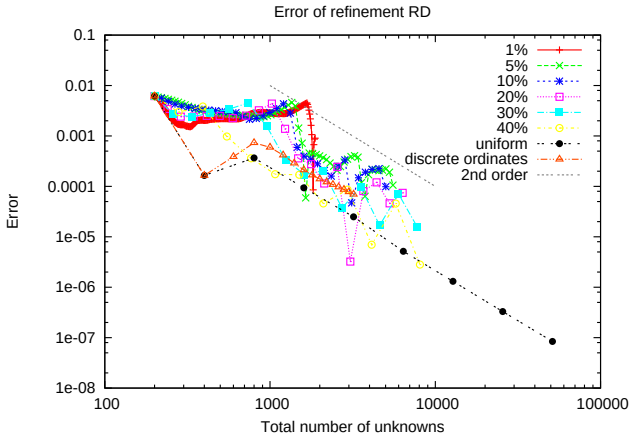

(c) *Traditional estimator.*

Figure 34: *Error of test case D, for different refinement ratio's, per refinement method. In most cases refining between 5% and 30% is most effective. However, a smaller percentage needs more iterations which takes more time. In the full adjoint error there is a sign change around 300 patches, which explains the dip in the error.*

8 Discussion

In this discussion section we will first present the main conclusions of this work, roughly in order of occurrence. The first part will be on the theoretical results we obtained in Section 3, the discretization of the neutron transport equation. Thereafter the conclusions of the uniform tests will be presented, these conclusions are on the behaviour of the uniform discontinuous Galerkin method compared to the widely used discrete ordinates method. Finally the results of the various adaptive algorithms is presented, where the comparison is made between traditional and goal-oriented refinement criteria. The second part of this chapter is a short elaboration of future work that can be done to further investigate the possibilities of the discontinuous Galerkin method.

8.1 Main conclusions

8.1.1 Theoretical results

Three different discretization methods were investigated on their ability to handle adaptivity and their feasibility of implementation in this work: the widely used discrete ordinates method, a discontinuous Galerkin method with wavelets as basis functions (wavelet method) and a discontinuous Galerkin method with polynomial basis functions (discontinuous Galerkin method).

The discrete ordinates method cannot handle adaptivity well, as most quadrature sets do not allow for directions to be added without altering the complete set of directions. The wavelet and discontinuous Galerkin method were therefore investigated as alternatives that do allow for adaptive algorithms, since both methods have a hierarchical structure of basis functions. For several reasons we preferred the discontinuous Galerkin method to the wavelet method. First of all the wavelet method resulted in a large non-sparse matrix equation that needs to be solved for each spatial element. This means that for fine wavelet distributions large filled matrices will have to be solved, which comes at high computational cost.

In the discrete ordinates description we showed that a cheap algorithm to solve the equation an be used, source iteration combined with a sweep algorithm. Since this algorithm is so cheap, we investigated the possibilities of using this algorithm in the adaptive algorithm, which is only partly possible in the wavelet method. Source iteration is still possible, but since the wavelets are not independent of each other we cannot apply the sweep algorithm. However, we found that both source iteration and the sweep algorithm can be applied in the discontinuous Galerkin method.

The third and last reason is that the discontinuous Galerkin method provides us with a much more flexible discretization than the wavelet method does. Polynomial basis functions can relatively easily be used to obtain higher order basis functions, which should lead to higher order convergence. The order of convergence of a certain wavelet as basis function is harder to predict. Also we found that the choice of wavelets largely depends on the ability to approximate spherical integrals on the wavelets well.

8.1.2 Uniform results

We compared the performance of the discontinuous Galerkin method with discrete ordinates by refining all patches uniformly. This test is a comparison between the set of directions obtained from the discontinuous Galerkin method and the set of quadrature directions of discrete ordinates. In general discrete ordinates provides us with a larger decrease in error than the discontinuous Galerkin method for the same number of unknowns in the discrete problem. This is due to two effects: the linear angular flux profile in diffusive materials and the performance of the set of directions when there is no coupling between the directions from scatter, which we will elaborate below.

The discontinuous Galerkin method was tested with constant basis function on the patches and linear basis functions on the spatial elements. The constant patches cannot approximate a linear flux profile well with few patches, while discrete ordinates does not need many directions to describe this flux profile well. We expect the discontinuous Galerkin method to perform much better in diffusive materials when linear basis functions are used on the patches.

When the scatter cross section is zero, $\sigma_s = 0$, there is no coupling between the discrete directions. A purely absorbing test problem is therefore a test of the performance of the distribution of directions on the angular domain. The discontinuous Galerkin patches are distributed uniformly throughout this domain, while the Gauss Legendre quadrature results in a larger density of directions around $\mu = 1$ and $\mu = -1$ than around $\mu = 0$. As expected this lead to an advantage of discrete ordinates in domains with a separate source and detector region. The neutrons that cover least ground to get to the detector are most important, as the likelihood of absorption is the smallest. The discrete ordinates methods gives a more accurate description of these neutrons.

In one kind of material the discontinous Galerkin method provided us with a larger decrease in error than the discrete ordinates method, for the same number of unknowns in the discrete problem. In thin scattering materials the effects of neutrons leaking from the domain through the vacuum boundaries propagate deeply into that domain. The angular flux around these vacuum boundaries is discontinuous at $\mu = 0$. The discontinuous Galerkin method can easily describe this discontinuity, as discontinuities are inherent to this method. However, the discrete ordinates method with the Gauss Legendre quadrature cannot handle discontinuities well. The discrete ordinates method could possibly perform better than the discontinuous Galerkin method when a double Gauss Legendre quadrature is used, which is discontinuous at $\mu = 0$. However, when we look at three-dimensional problems, the discontinuities in the angular flux can be anywhere on the sphere (depending on the shape of the domain). Discontiuous Galerkin will be more accurate than a discrete ordinates method in that case.

In all test cases (homogeneous slab and source detector geometries) and for both error measures, detector response error and node wise root mean square error, we showed that the discontinuous Galerkin method with constant basis functions on patches results in second order convergence. We therefore expect linear basis functions on patches to result in fourth order convergence.

8.1.3 Adaptive results

Using the dual or adjoint problem of the neutron transport equation, we derived an error estimator for the detector response error. In this derivation we expressed the estimator as a sum of contributions to the error of individual patches. This provided us with a goal-oriented refinement criterion to decide which patches will be refined, as the contribution of patches with the largest contribution is likeliest to decrease most when refined. Another refinement criterion was formulated using the change in the angular flux when a local refinement is performed. The refinement of the patches with the largest change in the angular flux are kept, the other patches are coarsened to their original distribution. This is called the traditional refinement criterion.

In general the goal-oriented adaptive algorithms performed well and decreased the detector response error quicker than uniform refinement, for the same number of unknowns. The largest gain from goal-oriented adaptive methods is seen when the spatial distribution of patches of the adaptive methods is not flat. When it is flat the uniform refinement is actually almost the optimal way of refinement. Comparing the goal-oriented adaptive algorithms with the discrete ordinates method we showed that in diffusive problems discrete ordinates still reduces the error more than the adaptive methods.

Two error measures were used to compare the goal-oriented and traditional adaptive methods, the error in the detector response and the node wise root mean square error of the scalar flux. We showed that the goal-

oriented adaptive methods result in a more accurate detector response than the traditional method does. In the other error measure, the rms error, we showed that the traditional method provides us the smallest error. This behaviour can be expected from the error measures, to get an accurate detector response the angular flux needs to be accurate around the detector. The traditional method does not take that into account, while the goal-oriented methods do. To obtain an overall accurate angular flux it suffices to look at the largest change in angular flux as refinement criterion.

The goal-oriented adaptive methods showed second order convergence for the detector response error measure. We therefore expect the convergence to be fourth order for linear patches with the goal-oriented adaptive methods.

Besides using the error estimators as a refinement criterion we investigated their use as indicator of the error. We can use the estimator that uses the full adjoint reliably in most cases. However, the local adjoint estimator never provides a reliable indicator to the error. The ratio of the full adjoint error estimator and the real error (which is approximated by a calculation on a much finer patch distribution) tends to unity, but not asymptotically. This is likely due to the fact that constant patches are used, using linear patches could improve this. Although the local adjoint estimator cannot be used as a reliable error estimate, the refinement criterion refines almost the same patches as the full adjoint estimator, making it a reliable refinement criterion.

The number of patches, given as a percentage, that is refined in each refinement iteration does not greatly affect the performance of the adaptive methods, when the error decrease at a certain number of unknowns is compared. In general the best results were obtained when a percentage between five and thirty is used. However, using larger refinement ratio's does result in a faster algorithm, as less refinement iterations are needed to reach a large error reduction. Therefore thirty per cent seems to be around the ideal ratio.

8.2 Future work

In the conclusions above we have seen that constant basis functions on patches do not provide a good description of the angular flux in diffusive materials. The angular flux profile is linear in these cases. Using linear basis functions on the patches is therefore expected to greatly enhance the performance in diffusive materials. Also in other materials the rate of convergence should be larger.

Introducing linear patches means that we need to solve more unknowns for each patch. This leads to a matrix equation that is four by four, instead of two by two. No other major changes will have to be made, although the calculation of the scalar flux and error contribution will have to be altered.

As all test cases were one-dimensional problems in this project, it is interesting to investigate how the discontinuous Galerkin method performs in two or three dimensions. In more dimensions one expects that goal-oriented adaptive methods will be relatively more efficient, compared to the uniform refinement. In one dimension neutrons can travel only two ways, left and right. In a source detector geometry all neutrons that travel, for example, to the right are important for an accurate detector response. In three dimensions the relative amount of neutrons that travel towards a small detector will be much smaller than in these one-dimensional test problems.

There are three main issues to be examined when expanding the model to three dimensions. The first is the patch distribution on the sphere, in three dimensions there is much more freedom to chose a patch structure. The evaluation of the angular integrals is more complicated and will have an effect on the choice of the patch distribution. Another issue is the sweep algorithm, which could be implemented in different ways. The easiest is to use a set of 'basis directions' that determine the order in which patches that lie in a certain octant of the sphere are computed. A more natural way seems to be to find the patches in the problem of which the upwind neighbouring patch is already updated. Since patches are independent of each other we can choose to update them only when the upwind patch is already updated. The final issue is practical, as in three dimensions the

number of unknowns grows roughly cubic with the inverse element size. It should be investigated whether it is still feasible to let each spatial element have its own angular patch distribution. An alternative would be to divide the domain into regions that have the same angular patch distribution.

The discontinuous Galerkin approach for both the angular and spatial dependence of the problem results in a description of the flux on the whole sphere, as opposed to the discrete ordinates method. This can be useful for solving other kinds of transport equations, for example the Fokker Planck equation. This equation can be used to describe charged particle transport. To get to the Fokker Planck equation from the transport equation used in this work a term that describes diffusion in the angular variables is introduced after a derivation using statistical physics. To get a physical interpretation of why adding this term leads to an equation for charged particle transport, think of a pencil beam of electrons. This beam, as the electrons travel through space, will become diffuse. The directions the electrons travel in spread slowly across the sphere, which can be described by a diffusion term. The discontinuous Galerkin method can be useful for solving this equation.

References

[1] Wolfgang Bangerth and Rolf Rannacher. *Adaptive finite element methods for differential equations*. Birkäuser Verlag, 2003. ISBN 3-7643-7009-2.

[2] Christian Blatter. *Wavelets: a primer*. CRC Press, January 1999. ISBN 1-5688-1095-4.

[3] A.G. Buchan, C.C. Pain, M.D. Eaton, R.P. Smedley-Stevenson, and A.J.H. Goddard. Linear and quadratic octahedral wavelets on the sphere for angular discretisations of the boltzmann transport equation. *Annals of Nuclear Energy*, 32:1224–1273, January 2005.

[4] Liangzhi Cao, Hongchun Wu, and Youqi Zheng. Solution of neutron transport equation using Daubechies' wavelet expansion in angular discretization. *Nuclear engineering and design*, 238:2292–2301, March 2008.

[5] Stephan Dahlke, Wolfgang Damen, Ilona Weinreich, and Eberhard Schmitt. Multiresolution analysis and wavelets on S^2 and S^3. *Numerical functional analysis and optimization*, 16(1):19–41, 1995.

[6] James J. Duderstadt and Louis J. Hamilton. *Nuclear Reactor Analysis*. John Wiley and Sons, 1942. ISBN 0-471-22363-8.

[7] Joshua J. Jarell and Marvin L. Adams. Discrete-ordinates quadrature sets based on linear discontinuous finite elements. In *International conference on mathematics and computational methods applied to nuclear science and engineering*, Rio de Janeiro, RJ, Brazil, May 2011. American Nuclear Society (ANS). ISBN 978-85-63688-00-2.

[8] Danny Lathouwers. Goal oriented spatial adaptivity for the S_N equations on unstructured triangular meshes. *Annals of Nuclear Energy*, 38:1373–1381, January 2011.

[9] E.E. Lewis and W.F. Miller. *Computational methods of neutron transport*. Wiley-Interscience, 1984. ISBN 0-471-09245-2.

[10] Peter Schröder and Wim Sweldens. Efficiently representing functions on the sphere, 1995.

[11] Joseph C. Stone and Marvin L. Adams. Adaptive discrete-ordinates algorithms and strategies. In *Mathematics and computation, supercomputing, reactor physics and nuclear and biological applications*, Palais des Papes, Avignon, France, September 2005. American Nuclear Society (ANS).

[12] Joseph C. Stone and Marvin L. Adams. Adaptive discrete-ordinates algorithms and strategies. In *Mathematics and computation, supercomputing, reactor physics and nuclear and biological applications*, page 5/12, Palais des Papes, Avignon, France, September 2005. American Nuclear Society (ANS).

[13] Todd A. Warening, John M. McGhee, Jim E. Morel, and Shawn D. Pautz. Discontinuous finite element S_N methods on three-dimensional unstructured grids. *Nuclear Science and Engineering*, 138:256–268, 2001.

[14] James S. Warsa. A continuous finite element-based, discontinuous finite element method for S_N transport. *Nuclear Science and Engineering*, 160:385–400, March 2008.

A Test Cases

Here we present the test cases used throughout this work, with specified geometries and material properties. For each test case we supply a short description, expected result, geometry and material properties. In the geometry diagram blue represents a volumetric source and green represents a volumetric detector.

A.1 Case A, Thick slab

The first test case is a uniform slab with a homogeneous source and detector. It is optically thick, which means that the neutrons have a small mean free path. The dimension of the slab is $1\ cm$. In Figure 35 a diagram of the geometry can be found and in Table 2 the material properties are listed. The boundary conditions of the slab are vacuum boundaries on both sides.

Since the boundary conditions are hard to satisfy properly it is expected that the mesh near the edges of the slab will be very fine.

Figure 35: *Homogeneous slab geometry.*

σ_t	$100\ cm^{-1}$
σ_s	$99\ cm^{-1}$
Source	$1\ cm^{-1}s^{-1}rad^{-1}$
Detector	$4\pi\ cm^{-1}$

Table 2: *Material properties for test problem A*

A.2 Case B, Thin slab

Test case B is again a homogeneous slab with the same dimensions as the test cases above. However, since the total cross section is much lower the mean free path of the neutrons is larger, which makes this an optically thin problem. Again the geometry can be found in Figure 35, while the material properties can be found in Table 3. This test case also has vacuum boundary conditions on both sides.

Refinement is expected to be similar to the refinement in test case A, although the effects of the edges will propagate much further into the domain, as this is an optically thin problem.

A.3 Case C, Thick source detector

This test case has a separate source and detector region in a homogeneous material. The boundaries of this slab geometry are again vacuum boundaries. A diagram of the geometry can be found in Figure 38. The material properties are listed in Table 4.

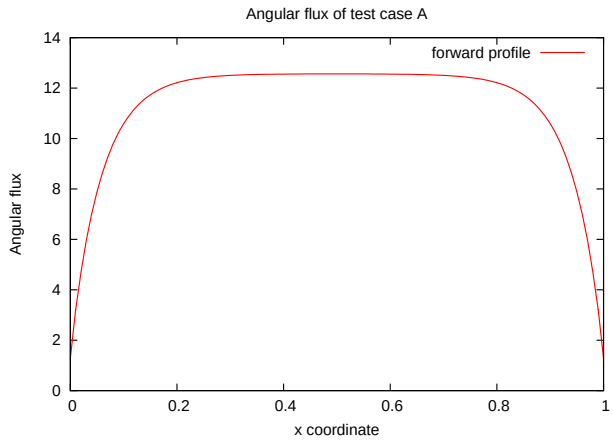

(a) *Solution of the forward scalar flux of test case A*

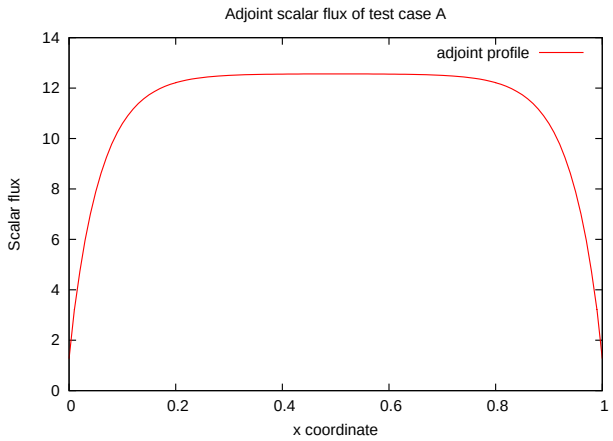

(b) *Solution of the adjoint scalar flux of test case A*

Figure 36: *Forward and adjoint solution of test case A.*

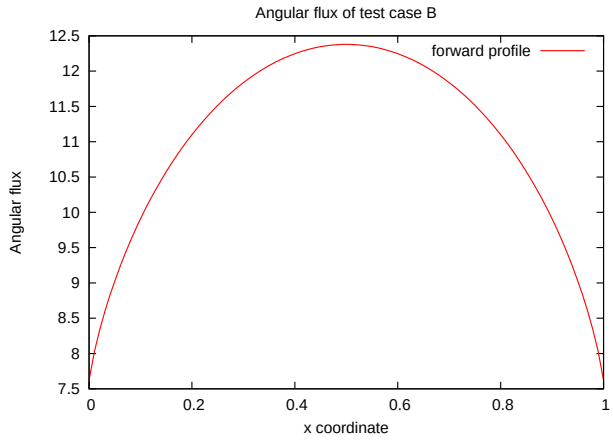

(a) *Solution of the forward scalar flux of test case B*

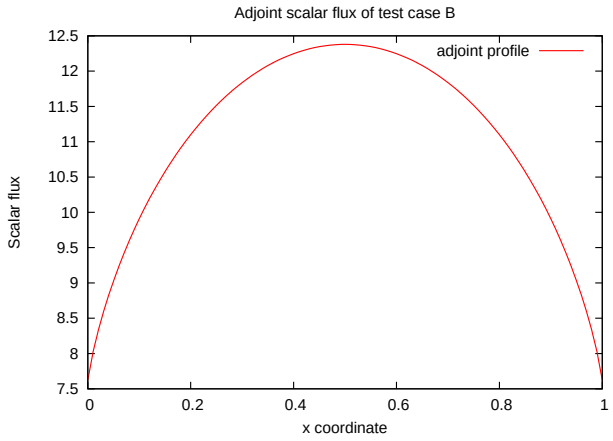

(b) *Solution of the adjoint scalar flux of test case B*

Figure 37: *Forward and adjoint solution of test case B.*

σ_t	$1\ cm^{-1}$
σ_s	$.5\ cm^{-1}$
Source	$1\ cm^{-1}s^{-1}rad^{-1}$
Detector	$4\pi\ cm^{-1}$

Table 3: *Material properties for test problem B*

In this test case it is important to have an accurate solution in the source and detector regions. Since the source is at the left hand side of the domain we also need an accurate solution of right going directions. Therefore we expect refinement in the detector source and regions, as well as refinement of right going directions.

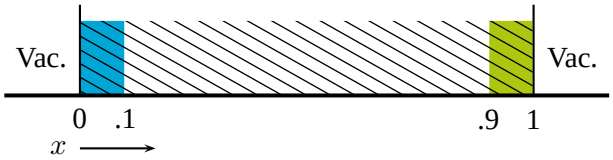

Figure 38: *Source detector slab geometry.*

σ_t	$100\ cm^{-1}$
σ_s	$99\ cm^{-1}$
Source	$1\ cm^{-1}s^{-1}rad^{-1}$
Detector	$4\pi\ cm^{-1}$

Table 4: *Material properties for test problem C*

A.4 case D, Thin source detector

This test case is also a source detector problem, but now with optically thin material. An illustration of the geometry can be found in Figure 38. Table 5 lists the material properties.

The expected behaviour is similar to that of test case C. However, since this is an optically thin problem the effects of the edges will propagate much further into the domain.

σ_t	$1\ cm^{-1}$
σ_s	$.5\ cm^{-1}$
thickness	$1\ cm$
Source	$1\ cm^{-1}s^{-1}rad^{-1}$
Detector	$4\pi\ cm^{-1}$

Table 5: *Material properties for test problem D*

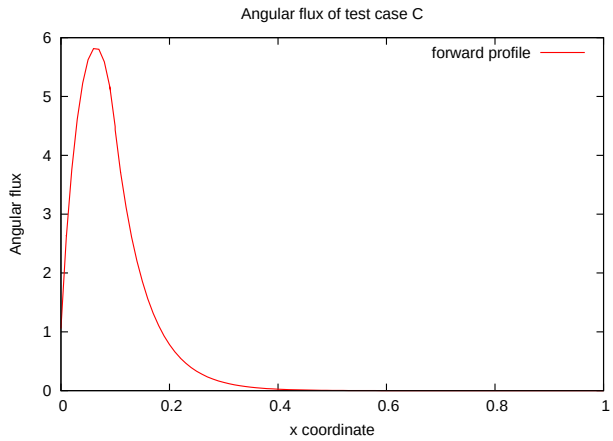

(a) *Solution of the forward scalar flux of test case C*

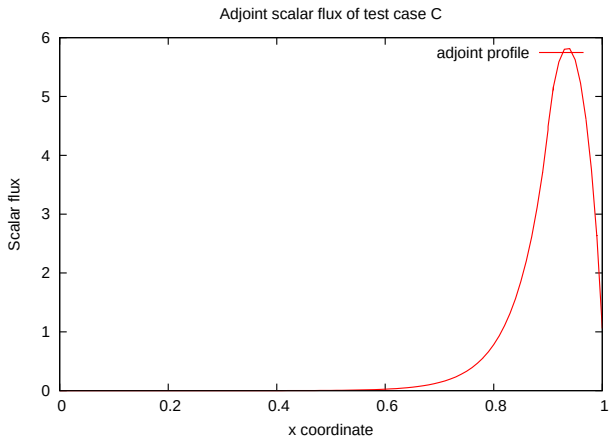

(b) *Solution of the adjoint scalar flux of test case C*

Figure 39: *Forward and adjoint solution of test case C.*

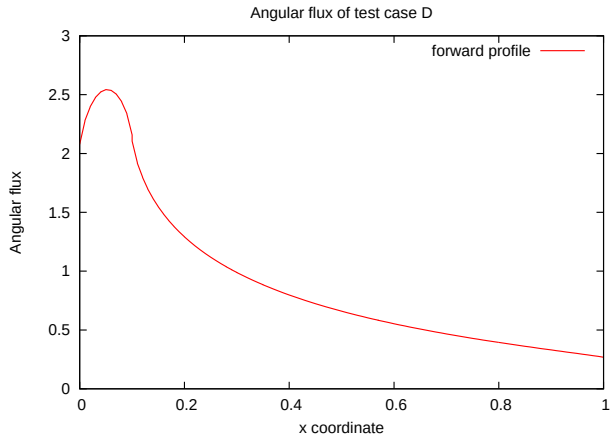

(a) *Solution of the forward scalar flux of test case D*

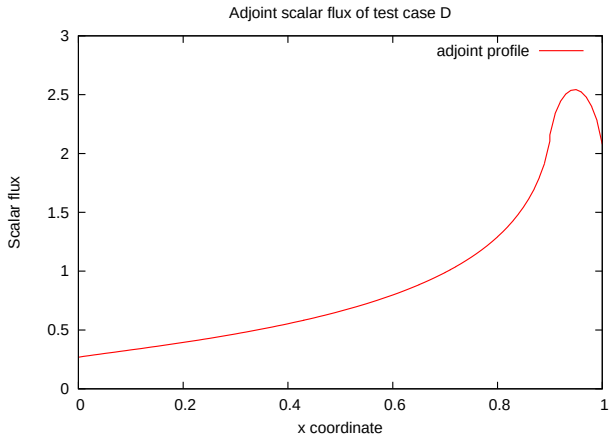

(b) *Solution of the adjoint scalar flux of test case D*

Figure 40: *Forward and adjoint solution of test case D.*

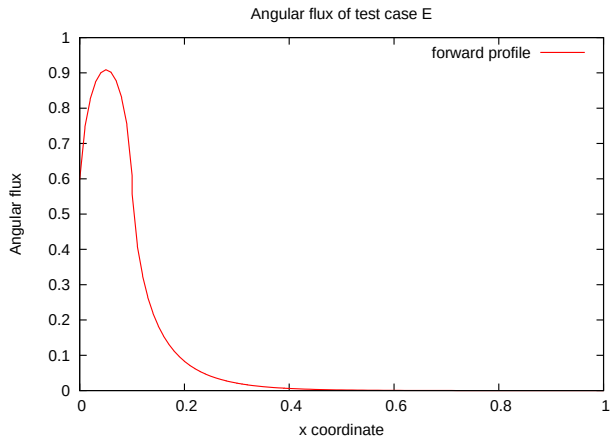

(a) *Solution of the forward scalar flux of test case E*

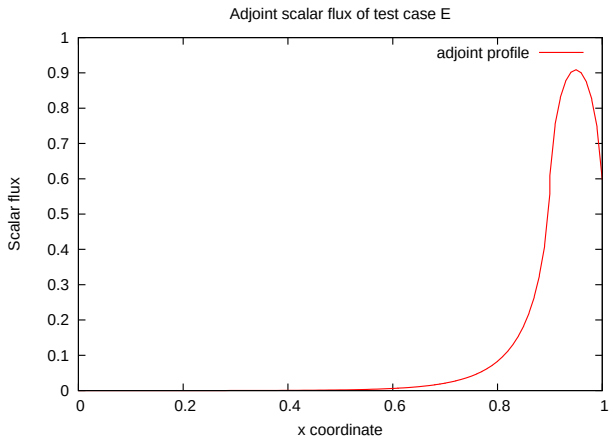

(b) *Solution of the adjoint scalar flux of test case E*

Figure 41: *Forward and adjoint solution of test case E.*

A.5 Case E, Highly absorbing source detector

This is also a source detector geometry as shown in Figure 38. However, the homogeneous material that is used in this problem is strongly absorbing. The material properties are listed in Table 6.

In this test case we expect the same results as for test case C, as this is also an optically thick problem.

σ_t	$10\ cm^{-1}$
σ_s	$1\ cm^{-1}$
Source	$1\ cm^{-1}s^{-1}rad^{-1}$
Detector	$4\pi\ cm^{-1}$

Table 6: *Material properties for test problem E*

A.6 Case F, Purely absorbing source detector

Test case F is the last separate source detector geometry as shown in Figure 38. The material is now purely absorbing, which means there is no scatter source in the right hand side of the transport equation. The material properties of this test case are listed in Table 7.

In this case there is no coupling between directions through the scatter, which will yield results on the choice of directions of the discontinuous Galerkin method.

σ_t	$10\ cm^{-1}$
σ_s	$0\ cm^{-1}$
Source	$1\ cm^{-1}s^{-1}rad^{-1}$
Detector	$4\pi\ cm^{-1}$

Table 7: *Material properties for test problem F*

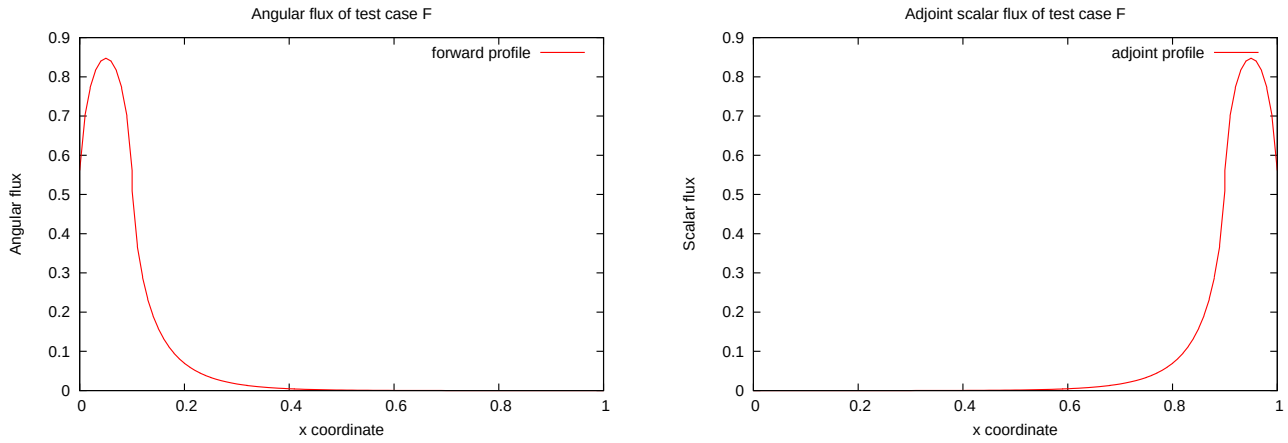

(a) *Solution of the forward scalar flux of test case F*

(b) *Solution of the adjoint scalar flux of test case F*

Figure 42: *Forward and adjoint solution of test case F.*

A.7 Case G, Thick boundary detector

Test case G is similar to test cases C, D, E and F, only the volumetric detector has been removed and the right boundary of the domain is a detector. The material properties are listed in Table 8. Also the forward and adjoint solution of this problem can be found in Figure 44. In Figure 43 the geometry of this test case is shown.

We expect the behaviour around the source to be the same as in the source volumetric detector cases. However, since the detector is at the boundary of the domain we do not expect much refinement to be needed at that end of the domain. There does not need to be an accurate solution of the flux in a region, only the current of neutrons is important near the edge of the domain.

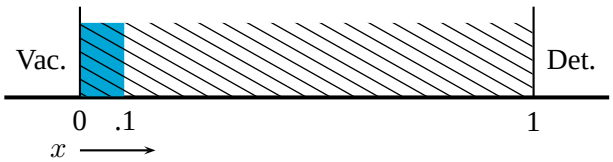

Figure 43: *Separate source and boundary detector geometry.*

σ_t	$100\ cm^{-1}$
σ_s	$99\ cm^{-1}$
Source	$1\ cm^{-1}s^{-1}rad^{-1}$

Table 8: *Material properties for test problem G*

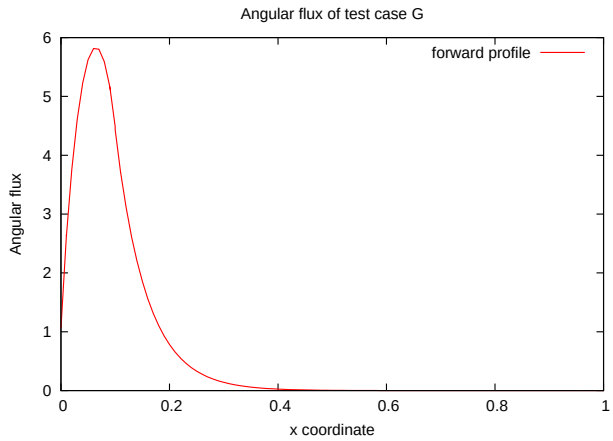

(a) *Solution of the forward scalar flux of test case G*

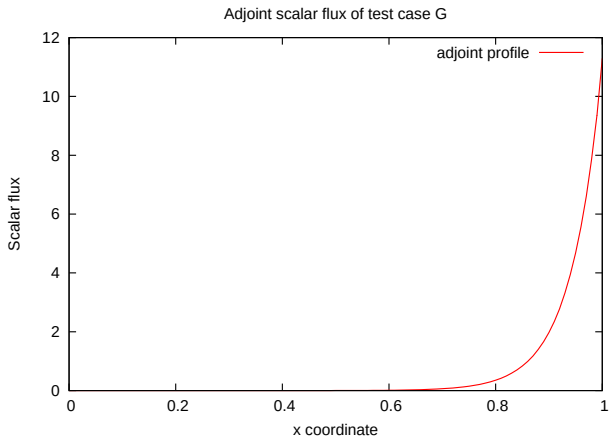

(b) *Solution of the adjoint scalar flux of test case G*

Figure 44: *Forward and adjoint solution of test case G.*

A.8 Case H, Thin boundary detector

The geometry of this test case is the same as that of test case G and is shown in Figure 43. However, the material properties are different and are listed in Table 9. The forward and adjoint solution for this test case can be found in Figure 45

σ_t	$1\ cm^{-1}$
σ_s	$0.5\ cm^{-1}$
Source	$1\ cm^{-1}s^{-1}rad^{-1}$

Table 9: *Material properties for test problem H*

A.9 Case I, Shielding

This test case is an extension of test case C. There is again a separate source and detector, however, the detector is behind a shield. A region of $0.05\ cm$ in the middle of the slab has a large total cross section, making it a neutron shield. The properties of the other regions remain the same. A diagram of the geometry is shown in Figure 46. The material properties are listed in Table 10, the source and detector are only present in the specified regions.

As this test case is similar to test case C we expect the refinement to be almost the same. Only the source region is not very important now, as only a few neutrons will traverse the shielding. Therefore it is more important to get an accurate flux in the shielding region. It is expected that refinement takes place in the shielding and detector region, as well as for right going directions.

A.10 Case J, Purely absorbing shielding

Test case H has the same geometry as the previous test case, shown in Figure 46. Now both the medium and the neutron shield are purely absorbing. The material properties are listed in Table 11.

Expectations on refinement are the same as in the other shielding test case, case I.

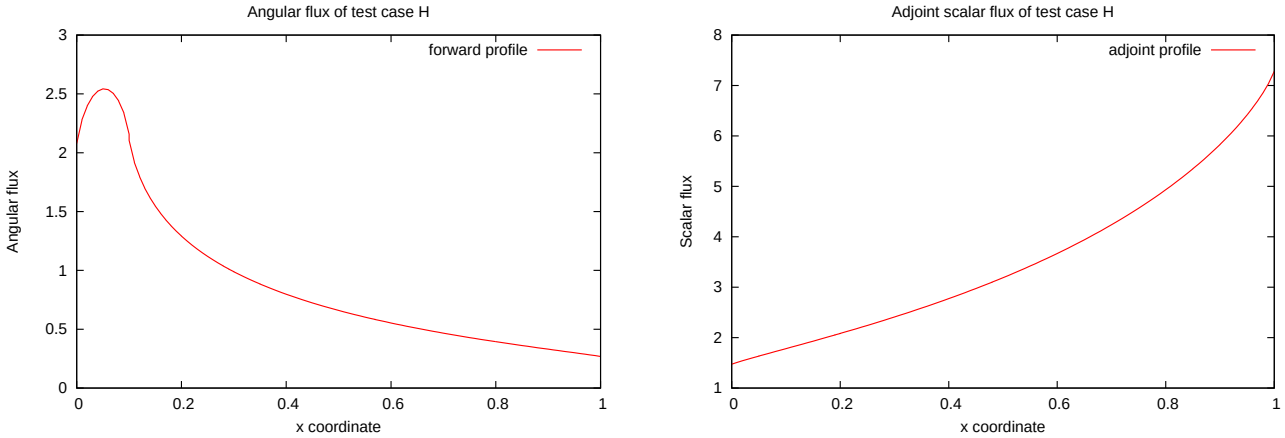

(a) *Solution of the forward scalar flux of test case H*

(b) *Solution of the adjoint scalar flux of test case H*

Figure 45: *Forward and adjoint solution of test case H.*

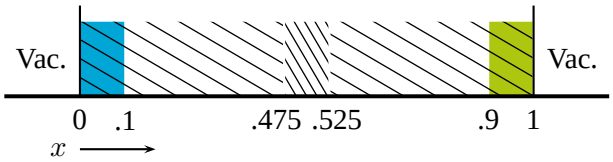

Figure 46: *Shielding slab geometry.*

Property	Material	Shielding
σ_t	$100\ cm^{-1}$	$50\ cm^{-1}$
σ_s	$99\ cm^{-1}$	$5\ cm^{-1}$
thickness	$2 \times .475\ cm$	$0.05\ cm$
Source	$1\ cm^{-1}s^{-1}rad^{-1}$	$0\ cm^{-1}s^{-1}rad^{-1}$
Detector	$4\pi\ cm^{-1}$	$0\ cm^{-1}$

Table 10: *Material properties for test problem I.*

Property	Material	Shielding
σ_t	$1\ cm^{-1}$	$100\ cm^{-1}$
σ_s	$0\ cm^{-1}$	$0\ cm^{-1}$
thickness	$2 \times .475\ cm$	$0.05\ cm$
Source	$1\ cm^{-1}s^{-1}rad^{-1}$	$0\ cm^{-1}s^{-1}rad^{-1}$
Detector	$4\pi\ cm^{-1}$	$0\ cm^{-1}$

Table 11: *Material properties for test problem J*

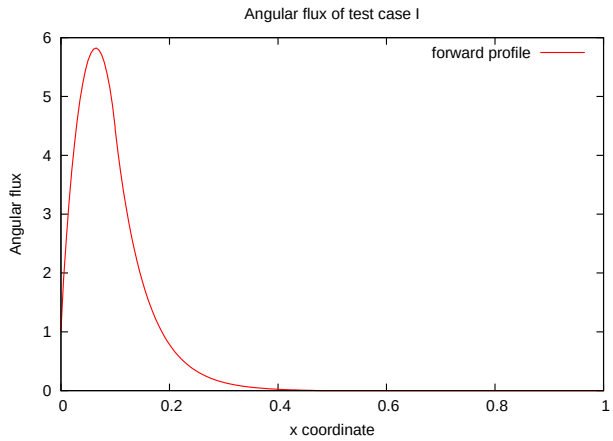

(a) *Solution of the forward scalar flux of test case I*

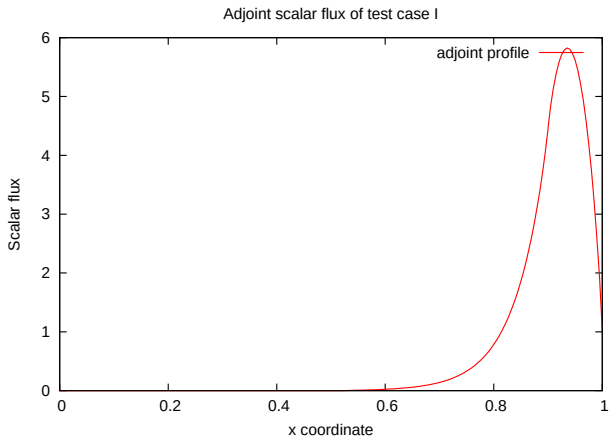

(b) *Solution of the adjoint scalar flux of test case I*

Figure 47: *Forward and adjoint solution of test case I.*

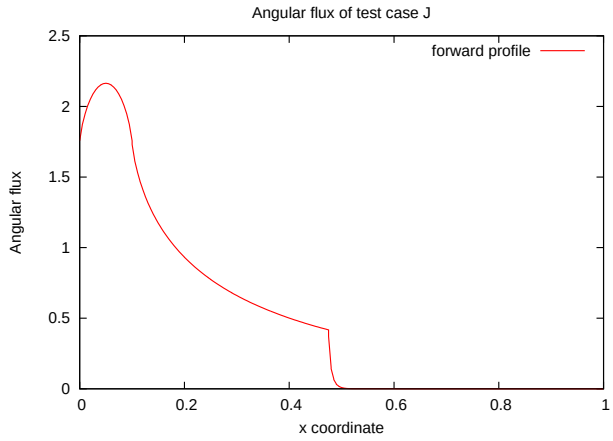

(a) *Solution of the forward scalar flux of test case J*

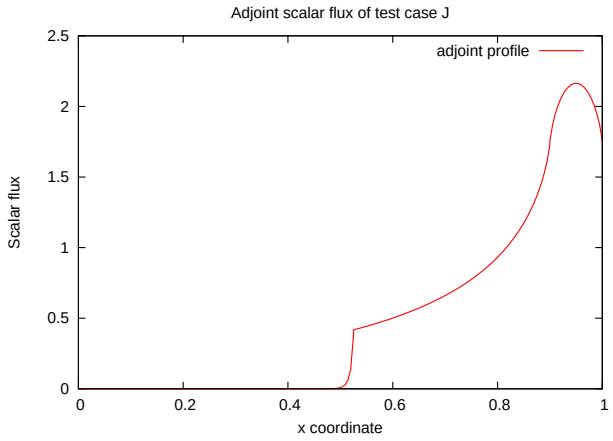

(b) *Solution of the adjoint scalar flux of test case J*

Figure 48: *Forward and adjoint solution of test case J.*

B Error Estimate Derivation

In this appendix the derivation of the error estimator is presented. From this derivation a criterion to decide which patches to refine is distilled. We will start with some preparatory definitions, before applying the discontinuous Galerkin method to the transport equation. After this we can write the equation in a bilinear and linear form, which are used to derive an error estimator.

We start with the single group, steady state, radiation transport equation with only an isotropic scattering term:

$$\hat{\boldsymbol{\Omega}} \cdot \nabla \phi(\boldsymbol{r}, \hat{\boldsymbol{\Omega}}) + \sigma_t \phi(\boldsymbol{r}, \hat{\boldsymbol{\Omega}}) = \frac{\sigma_s}{4\pi} \int_{4\pi} \phi(\boldsymbol{r}, \hat{\boldsymbol{\Omega}}) d\hat{\boldsymbol{\Omega}} + S \tag{B.1}$$

In our problem we use two different kinds of boundary conditions, Dirichlet and reflective:

$$\phi(\boldsymbol{r}, \hat{\boldsymbol{\Omega}}) = g, \qquad \boldsymbol{r} \in \partial V_D, \hat{\boldsymbol{\Omega}} \cdot \hat{\boldsymbol{n}} < 0 \tag{B.2}$$

$$\phi(\boldsymbol{r}, \hat{\boldsymbol{\Omega}}) = \phi_r = \phi(\boldsymbol{r}, \hat{\boldsymbol{\Omega}}_r), \qquad \boldsymbol{r} \in \partial V_R, \hat{\boldsymbol{\Omega}} \cdot \hat{\boldsymbol{n}} < 0 \tag{B.3}$$

First we introduce some sets that are needed for expressions later on. The domain in phase space of one element can be written as a set that takes care of the spatial part and one that takes care of the angular part.

$$e = \{\boldsymbol{r} \in \text{element e}\} \tag{B.4}$$

$$\Omega = \{\hat{\boldsymbol{\Omega}} \in 4\pi\} \tag{B.5}$$

$$\tag{B.6}$$

We can divide the angular set Ω into two sets, one for in flowing and one for outflowing directions on an edge δe.

$$\Omega^+ = \{\hat{\boldsymbol{\Omega}} \in \Omega | \hat{\boldsymbol{\Omega}} \cdot \hat{\boldsymbol{n}}_{\delta e} > 0\} \tag{B.7}$$

$$\Omega^- = \{\hat{\boldsymbol{\Omega}} \in \Omega | \hat{\boldsymbol{\Omega}} \cdot \hat{\boldsymbol{n}}_{\delta e} < 0\} \tag{B.8}$$

$$\tag{B.9}$$

Furthermore we need to discern the edges and directions that are specified by the boundary conditions of the problem. BC in the following expression is the abbreviation for boundary condition, which can be any of the elements of $\{U, R, D\}$, upwind, reflective and Dirichlet boundary conditions. There is an upwind 'boundary condition' as a result of applying the discontinuous Galerkin method is that all patches can be solved independently, therefore the upwind flux can be taken as a boundary condition for that patch.

$$\Omega_i^- = \{\hat{\boldsymbol{\Omega}} \in \Omega^- | BC = i\} \tag{B.10}$$

$$\partial V_i = \{\boldsymbol{r} \in \partial e^- | BC = i\} \tag{B.11}$$

The Galerkin procedure for spatial elements consists of multiplying the equation by a test function $v_{e,p}(\boldsymbol{r}, \hat{\boldsymbol{\Omega}})$ and integrating over the domain. The indices e and p are respectively the element and the patch index. This results in

$$
\begin{aligned}
&- \int_{4\pi}\int_e \phi\hat{\boldsymbol{\Omega}}\cdot\nabla v d\boldsymbol{r}d\hat{\boldsymbol{\Omega}} + \int_{4\pi}\int_e \sigma_t\phi^{int}v^{int}d\boldsymbol{r}d\hat{\boldsymbol{\Omega}} - \int_{4\pi}\int_e \frac{\sigma_s}{4\pi}\Phi v^{int}d\boldsymbol{r}d\hat{\boldsymbol{\Omega}} \\
&+ \int_{\Omega^+}\int_{\partial e^+}(\hat{\boldsymbol{\Omega}}\cdot\hat{\boldsymbol{n}})\phi^{int}v^{int}d\boldsymbol{r}d\hat{\boldsymbol{\Omega}} + \int_{\Omega_U^-}\int_{\partial e^-\setminus\{\partial V_R\cup\partial V_D\}}(\hat{\boldsymbol{\Omega}}\cdot\hat{\boldsymbol{n}})\phi^{ext}v^{int}d\boldsymbol{r}d\hat{\boldsymbol{\Omega}} \\
&\qquad + \int_{\Omega_R^-}\int_{\partial e^-\cap\partial V_R}(\hat{\boldsymbol{\Omega}}\cdot\hat{\boldsymbol{n}})\phi_r v^{int}d\boldsymbol{r}d\hat{\boldsymbol{\Omega}} \\
&= \int_{4\pi}\int_e Sv^{int}d\boldsymbol{r}d\hat{\boldsymbol{\Omega}} - \int_{\Omega_D^-}\int_{\partial e^-\cap\partial V_D}(\hat{\boldsymbol{\Omega}}\cdot\hat{\boldsymbol{n}})gv^{int}d\boldsymbol{r}d\hat{\boldsymbol{\Omega}} \qquad \text{(B.12)}
\end{aligned}
$$

By summing this equation over all elements we can identify a bilinear form and linear form such that we can write the discretized transport equation as

$$B(\phi, v) = l(v), \forall v \in V_h \qquad \text{(B.13)}$$

where V_h is the space of all test functions. An explicit expression for B and l is given by

$$
\begin{aligned}
B(\phi,v) &= \sum_e \Big\{ - \int_{4\pi}\int_e \phi\hat{\boldsymbol{\Omega}}\cdot\nabla v d\boldsymbol{r}d\hat{\boldsymbol{\Omega}} + \int_{4\pi}\int_e \sigma_t\phi^{int}v^{int}d\boldsymbol{r}d\hat{\boldsymbol{\Omega}} - \int_{4\pi}\int_e \frac{\sigma_s}{4\pi}\Phi v^{int}d\boldsymbol{r}d\hat{\boldsymbol{\Omega}} \\
&\quad + \int_{\Omega^+}\int_{\partial e^+}(\hat{\boldsymbol{\Omega}}\cdot\hat{\boldsymbol{n}})\phi^{int}v^{int}d\boldsymbol{r}d\hat{\boldsymbol{\Omega}} + \int_{\Omega_U^-}\int_{\partial e^-\setminus\{\partial V_R\cup\partial V_D\}}(\hat{\boldsymbol{\Omega}}\cdot\hat{\boldsymbol{n}})\phi^{ext}v^{int}d\boldsymbol{r}d\hat{\boldsymbol{\Omega}} \\
&\quad + \int_{\Omega_R^-}\int_{\partial e^-\cap\partial V_R}(\hat{\boldsymbol{\Omega}}\cdot\hat{\boldsymbol{n}})\phi_r v^{int}d\boldsymbol{r}d\hat{\boldsymbol{\Omega}}\Big\} \qquad \text{(B.14)} \\
l(v) &= \sum_e \Big\{ \int_{4\pi}\int_e Sv^{int}d\boldsymbol{r}d\hat{\boldsymbol{\Omega}} - \int_{\Omega_D^-}\int_{\partial e^-\cap\partial V_D}(\hat{\boldsymbol{\Omega}}\cdot\hat{\boldsymbol{n}})gv^{int}d\boldsymbol{r}d\hat{\boldsymbol{\Omega}}\Big\} \qquad \text{(B.15)}
\end{aligned}
$$

We will now introduce patches with constant basis functions. The test function $v_{e,p}$ is therefore assumed to be of the form

$$v_{e,p}(\boldsymbol{r}, \hat{\boldsymbol{\Omega}}) = \phi_e(\boldsymbol{r})G_{e,p}(\hat{\boldsymbol{\Omega}}) \qquad \text{(B.16)}$$

The spatial part, $\phi_e(\boldsymbol{r})$, consists of linear functions. Each patch, $G_{e,p}(\hat{\boldsymbol{\Omega}})$, has a constant basis function. The linear form can then be written as:

$$l(v) = \sum_e \Big\{ \sum_p \int_e \Delta G_{e,p}S_{e,p}v_{e,p}^{int}d\boldsymbol{r} - \sum_{p\in\Omega_D^-}\int_{\partial e^-\cap\partial V_D}(\hat{\boldsymbol{\Omega}}_{e,p}\cdot\hat{\boldsymbol{n}})G_{e,p}v_{e,p}^{int}d\boldsymbol{r}\Big\} \qquad \text{(B.17)}$$

where $\hat{\boldsymbol{\Omega}}_{e,p}$ denotes $\int_{\Delta G_{e,p}}\hat{\boldsymbol{\Omega}}d\hat{\boldsymbol{\Omega}}$. With this notation no approximation is made, the integrals over the directions are exact. Since the patches have a constant basis function we can write the 4π integrals as sums with the size of the patch as weights, as stated earlier.

The bilinear form will become:

$$
\begin{aligned}
B(\phi, v) \;=\; & \sum_e \Big\{ -\sum_p \int_e \phi \hat{\boldsymbol{\Omega}}_{e,p} \cdot \nabla v_{e,p} d\boldsymbol{r} + \sum_p \int_e \Delta G_{e,p} \sigma_t \phi^{int} v_{e,p}^{int} d\boldsymbol{r} - \sum_p \int_e \Delta G_{e,p} \frac{\sigma_s}{4\pi} \Phi v_{e,p}^{int} d\boldsymbol{r} \\
& + \sum_{p \in \Omega^+} \int_{\partial e^+} (\hat{\boldsymbol{\Omega}}_{e,p} \cdot \hat{\boldsymbol{n}}) \phi^{int} v_{e,p}^{int} d\boldsymbol{r} + \sum_{p \in \Omega_U^-} \int_{\partial e^- \setminus \{\partial V_R \cup \partial V_D\}} (\hat{\boldsymbol{\Omega}}_{e,p} \cdot \hat{\boldsymbol{n}}) \phi^{ext} v_{e,p}^{int} d\boldsymbol{r} \\
& + \sum_{p \in \Omega_R^-} \int_{\partial e^- \cap \partial V_R} (\hat{\boldsymbol{\Omega}}_{e,p} \cdot \hat{\boldsymbol{n}}) \phi_r v_{e,p}^{int} d\boldsymbol{r} \Big\} \qquad \text{(B.18)}
\end{aligned}
$$

We can now turn to the quantity of which we want to minimize the error $J(\phi) - J(\phi_h)$, where J is the detector response.

$$
J(\phi) = \int_V \int_{4\pi} \sigma_D(\boldsymbol{r}) \phi(\boldsymbol{r}, \hat{\boldsymbol{\Omega}}) d\hat{\boldsymbol{\Omega}} d\boldsymbol{r} \qquad \text{(B.19)}
$$

A short derivation shows how we can write the error as a function of the linear and bilinear form, using respectively: linearity, dual problem, Galerkin orthogonality and consistency [8].

$$
\begin{aligned}
\Delta J &= J(\phi) - J(\phi_h) && \text{(B.20)} \\
&= J(\phi - \phi_h) && \text{(B.21)} \\
&= B(\phi - \phi_h, \phi^*) && \text{(B.22)} \\
&= B(\phi - \phi_h, \phi^* - \phi_h^*) && \text{(B.23)} \\
&= l(\phi^* - \phi_h^*) - B(\phi_h, \phi^* - \phi_h^*) && \text{(B.24)}
\end{aligned}
$$

Here ϕ_h is the computed solution and ϕ is the exact or reference solution. Since the exact solution is not always available one can use an approximation by using a solution on a very fine mesh.

Plugging in our expressions for l and B and subsequent partial integration yields

$$
\begin{aligned}
\Delta J \;=\; & \sum_e \sum_p \Big\{ \int_e \Delta G_{e,p} S_{e,p} (\phi^* - \phi_h^*) d\boldsymbol{r} - \mathbf{1}_{p \in \Omega_D^-} \int_{\partial e^- \cap \partial V_D} (\hat{\boldsymbol{\Omega}}_{e,p} \cdot \hat{\boldsymbol{n}}) g_{e,p} (\phi^* - \phi_h^*) d\boldsymbol{r} \\
& + \int_e \phi \hat{\boldsymbol{\Omega}}_{e,p} \cdot \nabla (\phi^* - \phi_h^*) d\boldsymbol{r} - \int_e \Delta G_{e,p} \sigma_t \phi_h^{int} (\phi^* - \phi_h^*) d\boldsymbol{r} + \int_e \Delta G_{e,p} \frac{\sigma_s}{4\pi} \Phi (\phi^* - \phi_h^*) d\boldsymbol{r} \\
& - \mathbf{1}_{p \in \Omega^+} \int_{\partial e^+} (\hat{\boldsymbol{\Omega}}_{e,p} \cdot \hat{\boldsymbol{n}}) \phi_h^{int} (\phi^* - \phi_h^*) d\boldsymbol{r} - \mathbf{1}_{p \in \Omega_U^-} \int_{\partial e^- \setminus \{\partial V_R \cup \partial V_D\}} (\hat{\boldsymbol{\Omega}}_{e,p} \cdot \hat{\boldsymbol{n}}) \phi_h^{ext} (\phi^* - \phi_h^*) d\boldsymbol{r} \\
& - \mathbf{1}_{p \in \Omega_R^-} \int_{\partial e^- \cap \partial V_R} (\hat{\boldsymbol{\Omega}}_{e,p} \cdot \hat{\boldsymbol{n}}) \phi_r (\phi^* - \phi_h^*) d\boldsymbol{r} \Big\} \qquad \text{(B.25)}
\end{aligned}
$$

which is actually a sum over all patches. The sum is weighted by the patch size, which becomes clear when we interpret $\hat{\boldsymbol{\Omega}}_{e,p}$ as the 'average' angle times the size of the patch:

$$\hat{\mathbf{\Omega}}_{e,p} = \int_{\Delta G_{e,p}} \hat{\mathbf{\Omega}} d\mathbf{\Omega} \tag{B.26}$$

$$= \frac{\int_{\Delta G_{e,p}} \hat{\mathbf{\Omega}} d\hat{\mathbf{\Omega}}}{\Delta G_{e,p}} \Delta G_{e,p} \tag{B.27}$$

$$= \hat{\mathbf{\Omega}}'_{e,p} \Delta G_{e,p} \tag{B.28}$$

The sum over all the patches then becomes

$$\begin{aligned}
\Delta J = & \sum_e \sum_p \Delta G_{e,p} \Big\{ \int_e S_{e,p}(\phi^* - \phi_h^*) d\boldsymbol{r} - \mathbf{1}_{p \in \Omega_D^-} \int_{\partial e^- \cap \partial V_D} (\hat{\mathbf{\Omega}}'_{e,p} \cdot \hat{\boldsymbol{n}}) g_{e,p} (\phi^* - \phi_h^*) d\boldsymbol{r} \\
& + \int_e \phi^{int} \hat{\mathbf{\Omega}}'_{e,p} \cdot \nabla (\phi^* - \phi_h^*) d\boldsymbol{r} - \int_e \sigma_t \phi_h^{int} (\phi^* - \phi_h^*) d\boldsymbol{r} + \int_e \frac{\sigma_s}{4\pi} \Phi (\phi^* - \phi_h^*) d\boldsymbol{r} \\
& - \mathbf{1}_{p \in \Omega^+} \int_{\partial e^+} (\hat{\mathbf{\Omega}}'_{e,p} \cdot \hat{\boldsymbol{n}}) \phi_h^{int} (\phi^* - \phi_h^*) d\boldsymbol{r} - \mathbf{1}_{p \in \Omega_U^-} \int_{\partial e^- \setminus \{\partial V_R \cup \partial V_D\}} (\hat{\mathbf{\Omega}}'_{e,p} \cdot \hat{\boldsymbol{n}}) \phi_h^{ext} (\phi^* - \phi_h^*) d\boldsymbol{r} \\
& - \mathbf{1}_{p \in \Omega_R^-} \int_{\partial e^- \cap \partial V_R} (\hat{\mathbf{\Omega}}'_{e,p} \cdot \hat{\boldsymbol{n}}) \phi_r (\phi^* - \phi_h^*) d\boldsymbol{r} \Big\}
\end{aligned} \tag{B.29}$$

It is interesting to compare the weights of the sum in this expression and the weights of a quadrature set that is used in the discrete ordinates method. In that method one chooses a set of directions and weights on which one demands the equation to hold. The integrals over the angular domain are then performed by computing a sum of weighted angular fluxes. In this case the angular integrals change into weighted sums naturally, where the weights are not free to chose, but are equal to the size of the patch.

Since the expression for ΔJ is a sum over all elements and all patches we can define an error contribution for each patch, call it $\eta_{e,p}$. The $\eta_{e,p}$'s will eventually tell us where to refine or coarsen the spatial or angular discretization. The total error estimate then looks like:

$$\Delta J = \sum_e \sum_p \Delta G_{e,p} \eta_{e,p} \tag{B.30}$$

after some manipulation and partial integration we see that $\eta_{e,p}$ is of the form:

$$\begin{aligned}
\eta_{e,p} = & \int_e R_h (\phi^* - \phi_h^*) d\boldsymbol{r} + \mathbf{1}_{p \in \Omega_U^-} \int_{\partial e^- \setminus \{\partial V_D \cup \partial V_R\}} (\hat{\mathbf{\Omega}}'_{e,p} \cdot \hat{\boldsymbol{n}}) r_{h,U} (\phi^* - \phi_h^*)^{int} d\boldsymbol{r} \\
& + \mathbf{1}_{p \in \Omega_D^-} \int_{\partial e^- \cap \partial V_D} (\hat{\mathbf{\Omega}}'_{e,p} \cdot \hat{\boldsymbol{n}}) r_{h,D} (\phi^* - \phi_h^*)^{int} d\boldsymbol{r} \\
& + \mathbf{1}_{p \in \Omega_R^-} \int_{\partial e^- \cap \partial V_R} (\hat{\mathbf{\Omega}}'_{e,p} \cdot \hat{\boldsymbol{n}}) r_{h,R} (\phi^* - \phi_h^*)^{int} d\boldsymbol{r}
\end{aligned} \tag{B.31}$$

with:

$$R_h = S_{e,p} + \frac{\sigma_s}{4\pi}\Phi_h - \hat{\mathbf{\Omega}}'_{e,p} \cdot \nabla\phi_{h;e,p} - \sigma_t\phi_{h;e,p} \tag{B.32}$$

$$r_{h,U} = \phi^{int}_{h;e,p} - \phi^{ext}_{h;e,p} \tag{B.33}$$

$$r_{h,D} = \phi^{int}_{h;e,p} - g_{e,p} \tag{B.34}$$

$$r_{h,R} = \phi^{int}_{h;e,p} - \phi^{r}_{h;e,p} \tag{B.35}$$

The error contribution of a patch, $\eta_{e,p}$, is now an integral over the domain in phase space of that patch. The integrand is the product of the residual and the importance of the location in phase space, since R_h, $r_{h,U}$, $r_{h,D}$ and $r_{h,R}$ turn out to be the residual of the discrete transport equation. The importance is given by the adjoint solution, for more on the adjoint solution and the interpretation of the importance we refer to Appendix D. Finally the contribution $\eta_{e,p}$ is multiplied by the size of the patch $\Delta G_{e,p}$.

R_h is the spatial and the r's are the boundary residuals of the equation. $r_{h,D}$ and $r_{h,R}$ are the Dirichlet and reflective boundary residuals, while $r_{h,U}$ is the upwind residual. This upwind residual is non zero between elements (it is zero on the boundary of the domain). This residual is a result of the 'jumps' that are allowed in the solution in the discontinuous Galerkin method.

We can use this expression to estimate the error of the solution, without the need for an explicit expression of the exact solution. However, we can also formulate the criterion for refinement from this expression. We now have a contribution to the error of each patch $\Delta G_{e,p}\eta_{e,p}$. When these contribution are sorted we find which patches contribute most to the error. A fixed percentage of patches will be refined in each refinement iteration, which leads to the natural choice of refining the patches that contribute most to the error.

C Wavelet mathematics

Using wavelets as basis functions for the Galerkin discretization method results in large matrix systems that need to be solved. To see what matrices are needed a derivation of the discretized equations using wavelets is presented below. Some remarks for wavelets are made at the end of this section.

We start with the steady-state isotropic scatter neutron transport equation (see Equation 2.2)

$$\hat{\boldsymbol{\Omega}} \cdot \nabla\phi(\boldsymbol{r}, \hat{\boldsymbol{\Omega}}) + \sigma_t(\boldsymbol{r})\phi(\boldsymbol{r}, \hat{\boldsymbol{\Omega}}) = \frac{\sigma_s}{4\pi}\Phi(\boldsymbol{r}) + s(\boldsymbol{r}, \hat{\boldsymbol{\Omega}}) \tag{C.1}$$

The expansion of the angular flux into wavelets can be written as a general expansion

$$\phi(\boldsymbol{r}, \hat{\boldsymbol{\Omega}}) \approx \sum_{w=1}^{W} \phi_w(\boldsymbol{r}) G_w(\hat{\boldsymbol{\Omega}}) \tag{C.2}$$

where $G_w(\hat{\boldsymbol{\Omega}})$ a wavelet function. By applying the Galerkin method we obtain the following result

$$\int_{4\pi} G_v \left[(\hat{\boldsymbol{\Omega}} \cdot \nabla + \sigma_t) \sum_{w=1}^{W} \phi_w(\boldsymbol{r}) G_w(\hat{\boldsymbol{\Omega}}) - s + \frac{\sigma_s}{4\pi}\Phi \right] = 0 \tag{C.3}$$

For an easy representation of the transport equation we introduce some widely used notation for the streaming term. The inner product between $\hat{\boldsymbol{\Omega}}$ and ∇ becomes

$$\hat{\boldsymbol{\Omega}} \cdot \nabla = \Omega_x \frac{\partial}{\partial x} + \Omega_y \frac{\partial}{\partial y} + \Omega_z \frac{\partial}{\partial z} \tag{C.4}$$

where the components of the unit vector $\hat{\boldsymbol{\Omega}}$ are described by

$$\Omega_x = \sqrt{1-\mu^2}\cos\omega \tag{C.5}$$
$$\Omega_y = \sqrt{1-\mu^2}\sin\omega \tag{C.6}$$
$$\Omega_z = \mu \tag{C.7}$$

where μ is the cosine of the polar angle and ω is the azimuthal angle. The equation we obtain by applying the Galerkin method, Equation C.3, can now be written as

$$\boldsymbol{A_x}\frac{\partial \boldsymbol{\phi}}{\partial x} + \boldsymbol{A_y}\frac{\partial \boldsymbol{\phi}}{\partial y} + \boldsymbol{A_z}\frac{\partial \boldsymbol{\phi}}{\partial z} + \boldsymbol{H}(\boldsymbol{r})\boldsymbol{\phi} = \boldsymbol{S}(\boldsymbol{r}) \tag{C.8}$$

The matrices $\boldsymbol{A_x}$, $\boldsymbol{A_y}$, $\boldsymbol{A_z}$ and $\boldsymbol{H}$ are of size $W \times W$ and the vector $\boldsymbol{\phi}$ holds all wavelet expansion coefficients. All matrices and vectors are specified below, except the matrix $\boldsymbol{H}$, which is described later.

$$\boldsymbol{A}_{xvw} = \int_{4\pi} \Omega_x G_v(\hat{\boldsymbol{\Omega}}) G_w(\hat{\boldsymbol{\Omega}}) d\hat{\boldsymbol{\Omega}} = \int_0^{2\pi}\int_{-1}^{1} \sqrt{1-\mu^2}\cos\omega G_v(\hat{\boldsymbol{\Omega}}) G_w(\hat{\boldsymbol{\Omega}}) d\mu d\omega \tag{C.9}$$

$$\boldsymbol{A}_{yvw} = \int_{4\pi} \Omega_y G_v(\hat{\boldsymbol{\Omega}}) G_w(\hat{\boldsymbol{\Omega}}) d\hat{\boldsymbol{\Omega}} = \int_0^{2\pi}\int_{-1}^{1} \sqrt{1-\mu^2}\sin\omega G_v(\hat{\boldsymbol{\Omega}}) G_w(\hat{\boldsymbol{\Omega}}) d\mu d\omega \tag{C.10}$$

$$\boldsymbol{A}_{zvw} = \int_{4\pi} \Omega_z G_v(\hat{\boldsymbol{\Omega}}) G_w(\hat{\boldsymbol{\Omega}}) d\hat{\boldsymbol{\Omega}} = \int_0^{2\pi}\int_{-1}^{1} \mu G_v(\hat{\boldsymbol{\Omega}}) G_w(\hat{\boldsymbol{\Omega}}) d\mu d\omega \tag{C.11}$$

$$S_w = \int_{4\pi} s(\boldsymbol{r}) G_w(\hat{\boldsymbol{\Omega}}) d\hat{\boldsymbol{\Omega}} = \int_0^{2\pi}\int_{-1}^{1} s(\boldsymbol{r}, \hat{\boldsymbol{\Omega}}) G_w(\hat{\boldsymbol{\Omega}}) d\mu d\omega \tag{C.12}$$

Matrix $\boldsymbol{H}$ specifies the scatter and total removal operators and can be specified in several different ways. The most common way is using the Legendre expasion of the scattering cross section. This results in the following expression [3]

$$H_{vw} = \int_{4\pi} \sigma_t G_v G_w d\hat{\mathbf{\Omega}} - \left[\sum_{l=0}^{L} \sigma_{sl} \alpha_v^{e,l,0} \alpha_w^{e,l,0} + 2\sum_{l=1}^{L} \sigma_{sl} \sum_{m=1}^{l} [\alpha_v^{e,l,m} \alpha_w^{e,l,m} + \alpha_v^{o,l,m} \alpha_w^{o,l,m}]\right] \tag{C.13}$$

where

$$\alpha_v^{e,l,m} = \int_{4\pi} G_v Y_{l,m}^e d\hat{\mathbf{\Omega}} \tag{C.14}$$

$$\alpha_v^{o,l,m} = \int_{4\pi} G_v Y_{l,m}^o d\hat{\mathbf{\Omega}} \tag{C.15}$$

and $Y_{l,m}^e$ and $Y_{l,m}^o$ are the real and complex parts of the spherical harmonic function $Y_{l,m}$.

In this report we used isotropic scatter, which simplifies the matrix $\boldsymbol{H}$. We can then write it as

$$H_{vw} = \int_{4\pi} \sigma_t G_v G_w d\hat{\mathbf{\Omega}} - \frac{\sigma_s}{4\pi} \int_{4\pi} G_v d\hat{\mathbf{\Omega}} \int_{4\pi} G_w d\hat{\mathbf{\Omega}} \tag{C.16}$$

Another less common method would be to use binning, which means that the scatter cross section is described as a ratio of neutrons that end up in a certain 'bin' in the angular variable.

In Section 3.3 some properties of wavelets are mentioned, including the orthogonality relations between wavelets. They can be expressed as

$$< G_v, G_w >= \begin{cases} 0 & \text{if} \quad v \neq w \\ 1 & \text{if} \quad v = w \end{cases} \tag{C.17}$$

However, in the case of wavelets we also have integrals with the angular coefficients Ω_x, Ω_y and Ω_z in the integrand, which throw off the orthogonality relations. Therefore the matrices $\boldsymbol{A}_x$, $\boldsymbol{A}_y$ and $\boldsymbol{A}_z$ will not be sparse. The integrals in Equations C.9 through C.11 cannot be interpreted as inner products, since they are not positive-definite. When the support of the wavelets G_v and G_w do not overlap the integral will evaluate to zero, however these wavelets are not the zero element in the wavelet function space. One could look for wavelets that will produce sparse matrices, however these will not be easy to find, as they will have to satisfy 'orthogonality' relations with respect to four different integrals.

D Adjoint Neutron Transport

In this section the adjoint operator of a simplified version of the transport equation is derived. This equation reads, see Equation 2.2,

$$\hat{\mathbf{\Omega}} \cdot \nabla \phi(\boldsymbol{r}, \hat{\mathbf{\Omega}}) + \sigma_t(\boldsymbol{r})\phi(\boldsymbol{r}, \hat{\mathbf{\Omega}}) = \frac{\sigma_s}{4\pi}\Phi(\boldsymbol{r}) + S(\boldsymbol{r}, \hat{\mathbf{\Omega}}) \tag{D.1}$$

An alternate expression for this equation is in terms of the operator L and the external source S

$$L\phi = S \tag{D.2}$$

The adjoint operator or equation can be derived using inner products. An inner product in this case is an integral over the whole phase space of a product of two functions, or in mathematical notation

$$< f, g >= \int_V \int_{4\pi} f(\boldsymbol{r}, \hat{\mathbf{\Omega}}) g(\boldsymbol{r}, \hat{\mathbf{\Omega}}) d\hat{\mathbf{\Omega}} dV \tag{D.3}$$

With this notation the adjoint operator can be derived as follows

$$< \phi^*, L\phi >=< \phi^*, S > \qquad \Longleftrightarrow \qquad < L^*\phi^*, \phi >=< \phi^*, S > \tag{D.4}$$

where L is the forward operator and L^* is the adjoint operator. We can chose the right hand side of the adjoint problem equal to the detector cross section, in other words $L^*\phi^* = \sigma_D$. This leads to

$$< L^*\phi^*, \phi >=< \sigma_D, \phi >=< \phi^*, S >= J \tag{D.5}$$

where J is the detector response. The relation $< \sigma_D, \phi >=< \phi^*, S >$ is known as the duality relation. The explicit expression for the forward operator L in our case is

$$L = \hat{\mathbf{\Omega}} \cdot \nabla + \sigma_t - \frac{\sigma_s}{4\pi} \int_{4\pi} d\hat{\mathbf{\Omega}} \tag{D.6}$$

To derive an explicit expression for the adjoint operator L^* we start by substituting the expression for L in the left hand side of equation D.4

$$< \phi^*, L\phi >= \int_V \int_{4\pi} (\phi^* \hat{\mathbf{\Omega}} \cdot \nabla \phi + \phi^* \sigma_t \phi - \phi^* \frac{\sigma_s}{4\pi} \Phi) d\hat{\mathbf{\Omega}} dV \tag{D.7}$$

We will now rewrite each term to obtain the operator L^*. Note that the operator L^* works on ϕ^*, instead of ϕ. Rewriting each term must therefore result in an expression with an operator that works on ϕ^*. We will start with the total removal, the second term on the right hand side in Equation D.7

$$\int_V \int_{4\pi} \phi^* \sigma_t \phi d\hat{\mathbf{\Omega}} dV = \int_V \int_{4\pi} \phi \sigma_t \phi^* d\hat{\mathbf{\Omega}} dV \tag{D.8}$$

The next term we consider is the scatter source, the third term in Equation D.7. By rearranging angular integrals we can switch the two angular solutions ϕ and ϕ^*, resulting in the operator working on the other function.

$$\int_V \int_{4\pi} \phi^* \frac{\sigma_s}{4\pi} \Phi d\hat{\mathbf{\Omega}} dV = \int_V \int_{4\pi} \phi^* d\hat{\mathbf{\Omega}} \frac{\sigma_s}{4\pi} \int_{4\pi} \phi d\hat{\mathbf{\Omega}} dV \tag{D.9}$$

$$= \int_V \int_{4\pi} \phi d\hat{\mathbf{\Omega}} \frac{\sigma_s}{4\pi} \int_{4\pi} \phi^* d\hat{\mathbf{\Omega}} dV \tag{D.10}$$

$$= \int_V \int_{4\pi} \phi \frac{\sigma_s}{4\pi} \Phi^* d\hat{\mathbf{\Omega}} dV \tag{D.11}$$

The streaming term needs a bit more work than the two other terms. We start by applying the product rule for derivatives

$$\int_V \int_{4\pi} \phi^* \hat{\mathbf{\Omega}} \cdot \nabla \phi d\hat{\mathbf{\Omega}} dV = \int_V \int_{4\pi} (\hat{\mathbf{\Omega}} \cdot \nabla(\phi^* \phi) - \phi \hat{\mathbf{\Omega}} \cdot \nabla \phi^*) d\hat{\mathbf{\Omega}} dV \tag{D.12}$$

Taking a closer look at the first term on the right hand side reveils that we can get rid of this term by applying certain boundary conditions. This becomes clear when we apply the divergence theorem to this term

$$\int_V \int_{4\pi} \hat{\mathbf{\Omega}} \cdot \nabla(\phi^* \phi) d\hat{\mathbf{\Omega}} dV = \int_S \int_{4\pi} \hat{\mathbf{\Omega}} \cdot \hat{\boldsymbol{n}} \phi^* \phi d\hat{\mathbf{\Omega}} dS \tag{D.13}$$

The boundary conditions for the forward problem (corresponding to the solution ϕ) stipulate a flux on the incoming directions. This contribution to the integral can be cancelled by stipulating an equal flux of ϕ^* in the opposite direction. Cancellation will take place because the inner product $\hat{\mathbf{\Omega}} \cdot \hat{\boldsymbol{n}}$ will only change sign for opposite directions and the product $\phi^* \phi$ will be the same for the two opposite directions. Therefore we stipulate as boundary conditions a flux for outgoing directions for the adjoint problem.

Now that we showed that the first term of Equation D.12 does not contribute, we observe that the second term is already in the form we want it to be in. The expression in Equation D.7 now becomes

$$< L^* \phi^*, \phi >= \int_V \int_{4\pi} (-\phi \hat{\mathbf{\Omega}} \cdot \nabla \phi^* + \phi \sigma_t \phi^* - \phi \frac{\sigma_s}{4\pi} \Phi^*) d\hat{\mathbf{\Omega}} dV \tag{D.14}$$

from this it follows that the operator L^* can be expressed as

$$L^* = -\hat{\mathbf{\Omega}} \cdot \nabla + \sigma_t - \frac{\sigma_s}{4\pi} \int_{4\pi} d\hat{\mathbf{\Omega}} \tag{D.15}$$

The physical interpretation of this operator is that it describes the 'importance' of a location in phase space to the detector response. This follows from the expression for the detector response, $J =< \phi^*, S >$. When we chose $S = \delta(\boldsymbol{r}, \hat{\mathbf{\Omega}})$ we see that the inner product reduces to $J = \phi^*(\boldsymbol{r}, \hat{\mathbf{\Omega}})$. Therefore the contribution of that location of phase space is given by the adjoint solution.

This importance flows oppositely to neutrons, therefore a minus sign is in front of the streaming term. Furthermore the boundary conditions stipulate the importance flowing out of the domain, instead of neutrons flowing into the domain. This interpretation can be used to decide which patches to refine in order to obtain a more accurate detector response.